The role of systemic endothelial dysfunction in an experimental model of aortic valve stenosis

Inaugural-Dissertation

Zur Erlangung des Doktorgrades
der Mathematisch-Naturwissenschaftlichen Fakultät
der Heinrich-Heine-Universität Düsseldorf

vorgelegt von

Isabella Gyamfi Poku
aus Oberhausen

Düsseldorf, Dezember 2021

aus der Klinik für Kardiologie, Pneumologie und Angiologie

des Universitätsklinikums der Heinrich-Heine-Universität Düsseldorf

Direktor: Univ.-Prof. Dr. Malte Kelm

Gedruckt mit der Genehmigung der
Mathematisch-Naturwissenschaftlichen Fakultät der
Heinrich- Heine-Universität Düsseldorf

Berichterstatter

1. Univ.-Prof. Dr. Axel Gödecke

2. Univ.-Prof. Dr. Malte Kelm

Tag der mündlichen Prüfung: 21.06.2022

Ich versichere an Eides Statt, dass die Dissertation von mir selbstständig und ohne unzulässige fremde Hilfe unter Beachtung der „Grundsätze zur Sicherung guter wissenschaftlicher Praxis an der Heinrich-Heine-Universität Düsseldorf“ erstellt worden ist.

Diese Dissertation wurde weder in gleicher noch in ähnlicher Form in einem anderen Prüfungsverfahren vorgelegt. Außerdem erkläre ich, dass ich bisher noch keine weiteren akademischen Grade erworben oder zu erwerben versucht habe.

Düsseldorf, den 03.03.2022

Isabella Gyamfi Poku

To Elisabeth and Kwame

"*It always seems impossible until it's done*"

Nelson Mandela

Parts of this dissertation were already published in scientific journals or presented on scientific conferences:

Original publications:

Niepmann, S. T., Steffen, E., Zietzer, A., Adam, M., Nordsiek, J., **Gyamfi-Poku, I.**, Piayda, K., Sinning, J.-M., Baldus, S., Kelm, M., Nickenig, G., Zimmer, S., & Quast, C. (2019). Graded murine wire-induced aortic valve stenosis model mimics human functional and morphological disease phenotype. *Clinical Research in Cardiology*, *108 (8),* 847–856. https://doi.org/10.1007/s00392-019-01413-1

The contribution to the publication "Graded murine wire-induced aortic valve stenosis model mimics human functional and morphological disease phenotype" consisted of planning, implementation, and analysis of parts of the echocardiographic data and histological analysis.

Quast, C., Kober, F., Becker, K., Zweck, E., Hoffe, J., Jacoby, C., Flocke, V., **Gyamfi Poku, I.**, Keyser, F., Piayda, K., Erkens, R., Niepmann, S., Adam, M., Baldus, S., Zimmer, S., Nickenig, G., Grandoch, M., Bönner, F., Kelm, M., & Flögel, U. (2022). Multiparametric MRI identifies subtle adaptations for demarcation of disease transition in murine aortic valve stenosis. *Basic Research in Cardiology*, *117*(1), 29. https://doi.org/10.1007/s00395-022-00936-5

The contribution to the publication "Multiparametric MRI identifies subtle adaptations for demarcation of disease transition in murine aortic valve stenosis" consisted of planning of surgical procedures, implementation, and analysis of parts of the echocardiographic data, which were the basis for further magnetic resonance imaging.

Poster:

15.-18.04.2021 87. Annual Meeting of the German Cadiac Society (DGK):
Gyamfi Poku, I., Paul-Krahé, K., Kelm, M., Quast, C. Characterization of red blood cell integrity and endothelial function in a murine model of aortic valve stenosis.

07.-10.04.2020 86. Annual Meeting of the German Cadiac Society (DGK):
Gyamfi Poku, I., Chennupati, R., Becker, K., Gödecke, A., Kelm, M., Quast, C.
Cell-free hemoglobin plays a crucial role in systemic endothelial dysfunction in an experimental model aortic valve stenosis.

Abstract

Background: The endothelium is the indispensable paracrine organ whose function is closely related to the bioavailability of nitric oxide (NO) – a key player in endothelium-dependent relaxation. A convincing body of literature identified decreased endothelium-dependent flow-mediated dilation (FMD) in patients with aortic valve stenosis (AS), widely used as a read-out for NO bioavailability. The morphological alterations of the aortic valve promote an increase in left ventricular afterload and turbulent blood flow in the ascending aorta. These turbulences result in increased shear stress on red blood cells (RBCs), which were shown to be in the threshold range for subhemolytic alterations of the RBCs membrane and an increase in cell-free hemoglobin (Hb). However, the underlying mechanisms driving impaired endothelium-dependent relaxation in AS are complex and still not fully understood.

Hypothesis & Aims: This work hypothesized that aortic valve stenosis affects vascular endothelial function by reduced NO bioavailability due to turbulent blood flow conditions in the ascending aorta. Therefore, the global aim of the present work was to elucidate endothelial function in an experimental model of AS.

Methods: Male C57BL6 mice were subjected to wire-injury of the aortic valve to induce AS. Characterization of transvalvular blood flow, cardiac function and valvular alterations were conducted by echocardiography, magnetic resonance imaging, or histology, respectively. FMD studies were used to assess endothelial function *in vivo*, whereas wire-myography was used to examine endothelium-dependent relaxation in isolated segments of the aorta and femoral arteries. RBCs integrity was assessed by blood count, flow cytometry, cell-free Hb levels and ectacytometry.

Results: Manipulation of the aortic valve caused restricted aortic valve opening with a significant increase in pressure gradients across the valve and turbulences in the ascending aorta. LV function was preserved with mild hypertrophy of the myocardium. Histological analysis revealed significant thickening of the aortic valve with fibrosis and infiltration of macrophages. Importantly, we observed a significant impairment of FMD in AS animals. Administration of haptoglobin, the physiological scavenger of cell-free Hb, improved FMD in AS animals. In contrast, *ex vivo* vascular reactivity studies showed fully preserved acetylcholine-induced relaxation responses in the femoral artery. Moreover, the analysis of vascular reactivity in isolated aortic segments revealed impaired NO-mediated relaxation responses in mice with AS. In addition, aortic eNOS protein expression levels were significantly elevated in AS animals with a concomitant decrease in GSH/GSSG ratio. No

differences in NO metabolites were observed in plasma, heart, or aorta of sham and AS animals. Furthermore, we observed an increase in Annexin V positive RBCs with a simultaneous increase in cell-free plasma Hb levels. However, RBCs deformability was fully preserved.

Conclusion: Taken together, this work provides novel evidence that the wire-injury model of AS is associated with systemic endothelial dysfunction. The results of the present work suggest that subhemolytic release of cell-free Hb likely drives reduction in NO bioavailability and thereby limits endothelium-derived NO to induce vascular smooth muscle cells (VSMCs) relaxation response.

Zusammenfassung

Hintergrund: Das Endothel ist ein unverzichtbares parakrines Organ, dessen Funktion eng mit der Bioverfügbarkeit von Stickstoffmonoxid (NO) verknüpft ist. NO spielt eine Schlüsselrolle bei der endothelabhängigen Dilatation. In der Fachliteratur wurde eine verminderte endothelabhängige flussvermittelte Dilatation (FMD) bei Patienten mit Aortenklappenstenose (AS) festgestellt, die häufig als Indikator für die NO-Bioverfügbarkeit verwendet wird. Die morphologischen Veränderungen der Aortenklappe begünstigen einen Anstieg der linksventrikulären Nachlast und einen turbulenten Blutfluss in der Aorta ascendens. Diese Turbulenzen führen zu einer erhöhten Scherbeanspruchung der Erythorzyten, die nachweislich im Schwellenbereich für subhämolytische Veränderungen der Erythrozytenmembran liegen und mit einem Anstieg des zellfreien Hämoglobins (Hb) einhergehen kann. Die zugrundeliegenden Mechanismen, die zu einer Beeinträchtigung der endothelabhängigen Dilatation bei AS führen, sind komplex und noch nicht vollständig geklärt.

Hypothese & Ziele: Die Hypothese dieser Arbeit war, dass die Aortenklappenstenose die vaskuläre Endothelfunktion durch eine reduzierte Bioverfügbarkeit von NO aufgrund turbulenter Strömungsbedingungen in der Aorta ascendens beeinflusst. Daher war das globale Ziel dieser Arbeit, die Endothelfunktion in einem experimentellen Modell von AS zu untersuchen.

Methoden: Männliche C57BL6-Mäuse wurden einer „wire-injury“ der Aortenklappe unterzogen, um eine AS zu induzieren. Die Charakterisierung des transvalvulären Blutflusses, der Herzfunktion und der Klappenveränderungen wurden mittels Echokardiographie, Magnetresonanztomographie bzw. Histologie durchgeführt. Die FMD diente zur Analyse der Endothelfunktion *in vivo*, während die „wire-myography“ zur Untersuchung der endothelabhängigen Relaxation in isolierten Segmenten der Aorta und der Femoralarterie eingesetzt wurde. Die Integrität der Erythrozyten wurde mittels Blutbild, Durchflusszytometrie, zellfreiem Hb-Wert und Ektazytometrie beurteilt.

Ergebnisse: Die Manipulation der Aortenklappen führte zu einer reduzierten Aortenklappenöffnungsfläche mit einem signifikanten Anstieg des Druckgradienten über der Klappe und Turbulenzen in der aufsteigenden Aorta. Die linksventrikuläre Funktion blieb bei leichter Hypertrophie des Myokards erhalten. Die histologische Analyse ergab eine deutliche Verdickung der Aortenklappe mit Fibrose und Infiltration von Makrophagen. Darüber hinaus wurde bei den AS-Tieren eine signifikante Beeinträchtigung der FMD

beobachtetet. Die Verabreichung von Haptoglobin, dem physiologischen „scavenger“ von zellfreiem Hb, konnte die FMD bei AS-Tieren verbessern. Im Gegensatz dazu zeigten *ex-vivo* Studien zur Gefäßreaktivität, dass die Acetylcholin-induzierte Relaxation in der Femoralarterie vollständig erhalten blieb. Die Analyse der Gefäßreaktivität in isolierten Aortensegmenten zeigte hingegen, dass die NO-vermittelte Relaxation bei Mäusen mit AS beeinträchtigt war. Darüber hinaus war die Expression des eNOS-Proteins in der Aorta bei AS-Tieren signifikant erhöht, was mit einer Abnahme des GSH/GSSG-Verhältnisses einherging. Es wurden keine Unterschiede bei den NO-Metaboliten im Plasma, im Herzen oder in der Aorta zwischen Kontrolltieren und AS-Tieren festgestellt. Des Weiteren wurde eine Zunahme der Annexin V-positiven Erythrozyten bei gleichzeitigem Anstieg der zellfreien Hb-Werte im Plasma beobachtet. Die Verformbarkeit der Erythrozyten blieb jedoch vollständig erhalten.

Schlussfolgerung: Zusammenfassend liefert diese Arbeit neue Erkenntnisse, dass die durch „wire-injury“ induzierte AS mit einer systemischen endothelialen Dysfunktion einhergeht. Die Ergebnisse der vorliegenden Arbeit deuten darauf hin, dass die subhämolytische Freisetzung von zellfreiem Hb zu einer Verringerung der NO-Bioverfügbarkeit führt und dadurch das aus dem Endothel stammende NO zur Dilatation an den glatten Gefäßmuskelzellen reduziert wird.

Table of contents

Table of figures

Abbreviations

AS	aortic valve stenosis
AC	adenylate cyclase
Ach	acetylcholine
AR	aortic regurgitation
AUC	area under the curve
cAMP	cyclic adenosine monophosphate
cGMP	cyclic guanosine monophosphate
CLD	chemiluminescence detection
Ctrl	control
CVD	cardiovascular disease
CO	cardiac output
EC	endothelial cell
EI	elongation index
EImax	maximal elongation index
Emax	maximal dilation
EDHF	endothelium-derived hyperpolarization factor
EDRF	endothelium-derived relaxing factor
EDV	end-diastolic volume
EF	ejection fraction
eNOS	endothelial nitric oxide synthase
ESV	end-systolic volume
FMD	flow-mediated dilation
Grs	glutathione reductase
GSH	glutathione
GSSG	glutathione disulfide
Gpx	glutathione peroxidase
H_2O_2	hydrogen peroxide
Hb	hemoglobin
Hp	haptoglobin
HR	heart rate
IVSd	interventricular septum thickness, diastole
KO	knock out
L-NAME	N^G-nitro-L-arginine methyl ester

LORCA	laser optical rotational cell analyzer
LV	left ventricle
LVIDd	left ventricular inner diameter, diastole
MAP	mean arterial pressure
mRNA	messenger RNA
MRI	magnetic resonance imaging
NADPH	nicotinamide adenine dinucleotide phosphate
NO	nitric oxide
NOS	nitric oxide synthase
NO_3^-	nitrate
NO_2^-	nitrite
NO_x	nitric oxide metabolites
$ONOO^-$	peroxynitrite
OxyHb	oxygenated hemoglobin
PED	end-diastolic pressure
PES	end-systolic pressure
PBS	phosphate buffered saline
PWV	pulse wave velocity
RBC	red blood cell
RDW	red cell distribution width
ROS	reactive oxygen species
RXNO	sum of nitrosothiols and nitrosoamines
SEM	standard error of the mean
sGC	soluble guanylate cyclase
SNP	sodium nitroprusside
SOD	superoxidedismustase
SV	stroke volume
SVR	systemic vascular resistance
VSMC	vascular smooth muscle cell
WT	wild type

1 Introduction

1.1 Aortic valve stenosis

Aortic valve stenosis (AS) is the most common valvular heart disease of the elderly population in the western world (Osnabrugge et al., 2013). The prevalence of AS is likely to increase within the next decades as a consequence of our aging population. While congenital anomalies and the rheumatic form of AS are comparably rare in industrialized countries, age-related AS is the most common form and is thus of great medical and socioeconomic interest (Yadgir et al., 2020). The high risk for adverse cardiovascular events in patients with severe AS emphasizes its clinical importance, especially considering the lack of an effective medical treatment (Lancellotti et al., 2018). The disease precedes a long latent phase with sclerotic alterations of the aortic valve without clinically relevant hemodynamic changes. However, in the later phases, the disease characteristics are fibrotic, inflammatory, and calcific valve remodeling leading to progressive leaflet stiffening and narrowing of the aortic valve orifice area. As a consequence, the pressure afterload and ventricular wall stress increase, eventually inducing concentric hypertrophy of the left ventricle (LV). Echocardiography is the primary tool to assess the severity of AS by evaluation of aortic valve area, peak velocity, and mean pressure gradient (Baumgartner et al., 2009). Symptomatic patients experience dyspnoea, angina pectoris, and syncopation. Currently, there is no pharmacological treatment available that effectively decelerate disease progression (Marquis-Gravel et al., 2016). According to the latest guidelines for the management of valvular heart disease, surgical aortic valve replacement or transcatheter aortic valve implantation (TAVI) remains the only effective therapeutic option in patients with severe AS (Vahanian et al., 2021).

Once the compensatory mechanism becomes insufficient, the LV dilates, ultimately resulting in chronic heart failure. Hence, AS is a disease of the valve, the heart, and peripheral vascular system, as several studies highlighted the presence of vascular endothelial dysfunction in AS patients (Chenevard et al., 2006; Dweck et al., 2012; Moscarelli et al., 2019; Poggianti et al., 2003).

1.2 Pathophysiology of aortic valve stenosis

In the past decades, AS was considered as a consequence of degenerative processes. However, recent findings suggest that the development of AS is a complex and active process that consists of various stages regarding molecular and cellular alterations (Rajamannan et al., 2011). The tricuspid aortic valve consists of three semilunar cusps connected to the aortic wall. The primary function of the aortic valve is to maintain the unidirectional blood flow from the LV into the ascending aorta during systole and to prevent the backflow of blood during diastole into the ventricle. The aortic valve leaflets are composed of a distinct cellular architecture comprising four distinct layers (Misfeld & Sievers, 2007). The fibrosa is located at the aortic side, consisting of valvular interstitial cells (VICs) and type I and III collagen fibers, and is responsible for the mechanical strength of the valve (Schoen, 2008). The spongiosa is the middle layer and consists of VICs, and is also rich in proteoglycans and glycosaminoglycans, which facilitate compression changes and rearrangement of the collagen and elastin layers (Goody et al., 2020). The ventricularis is responsible for flexibility and is composed of VICs, elastic fibers, and smooth muscle cells. A single layer of endothelial cells (ECs) borders both the aortic and ventricular sides. Valvular ECs differ from vascular ECs regarding their response to mechanical forces and their gene expression profile (Butcher et al., 2004, 2006).

According to previous studies, AS features distinct disease stages, composed of endothelial injury/dysfunction, inflammation, fibrosis, and calcification (Kostyunin et al., 2019). The earliest stage of the pathogenesis of AS is attributed to an activation of valvular ECs (Sucosky et al., 2009). Importantly, side-specific EC heterogeneity between the endothelium on the aortic side and the ventricular side of the valve was identified, suggesting an explanation for the greater disease susceptibility of the aortic side of the valve (Simmons et al., 2005). This supports that altered blood flow conditions increase the expression of adhesion molecules and inflammatory markers on the aortic side of the leaflet (Richards et al., 2013a). Thus it is assumed that mechanical stress, also found in disease states like arterial hypertension, can induce valvular endothelial damage with an increased expression of adhesion molecules (Ghaisas et al., 2000; Liakos et al., 2017; Rieck et al., 2012; Thubrikar et al., 1986).

Endothelial damage and dysfunction trigger accumulation and oxidation of lipids and infiltration of inflammatory cells in the subendothelial fibrosa, which occurs in early aortic valve lesions (O'Brien et al. 1996, Olsson, Thyberg and Nilsson, 1999). Secretion of multiple proinflammatory mediators by inflammatory cells propagate activation and differentiation of VICs to myofibroblast in line with increased secretion of extracellular matrix and expression of matrix metalloproteinases (MMPs) enhancing fibrosis (Kaden et al., 2005). The differentiation to an osteoblast-like phenotype of myofibroblasts includes multiple pathways, such as receptor activator of nuclear kappa B (RANK), RANK ligand (RANKL)/OPG, runt-related transcription factor 2 (RUNX-2)/Notch, Wnt3-Lrp5-b catenin (Garg et al., 2005; Kawakami et al., 2016; Yang et al., 2009). Secretion of bone-related proteins like osteopontin and osteocalcin, bone morphogenetic protein 2 (BMP-2), alkaline phosphatase were found in AS (Srivatsa et al., 1997) and can contribute to calcification and lamellar bone formation (Mohler et al., 2001). Progressive calcification exacerbates valve thickening and stiffening, which further increases mechanical stress and injury, culminating in a downward spiral of disease progression (Pawade et al., 2015).

1.2.1 The role of eNOS in the development of aortic valve stenosis

Similar to vascular ECs, alterations in blood flow-induced shear stress affect the endothelial homeostasis with distinct changes in endothelium-derived NO signaling (Gould et al., 2013). The importance of endothelium-derived NO in initiating the disease process of AS was demonstrated by El Accaoui et al. (2014). They demonstrated that eNOS deficient mice developed greater aortic valve fibrosis than age-matched wild-type (WT) mice. Interestingly, valvular changes in mice lacking eNOS were already reported more than one decade earlier (T. C. Lee et al., 2000). These animals were identified with the presence of a bicuspid aortic valve. In a further study, it was demonstrated that NO signaling plays a critical role in the regulation of VICs by valvular ECs (Richards et al., 2013b). They demonstrated that the main source of NO in the aortic valve is the endothelium on the side of the ventricularis. Furthermore, they showed that NO can antagonize valvular calcification, whereas incubation with eNOS inhibitor N^G-nitro-L-arginine methyl ester (L-NAME) increases calcification. Taken together, there is a strong association between eNOS deficiency and the disease progression of AS.

1.3 Therapy of aortic valve stenosis

The high incidence of AS in the aging population and the poor prognosis of symptomatic, severe AS patients emphasize the high demand for effective therapy. However, today there is no medical treatment available to slow down disease progression. Recent studies focused on three major conceptual frameworks. These include lipid-lowering therapy, antihypertensive therapy and the therapy of valvular calcification (Marquis-Gravel et al., 2016).

The parallels to the etiopathology of arteriosclerosis and the association of increased levels of LDL and increase in aortic valve calcification (Smith et al., 2014) led to the hypothesis that statins could intervene in the progression of AS. Therefore, several studies in the broader literature have examined the effects of statin therapy on disease progression (Novaro et al., 2001; Rosenhek et al., 2004; Shavelle et al., 2002). Nevertheless, besides lowering LDL-cholesterol, none of the randomized studies were able to prove a deceleration of the progression of AS (Chan et al., 2010; Cowell et al., 2005; Dichtl et al., 2008; Rossebø et al., 2008). The only medical intervention recommended in the guidelines is the treatment of underlying hypertension (Vahanian et al., 2021). Studies demonstrated that drugs, which target the renin-angiotensin-aldosterone-system (RAAS) reduce aortic valve calcium (O'Brien et al., 2005), are associated with lower aortic valve weight (Côté et al., 2011) and decrease in left ventricular mass in asymptomatic AS patients (Bull et al., 2015). The differentiation of the VICs towards an osteoblast phenotype set another focus on drugs, which potentially inhibit valvular calcification. Bisphosphonates, which are frequently used in the therapy of osteoporosis, have been shown to decrease differentiation of myofibroblasts to osteoblasts and inhibit aortic valve calcification in an experimental model (Elmariah et al., 2010; Synetos et al., 2018). Further studies focused on targeting the RANK/RANKL/OPG signaling cascade involved in the calcification of the aortic valve. The human monoclonal antibody denosumab was identified to be a potential therapeutic target. Denosumab inhibits the RANK ligand interaction with RANK and inhibits osteoclast formation and, consequently, bone resorption (Hanley et al., 2012). However, recent data from a randomized clinical trial showed that denosumab does not affect calcification in patients with AS (Pawade et al., 2021). In summary, lacking proper medical therapy, aortic valve replacement is the only effective therapy to improve the outcome in patients with severe AS at the moment (Baron et al., 2019; Baumgartner et al., 2017).

1.4 The endothelium and its importance for the cardiovascular system

The importance of the endothelium within the cardiovascular system started to gain attention when Furchgott and Zawadski (1980) first described the importance of an intact endothelium for the vascular dilation response to acetylcholine. Intensive research revealed the complex and fundamental functions of the endothelium, especially regarding the synthesis of several vasoactive substances, from which the endothelium-derived relaxing factor (EDRF), later identified as nitric oxide (NO) is the most important one (Murad et al., 1983, Ignarro et al., 1987; Palmer et al., 1988). Thus the endothelium represents a paracrine organ, which regulates via the release of vasoactive mediators the dilation and constriction of vascular smooth muscle cells (VSMCs) to control vascular tone, blood flow (Gardiner et al., 1990; Gladwin et al., 2004), platelet aggregation (Radomski et al., 1987), leucocyte adhesion (Kubes et al., 1991) and angiogenesis (Murohara et al., 1998; Papapetropoulos et al., 1997). Considering NO as the key player in vasodilator control in muscular arteries, the hallmark of endothelial dysfunction is NO deficiency. This can be the consequence of impaired synthesis or reduced bioavailability via inactivation by, e.g., reactive oxygen species (ROS) or other scavenging molecules such as cell-free hemoglobin (Doherty et al., 1998; Rubanyi & Vanhoutte, 1986). *"After almost 30 years of NO-related research, reduced NO bioavailability has become synonymous with the condition broadly described as "endothelial dysfunction""*(Harris et al., 2010). To compensate for decreased bioavailability of NO, the endothelium is able to upregulate the release of other vasoactive substances, such as endothelium-derived hyperpolarization factor (EDHF), known to be a potent relaxing factor in the microcirculation (Ozkor & Quyyumi, 2011). Endothelial dysfunction is also associated with disturbed redox balance, endothelial cell activation, an increase of inflammatory reactions within the vessel, alterations in vascular permeability, vascular tone disruption, and decreased vasodilation (Liao, 2013; Thomas et al., 2008; C. Zhang, 2008).

Several studies have shown the predictive value of endothelial function assessment for future cardiovascular events (Gokce et al., 2003; Heiss et al., 2006; Maruhashi et al., 2018; Suwaidi et al., 2000). Yeboah and colleagues investigated the predictive value of brachial artery flow-mediated dilation (FMD) regarding the incidence of cardiovascular disease events in adults, which were not suffering from any cardiovascular disease so far (Yeboah et al., 2009). This Multi-Ethnic Study of Atherosclerosis (MESA) demonstrated that FMD correlated inversely with cardiovascular events regardless of other major risk factors. Therefore, the investigation

of endothelium-dependent vasodilation response is widely used to assess cardiovascular health (Corretti et al., 2002). In humans, the clinical standard tool for the assessment of endothelial function is FMD by the reactive hyperemia test, evaluated with the help of high-resolution ultrasound imaging. The method of FMD has been constantly developed over the past decades with the goal to induce a shear stress stimulus that creates a NO-dependent dilation response to use FMD as a read-out for NO bioavailability (Celermajer et al., 1992; Corretti et al., 2002; Green et al., 2011). The nature of the shear stress stimulus highly depends on the protocol used (cuff position, time and degree of ischemia) and entails the mechanistic dilation response (Pyke & Tschakovsky, 2005).

In animal studies, vascular reactivity is typically studied in isolated segments of arteries under mimicked physiological conditions such as temperature, nutrients, and oxygen (Mulvany and Halpern, 1976). In this method, the force developed by the vessel segment in response to pharmacological stimuli is studied. This technique allows to investigate the endothelial and smooth muscle cell function in various disease states with multiple pharmacological substances. Even though this represents a powerful method to study vasodilation and vasoconstriction responses of different arteries, the *in vivo* assessment of endothelial function would comprise the effects of flowing blood and the integrity of the vasculature and allows for repeated measurements. For this reason, the concept of FMD was transferred to rodents to study endothelial function in the living animal (Heiss et al., 2008; Schuler et al., 2014). In mice and rats, FMD assessment is performed in the femoral artery by hind limb occlusion according to the protocol used in humans.

1.5 Endothelial dysfunction and its role in aortic valve stenosis

Endothelial dysfunction is commonly considered as a crucial factor in the development of arteriosclerosis and is known to play an important role in cardiovascular disease states, such as coronary artery disease (Suwaidi et al., 2000). Aortic valve sclerosis (AVS) and AS are commonly associated with a series of cardiovascular events, suggesting that pathological alterations are not limited to the valve itself (Pohle et al., 2001; Coffey, Cox and Williams, 2014). Eventually, decreased FMD was identified in AVS (Poggianti et al., 2003) and AS patients (Chenevard et al., 2006, Horn et al., 2014). These studies suggest that turbulences might be co-responsible for abnormal endothelial function. In a recent study, it was shown that the improvement of FMD in AS patients correlates with endothelial integrity after aortic valve replacement (Horn et al., 2014). Nevertheless, the inconsistency of previous data regarding decreased NO bioavailability determining decreased FMD and AS emphasizes the importance of further research. Moreover, previous research has not taken into account whether NO reduction in AS is caused by turbulent blood flow conditions with regards to blood cell properties. The high transvalvular velocities in AS result in turbulent, disturbed flow patterns in the ascending aorta, with eccentrically elevated shear stress (Garcia et al., 2019; von Knobelsdorff-Brenkenhoff et al., 2016). RBC membrane damage occurs when shear stress exceeds a specific magnitude (Baskurt, 2012). As a consequence, morphological changes or membrane damage leads to hemolysis and the release of cell-free hemoglobin (Hb) (Baskurt, 2012). Recently, Vahidkhah et al. investigated in a multiscale approach the shear stress-induced damage to RBCs during high blood flow velocities in AS (Vahidkhah et al. , 2016). The study showed that increased shear stress levels are within the threshold range for membrane damage of RBCs. The authors concluded that RBC membrane damage is within the subhemolytic range in AS. Subhemolytic damage of RBCs is associated with a decrease in deformability, lifespan and release of RBC microparticles (Baskurt, 2012; Buerck et al., 2021). Intravascular hemolysis is a common, long-known condition in patients with prosthetic heart valves (Dasi et al., 2009; Mecozzi et al., 2002). Noteworthy, a few studies reported intravascular hemolysis in patients with native, moderate to severe AS (Jacobson et al., 1973; Sugiura et al., 2016; TSUJI et al., 2004).

However, the field of AS research had gradually broadened when animal models were employed to investigate disease progression. Most of these animal models are based on diet-induced AS or require genetic modifications (Sider et al., 2011). In a more recent study, Honda and colleague*s* published a new model of AS, based on wire-injury of the aortic valve, which was further modified in our lab (Honda et al., 2014; Niepmann et al., 2019).

1.6 The vasculature and blood vessel architecture

The vascular system represents the transport system within the body. It consists of the heart and highly branched tubular system, which supports transport function for blood carrying oxygen, carbon dioxide, nutrients and waste products within the body. This tubular system consists of arteries, arterioles, capillaries, veins and venules. Blood, rich in oxygen and nutrients, is pumped from the heart and transported via large arteries to tissues, where oxygen and nutrients are exchanged via small capillaries and venules. Deoxygenated, carbon dioxide-rich blood and metabolic waste products are transported back to the heart via the venous system.

Blood vessels are characterized by a distinct morphological architecture adapted to their mechanical and functional requirements within the vascular system (Chi et al., 2003). The general structure of a blood vessel features the three distinct layers tunica intima, tunica media, and tunica externa. The arterial endothelium is composed of a continuous monolayer of ECs that covers the entire surface of the vessel. Together with connective tissue, the internal elastic membranes and the endothelium represent the tunica intima of the vessel wall. ECs feature a great heterogeneity within their location in the vasculature and organs (Chi et al., 2003). The endothelium is classified according to the differences in intercellular junctions into a continuous, fenestrated and discontinuous type (Aird, 2007). The arterial endothelium is composed of continuous ECs connected via tight junctions. Fenestrated endothelium is characterized by transcellular pores covered with a diaphragm and found in tissues with high transcellular transport, e.g. endocrine glands, kidney glomeruli. The discontinuous endothelium of sinusoidal ECs of the liver features large fenestrae and a discontinuous basement membrane (Aird, 2012).

The underlying tunica media is composed of VSMCs, connective and elastic tissues. VSMCs represent the major cellular constituents of the vessel wall and determine the vessel's mechanical properties and vascular tone by actively dilating or constricting in response to

various biochemical stimuli. The amount of VSMCs layers varies depending on the function of the vessel wall. Similar to ECs, VSMCs exhibit great heterogeneity within the vasculature. Pathological states, including hypertension, provoke hypertrophic remodeling of VSMCs, resulting in an increased media thickness and reduction in lumen diameter. In contrast, inward eutrophic remodeling is associated with a decrease in lumen diameter and outer diameter and with unaltered media thickness (Laurent and Boutouyrie, 2015; Intengan and Schiffrin, 2000). In conducting arteries, like the aorta, the tunica media is composed of multiple layers of VSMCs with great elastic content related to its windkessel function. Muscular distributing arteries, e.g. femoral or brachial artery, are distinguished by a high ratio of VSMCs and less elastin. This accounts for the high capability of muscular arteries to dilate and constrict according to the peripheral blood requirements. Resistance arteries represent a network of small, peripheral arteries composed of a thin layer of VSMCs and ECs. They lack the external lamina and are encased by pericytes to stabilize the vessel and allow transendothelial transport. Resistance arteries are the primary regulator of blood flow and the key contributors of vascular resistance. The third, most outer layer is the tunica externa. This layer is composed of connective fibers connected to the tunica media via an external elastic lamina. This layer anchors the vessel within the tissue.

1.7 Endothelial cell signaling

The pivotal role of the endothelium is to control vascular tone by balancing the release of vasoactive substances in response to different stimuli. The first vasoactive substance to be identified was prostacyclin (PGI_2) (S Moncada et al., 1976). PGI_2 is a product of arachidonic acid metabolism and synthesized by PGI_2 synthase, which is highly expressed in ECs and also possesses a distinct anti-thrombotic function (Moncada and Higgs, 1977; Frangos et al., 1983). PGI_2 induces vasodilation through its binding on the PGI_2 receptor (IP) on VSMCs. This mediates the increase in cyclic adenosine monophosphate (cAMP) by converting adenosine triphosphate (ATP) via the enzyme adenylyl cyclase to induce vasodilation. As mentioned in the previous section, the second major vasoactive compound identified was NO, which is constitutively produced from substrate L-arginine (Palmer and Moncada, 1989). NO diffuses to underlying smooth muscle cells and activates soluble guanylate cyclase (Palacios et al., 1989). The existence of another critical relaxing factor has been extensively studied. Despite the inhibition of NO and prostaglandin production, persistent vasodilation was observed, which involves endothelium-dependent hyperpolarization of

VSMCs (Feletou & Vanhoutte, 1988; Garland & McPherson, 1992; Nagao & Vanhoutte, 1992). Initially, it was named the endothelium-derived hyperpolarization factor (EDHF) as its chemical nature was not clearly identified (Busse et al., 2002). EDHF primarily contributes to vasodilation in muscular and resistant arteries through hyperpolarization of the VSMCs (Luksha et al., 2009).

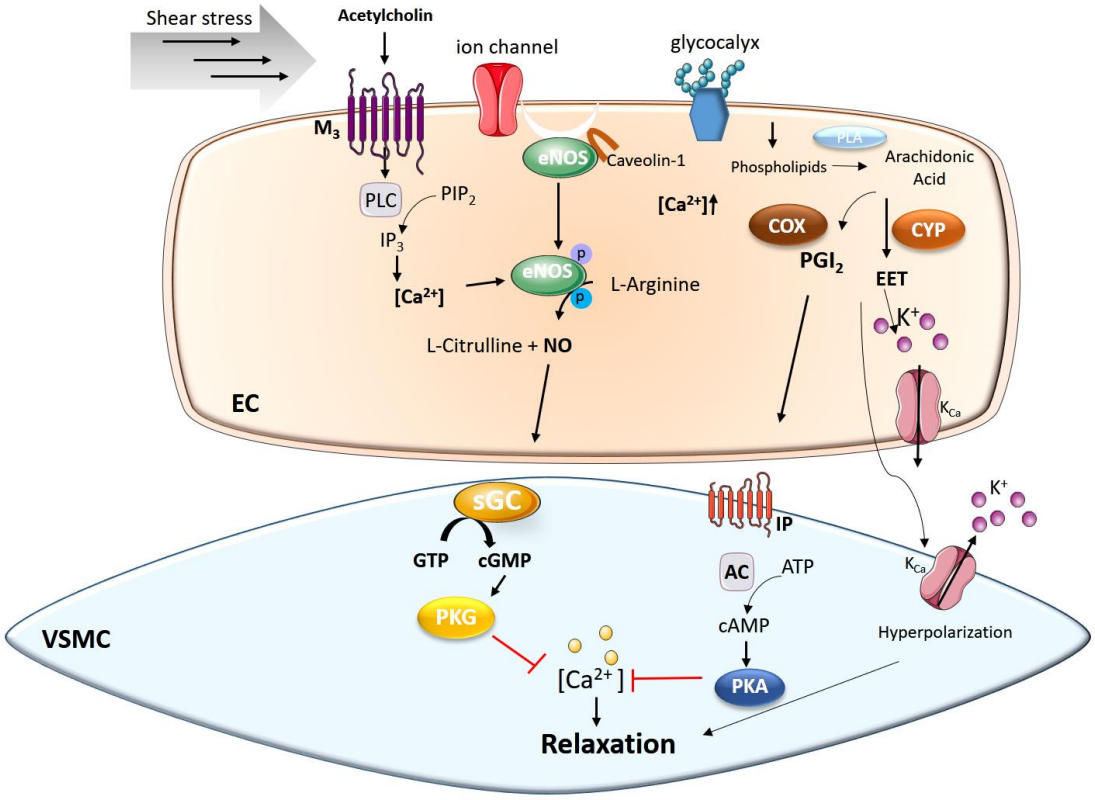

Figure 1 Intracellular mechanisms involved in endothelium-dependent vasodilation
Mechanosensitive structures (e.g., glycocalyx, ion channels) transduce the force generated by the streaming blood into a biochemical signal and cause the intracellular increase in calcium (Ca^{2+}) concentration. This increase in Ca^{2+} induces the synthesis of nitric oxide (NO) from substrate L-arginine by endothelial nitric oxide synthase (eNOS) in a calmodulin (CaM) dependent manner. Agonists induce NO production, e.g. through binding of acetylcholine to muscarinic M3 receptor, which induces cleavage of phosphatidylinositol 4,5-bisphosphate (PIP_2) by phospholipase C (PLC) to inositol 1,4,5-trisphosphate (IP_3), which finally increase Ca^{2+} concentration. NO diffuses to the vascular smooth muscle cell (VSMC), where it binds to the heme moiety of soluble guanylate cyclase (sGC), which catalyzes the dephosphorylation of guanosine-5'-triphosphate (GTP) to 3'5'-cyclic guanosine monophosphate (cGMP). cGMP, in turn, stimulates protein kinase G to inhibit Ca^{2+} release and influx. All of these mechanisms induce the relaxation of VSMCs. In addition, endothelial increase in Ca^{2+} stimulates the production of prostacyclin (PGI_2), epoxyeicosatrienoic acids (EET), and other prostanoids by cyclooxygenase (COX) or cytochrome P450 (CYP), respectively. PGI_2 induces VSMC relaxation by receptor-induced inhibition of Ca^{2+}. EET activates Ca^{2+}-activated potassium channels in the VSMC, which induce hyperpolarization.

1.8 The endothelial nitric oxide synthase

The free radical NO is produced by three different isoforms of NO synthases (NOS). The neuronal NOS (nNOS), the inducible NOS (iNOS), and the endothelial NOS (eNOS) (Knowles & Moncada, 1994). Endothelial NO synthase is the most abundant in the endothelium (Förstermann et al., 1994). NO synthase-dependent conversion of L-arginine to L-citrulline and NO is depicted in Figure 2. The endothelial NO enzyme is a homodimer, consisting of an N-terminal oxygenase domain linked via a regulatory calmodulin-binding domain and zinc to the C- terminal reductase domain. The oxygenase domain has binding sites for the substrate L-arginine, heme, and cofactor tetrahydrobiopterin (BH4) (Raman et al., 1998). The reductase domain binds the cofactors nicotinamide adenine dinucleotide phosphate (NADPH), flavin mononucleotide (FMN), flavin adenine dinucleotide (FAD) and calmodulin (CaM). For NO synthesis, the electron transfer by flavins, originated from NADPH to the heme iron in the oxygenase domain is required for binding and reduction of oxygen. The synthesis is calmodulin dependent (Bredt & Snyder, 1990; M. Zhang & Vogel, 1994). Oxygen reacts with the guanidine group of L-arginine to form the intermediate N^{ω} –hydroxy-L-arginine, from which NO is finally released (Stuehr et al., 1991).

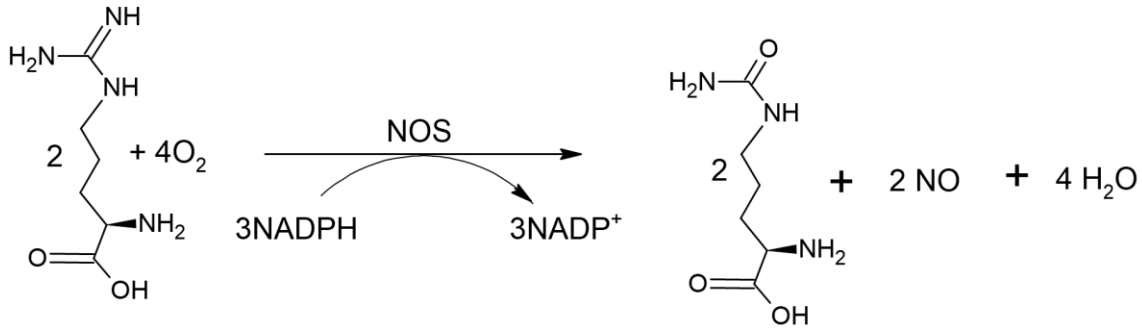

Figure 2 Chemical equation of nitric oxide synthesis

The consequences of lack of endothelial NO synthase were intensively studied in eNOS knock-out mice (Huang et al., 1995; Shesely et al., 1996; Gödecke et al., 1998; Kuhlencordt et al., 2001; Cook et al., 2004). The deficiency of eNOS phenotypically resulted in increased blood pressure and decreased heart rate (Huang et al., 1995). Noteworthy, spontaneous AS was observed in eNOS KO mice in an age-dependent matter (El Accaoui et al., 2014).

1.9 Regulation of eNOS activity

Endothelium-dependent NO release by eNOS depends on both mechanical and chemical stimuli. One of the most important stimuli for NOS activation is shear stress generated by the pulsatile flow of blood (Davies, 1995). The pivotal role of endothelium-dependent flow-mediated vasodilation response was known even before discovering NO as a relaxing factor (Rubanyi et al., 1986). Disturbed flow and low shear stress are associated with an altered eNOS expression and endothelial dysfunction (Balligand et al., 2009). The arterial branches and curvatures are typically characterized by disturbed flow and low shear stress. Thus, they are the first site of arteriosclerotic lesion formation in the vasculature (Asakura & Karino, 1990; Zarins et al., 1983). In contrast, laminar flow with high shear stress was demonstrated to exert protective effects on the endothelium, explaining less development of arteriosclerotic lesions in straight arterial regions (Chiu & Chien, 2011). Shear stress provokes eNOS activation in a calcium-dependent and calcium-independent manner, whereas the latter requires phosphorylation by kinases to maintain NO synthesis (Balligand et al., 2009; Fleming, 2010). Different endothelial cell-surface mechanosensors such as glycolalyx, G protein-coupled receptors (GPCR) or ion channels transduce the force generated by shear stress into a biochemical signal, thus enhancing eNOS activity by increasing intracellular calcium (Erkens et al., 2017). Membrane structures like caveolae represent invaginations of the plasma membrane and are essential for the control of eNOS localization (Ju et al., 1997). The increase in intracellular Ca^{2+} leads to the formation of a calcium-calmodulin complex, which binds to the binding site within the eNOS enzyme to link the oxygenase and reductase domain. This enables the electron flux from the reductase to the oxygen domain and enhances its activity (Fleming, 2010).

Moreover, shear stress-induced activation of cell surface proteins, junctional complexes and integrins involves posttranslational modification of kinases such as AKT1, PKA, PYK2 and others (Balligand et al., 2009). These phosphorylation sites include serine, threonine, or tyrosine residues and play a pivotal role in the activation of the enzyme (Fleming et al., 1998). While phosphorylation on threonine 495 attenuates the binding of calmodulin and consequently decreases the enzyme activity, phosphorylation on serine 1179 enhances the activity (Kolluru et al., 2010). The activation of PYK2 induces phosphorylation of tyrosine 657 and inhibits eNOS activity (Loot et al., 2009).

The activity of eNOS is strongly associated with the availability of cofactors and the substrate L-arginine. If substrate or cofactors are below the optimal concentrations, superoxide (O_2^-) can be generated instead of NO (Förstermann & Münzel, 2006). The substrate availability can be diminished due to enhanced activity of arginases, catalyzing the reaction of L-arginine to ornithine and urea (Shin et al., 2012). Increased enzymatic activity of arginases was observed in disease models of endothelial dysfunction, such as diabetes and ischemia-reperfusion (Hein et al., 2003). The other crucial cofactor essential for eNOS activity is tetrahydrobiopterin (BH_4). Reduced BH_4 levels were observed in disease states associated with enhanced oxidative stress in the vasculature, contributing to eNOS uncoupling. The uncoupling of eNOS results due to altered electron flux from the reductase domain to the oxygen domain, which is further associated with an oxidative decay favoring the generation of superoxide anion (O_2^-) (Siragusa & Fleming, 2016). Superoxide anion metabolism includes the formation of hydrogen peroxide (H_2O_2), hydroxyl radical ($\bullet HO^-$), and the reaction of O_2^- and NO to form peroxynitrite ($ONOO^-$), which diminishes NO availability. The production of $ONOO^-$ initiates a vicious circle in which BH_4 is further oxidized by $ONOO^-$, enhancing eNOS uncoupling.

1.10 The circulating NO pool

Apart from vasodilator effects, NO produced from endothelium and RBCs undergoes oxidation or nitrosylation into different bioactive metabolites, including nitrite (NO_2^-), nitrate (NO_3^-), nitrosated thiols (RSNO), or nitrosated amines (RNNO) (Kelm, 1999; Kleinbongard et al., 2003; Rassaf et al., 2002). This facilitates the transport of NO to different tissues throughout the body where NO production is altered (Lundberg et al., 2008). Moreover, RBCs were identified to contain a functional NO synthase and represent part of the circulating NO pool (Cortese-Krott *et al.*, 2012; Wood *et al.*, 2013, Cortese-Krott and Kelm, 2014). Under hypoxia or acidic conditions, the bioactive NO metabolites contribute to the eNOS-independent release of NO through chemical reduction by heme-containing proteins with nitrite reductase activity (Cosby et al., 2003; Gladwin et al., 2006; Rassaf et al., 2007; Zweier et al., 1995). Thus, NO possesses a critical endocrine function (Bryan et al., 2005) and eNOS-independent NO generation plays an essential role in physiological NO signaling (Amdahl et al., 2019). Importantly, in patients with endothelial dysfunction, levels of circulating NO metabolites are decreased (Heiss et al., 2006; Kleinbongard et al., 2006; Rassaf et al., 2006).

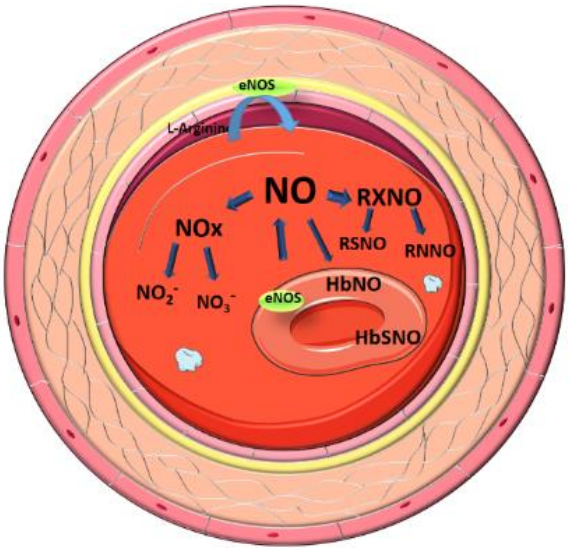

Figure 3 Endothelium-derived nitric oxide and red blood cell-derived nitric oxide contributes to the circulating nitric oxide pool.
Nitric oxide (NO) metabolites comprise nitrite (NO^{2-}), nitrate (NO^{3-}) and nitrosylated proteins (RXNO). The NO formation from these bioactive substances happens in dependency of the surrounding oxygen concentration via heme-containing proteins. Under normoxic conditions, NO is synthesized by the endothelial NO synthase (eNOS) in endothelial cells and can be oxidized to different bioactive metabolites, representing the NO storage pool. HbNO: nitrosated hemoglobin, HbSNO: S-nitroso hemoglobin.

1.11 Nitric oxide scavenging by cell-free hemoglobin

Over time, extensive literature has developed on the role of cell-free Hb on NO metabolism. Under physiological conditions, the highest Hb concentration is compartmentalized within the red blood cells (RBCs). Hb is a protein complex composed of four globin subunits, whereas each subunit comprises one heme, the oxygen-binding iron complex, based on a porphyrin structure (Perutz, 1978). This structure allows for the protein to meet its primary function as an oxygen transporter. The human Hb is composed of two α- and two β-globin chains, enabling the protein to bind four oxygen molecules simultaneously. In this heme group, iron is coordinated with four nitrogen atoms of the histidine originated imidazole rings within a planar complex (Perutz et al., 1998). Hence, the protein can undergo a conformational change from the tensed state to the relaxed state to facilitate further oxygen-binding (Monod Jacquez et al. 1965). The compartmentalization of Hb in the RBC limits the reaction of NO with oxyHb by approximately 600-fold (Liu et al., 1998). This limitation is attributed to a diffusional resistance created by the RBC-free zone generated by the flow, the unstirred layer around the RBCs and the RBC membrane (Vaughn *et al.*, 1998, 2000; Kavdia and Kavdia, 2013). When hemolysis occurs, cell-free Hb is released to the plasma and exists in an equilibrium of tetrameric and dimeric form. In the absence of diffusional barriers due to decompartmentalization, cell-free Hb rapidly reacts with NO to form methemoglobin and NO_3^-. Moreover, the smaller molecule size of the heterodimers enables the protein translocation from the vascular lumen in the subendothelial space, which leads to further NO depletion and oxidation, allowing accumulation of ferric Hb (Fe^{3+}) in the vascular wall (C. A. Schaer et al., 2016). Under these conditions, heme is likely to be released from Hb and can interact with lipids, which trigger a lipid-peroxidation cascade and contribute to Hb toxicity. With this regard, another scavenging molecule plays an important role, i.e., Hemopexin (Hx). Hx scavenges heme and prevents heme-induced damage on the endothelium (D. J. Schaer et al., 2014). The physiological binding protein of cell-free Hb in plasma is haptoglobin (Hp). Hp is a sensitive marker for hemolysis as its depletion is associated with acute or chronic hemolytic conditions. Hp is composed of two α- and two β-chains. The crosslinking of the α-subunit defines one of the three Hp phenotypes, such as dimeric or multimeric Hp (Hp 1-1, 1-2, 2-2) (Langlois & Delanghe, 1996). The irreversible binding of the Hp β-subunit and the β-hemoglobin dimer occur in a 1-1 stoichiometry (Lim et al., 2001). The complex is cleared from the circulation via receptor CD163 on

macrophages, which is highly expressed on macrophages of the spleen and liver Kupffer cells (Kristiansen et al., 2001). If the scavenging system gets exhausted during massive hemolysis, cell-free Hb can exert its toxic effects, as mentioned in the previous section. Recent studies investigated the potential benefits of Hp in preventing cell-free Hb-induced vasoconstriction by NO scavenging (Hugelshofer et al., 2019).

In disease states like sickle cell disease, higher amounts of cell-free Hb are released into the plasma. During a hemolytic crisis, complications such as pulmonary hypertension and ischemia were attributed to NO depletion by cell-free Hb (Reiter et al., 2002).

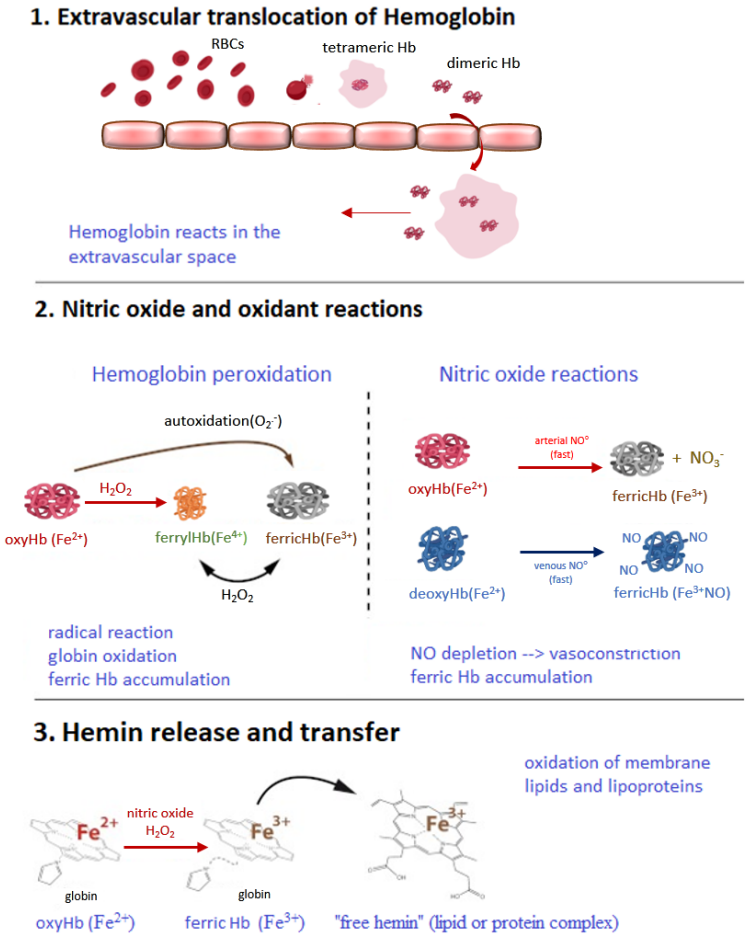

Figure 4 Mechanisms involved in cell-free hemoglobin-driven toxicity
The mechanism driving cell-free hemoglobin (Hb) toxicity comprise 1.) translocation of dimeric Hb in the subendothelial space. 2.) Oxidant and nitric oxide (NO) reactions: NO consumption by Hb under the formation of ferric Hb and nitrate (NO_3^-), iron nitrosylation of deoxyhemoglobin (deoxyHb) and Hb peroxidation reactivity with physiological oxidants. 3.) Accumulation of ferric Hb can promote the release of hemin and its transfer to plasma proteins and lipids to build hemin protein/lipid complexes, contributing to vascular injury. This illustration was adapted from Schaer et al., (2013).

2 Aim of the study

AS leads to complex changes in flow patterns in the ascending aorta. The hemodynamic consequences of AS are no longer assumed to be limited to the valve but were also shown to affect various compartments, including RBCs, the myocardium, and the vascular system. This becomes obvious when several studies identified endothelial dysfunction in patients with AS. However, the underlying mechanisms causing endothelial dysfunction in patients with AS are still incompletely understood. To date, no animal model of AS investigated the systemic consequences of AS on vascular endothelial and RBCs' functional properties. Therefore, the present work hypothesized that the turbulent blood flow in AS might induce endothelial dysfunction as a consequence of mechanical damage to RBCs, which induces the release of hemoglobin and results in a reduction of NO bioavailability.

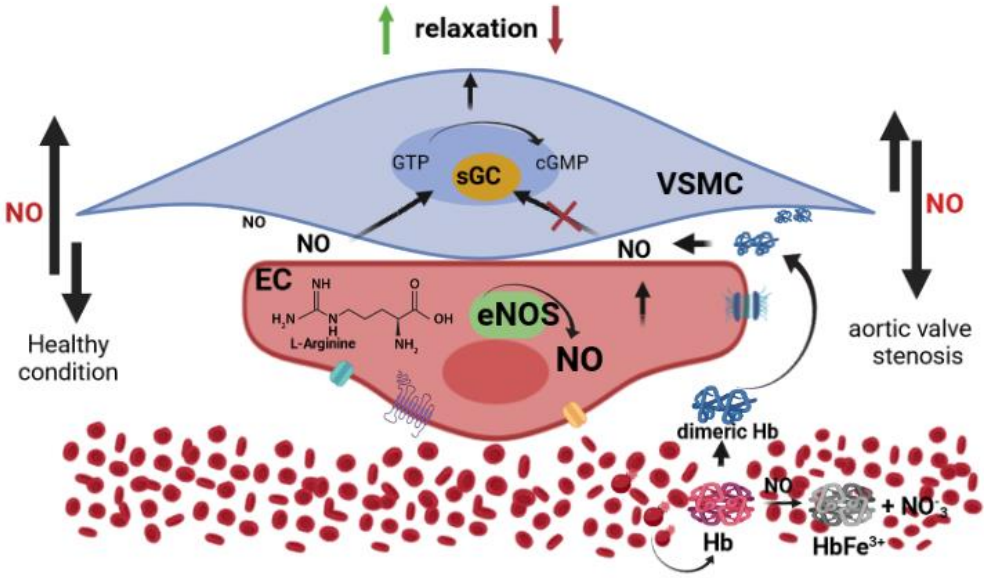

Figure 5 Graphical abstract
In healthy conditions, NO is synthesized by endothelial nitric oxide synthase (eNOS) in endothelial cells (EC). NO diffuses to vascular smooth muscle cells (VSMC), binds to the heme moiety of soluble guanylate cyclase (sGC), which induce VSMCs relaxation (green arrow) via the dephosphorylation of guanosine-5'-triphosphate (GTP) to 3'5'-cyclic guanosine monophosphate (cGMP). In the present study we hypothesized that endothelial dysfunction in aortic valve stenosis (AS) is attributable to turbulent blood flow induced red blood cell membrane damage, which may lead to the release of hemoglobin (Hb). Cell-free Hb scavenge NO, thus limits its ability to induce VSMCs relaxation (red arrow).

For this purpose, the following aspects were analyzed:

1. The first aim of this study was to perform a comprehensive characterization of the modified wire-injury model of AS regarding transvalvular blood flow, left ventricular and aortic valve morphological, and functional adaptions. Therefore, the model was validated by echocardiography, magnetic resonance imaging (MRI), and histology. As an additional attempt, the role of global eNOS deficiency in the progression of AS was investigated.

2. To investigate RBCs integrity and alterations in functional properties due to potential mechanical trauma resulting from turbulent flow, blood analysis was performed four weeks after induction of AS. For this purpose, blood count, levels of cell-free Hb and RBCs exposure of phosphatidylserine were analyzed. RBC membrane stability properties was evaluated as a function of deformability. To assess potential RBC damage and cell-free Hb release affecting NO metabolism by NO scavenging, NO metabolites were quantified by chemiluminescence and HPLC-based approach.

3. The third aim of the present work was to evaluate the effects of AS on vascular endothelial functional properties. For this purpose, endothelial function was assessed *in vivo* by FMD studies in the femoral artery, whereas vascular reactivity studies were conducted to evaluate endothelium-dependent and endothelium-independent relaxation in isolated segments of the thoracic aorta and femoral arteries.

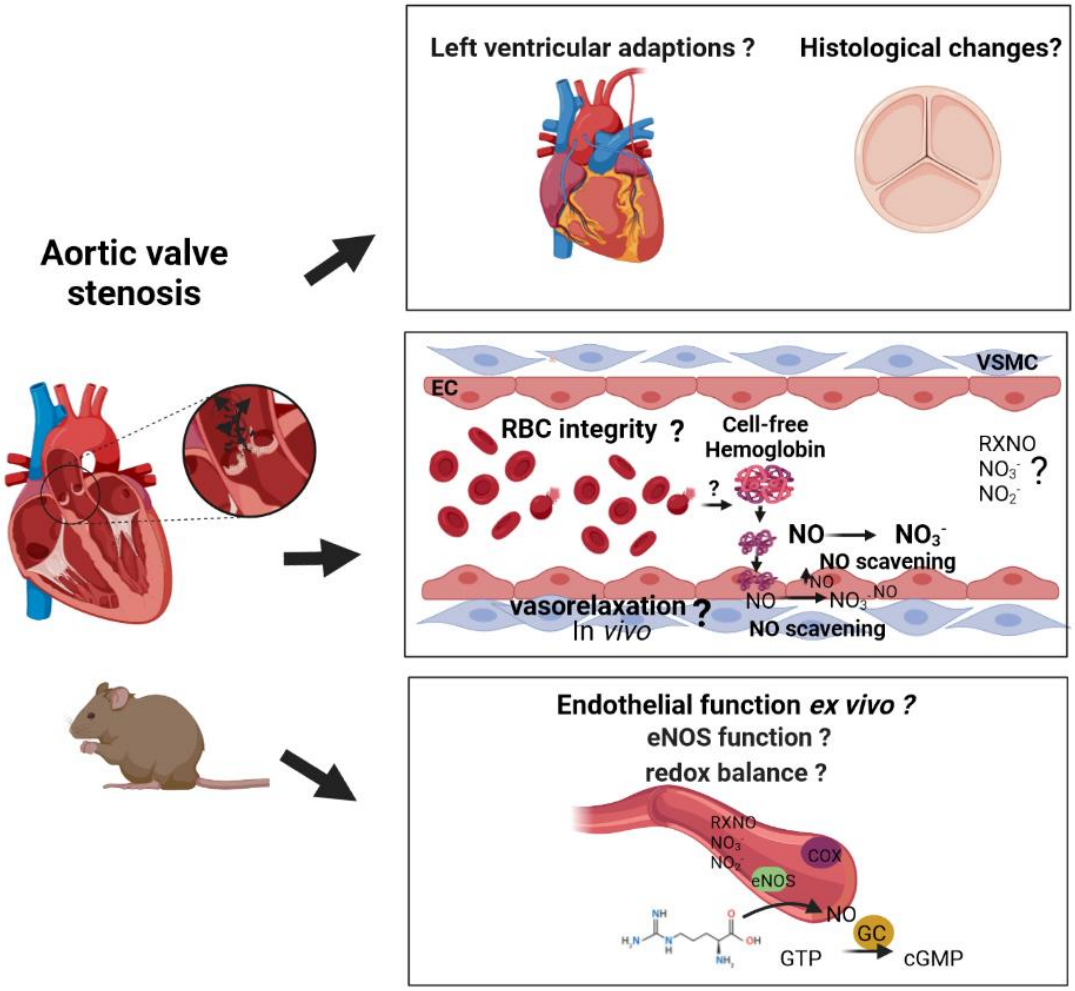

Figure 6 Overview aims

The aim of this study was to investigate the local and systemic consequences of aortic valve stenosis (AS) in our experimental model, which based on wire injury of the aortic valve. The following aims were investigated: 1.) Left ventricular function adaptions and valvular morphological changes in response to the wire- injury 2.) The effects of turbulent blood flow on red blood cell integrity, cell-free Hb release and consequences for NO metabolism. 3.) The effects of AS on vascular endothelial function, eNOS function and redox status in aorta and femoral artery. COX: cyclooxygenase, cGMP: cyclic guanosine monophosphate, EC: endothelial cell, eNOS: endothelial nitric oxide synthase, GC: guanylate cyclase, GTP: guanosine triphosphate, Hb: hemoglobin, NO: nitric oxide, RXNO: sum of nitrosothiols and nitrosoamines, VSMC: vascular smooth muscle cell.

3 Materials and Methods

3.1 Chemicals and Solution

All chemicals were purchased from Sigma-Aldrich (St. Louis, USA), Carl Roth GmbH (Karlsruhe, Germany), or Merck (Darmstadt, Germany) in the highest available purity if not stated differently. Solutions and buffers were prepared with distilled water or ultrapure water from the MilliQ® Reference water purification system (Merck, Darmstadt, Germany). Dulbeccos's phosphate Buffered Saline (DPBS) was purchased from Sigma Aldrich (St. Louis, USA).

3.2 Animal characteristics

All animal studies were approved by "Landesamt für Natur, Umwelt- und Verbraucherschutz" (LANUV) of Northrhine-Westfalia under the file numbers 84-02.04.2017.A172 and 032/19 in accordance with the animal welfare regulation. Male C57BL6 mice, aged 11-12 weeks, were purchased from Janvier Labs (Le Genest- Saint- Isle, France). Additional studies were performed on global eNOS KO mice, which were developed by Professor Axel Gödecke (Heinrich Heine University, Düsseldorf). All animals were housed in the central facility premises for animal research and scientific animal protection tasks (ZETT) at Heinrich Heine University. The mice were housed in standard cages at constant room temperature and humidity, with 12 hours light-12 hours dark cycle. The animals were fed a standard chow diet and tap water ad libitum.

3.3 In vivo studies

The following working program was performed to investigate the effects of experimental AS on vascular, myocardial, and RBC function:

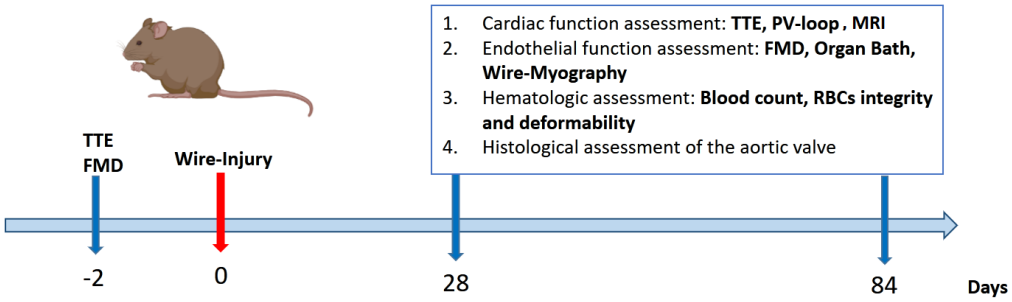

Figure 7 Work program
The work program comprised analysis of cardiac and endothelial function, as well as hematological assessment in mice with aortic valve stenosis (AS) induced by wire-injury of the aortic valve. These analyses were performed under baseline conditions and followed up after 28 or 84 days, respectively. Additionally, magnetic resonance imaging was performed after 28 days. FMD: Flow-mediated dilation, PV: pressure-volume, RBCs: red blood cells, TTE: transthoracic echocardiograph.

3.3.1 Wire- injury model of aortic valve stenosis

We used the wire-injury model of AS (Honda et al. 2014), which was further modified in our lab (Niepmann et al., 2019). Briefly, to induce AS, the mice were anesthetized by intraperitoneal injection with ketamine (Ketaset® Zoetis, Germany) (100 mg/kg body weight) and xylazine (Rompun® Serumwerk Bernburg AG, Germany) (10 mg/kg body weight). After intubation using an indwelling cannula (Vasofix® Safety 20 G, B. Braun Se, Germany), the animal was fixed in a supine position on an operating table preheated to 37 °C. Anesthesia was maintained via a respirator with a mixture of 1.5 % isoflurane (Piramal® Critical Care, India) with oxygen-enriched room air. After the fur was removed using hair removal cream (Veet, Reckitt Benckiser, Germany), a 1 cm skin incision was made in the medial neck area to expose the right common carotid artery. The common carotid artery was temporarily ligated with a hemostat (Micro Clamp, No.3, S&T® AG, Switzerland) and wrapped proximally with a silk thread. The artery was then incised to insert a prepared wire (High-torgue, Universal, 0.014mm, Abbot Laboratories, USA) into the vessel. The hemostat was removed to facilitate pushing the wire into the LV retrogradely. To ensure the correct position of the wire, the whole procedure was performed under echocardiographic control (parasternal long-axis view). By pushing the wire back and forth in a defined manner (50x), followed by rotating (100x), the valve endothelium was manipulated. The wire was removed, and the common carotid artery was immediately ligated with the previously positioned silk thread. Immediately after the procedure, color Doppler was used to verify intact valve function. Afterwards, anesthesia was slowly reduced,

and the animal was extubated as soon as reflexes were detectable. Analgesia was provided by subcutaneous injection of buprenorphine (0.05 mg/kg body weight). Mice underwent sham surgery were carried out to the same protocol, while the wire was only inserted into the carotid artery but was not guided to the LV, and thus touching of the valve was prevented. The surgical procedures were performed by Kathrin Paul-Krahé and Katrin Becker.

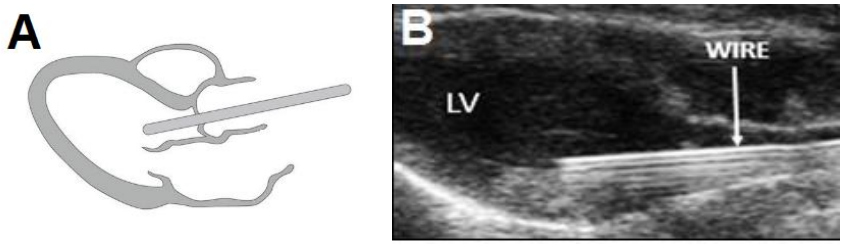

Figure 8 Parasternal long-axis view of the left ventricle during the surgical procedure of wire-injury.
(A) Scheme illustrating wire-induced AS. (B) The wire positioned in the left ventricle for aortic valve manipulation under echocardiographic AS: aortic valve stenosis, control. LV: left ventricle. The illustration was adapted from Niepmann et al., (2019).

3.3.2 Echocardiographic assessment

Cardiac function analysis was performed by high-resolution ultrasound (Vevo 3100 Preclinical Imaging System, Visual Sonics, Fujifilm, Japan) using the MS-400 transducer. Initially, the animals were anesthetized in an induction chamber with 3 % isoflurane (v/v) with oxygen-enriched room air. Next, animals were fixed in a supine position on the preheated examination table, and anesthesia was maintained through a respiratory mask (1.5 % (v/v) isoflurane). The fur was removed from the thorax up to the upper part of the abdomen with hair removal cream (Veet, Reckitt Benckiser, United Kingdom). During the entire examination, respiration, body temperature, and an electrocardiogram were continuously recorded. The following examination protocol was employed: 1.) Suprasternal position to visualize aorta ascendens with the aortic valve. Pulse wave Doppler was used to image and quantify flow profiles with eligible angle correction 2.) Parasternal long and short axis in B-mode and M-mode to visualize tissue movement 3.) Apical four-chamber view to assess diastolic function including tissue Doppler recordings of the medial and lateral mitral annulus 4.) Left lateral view of the aortic valve in the long and short axis in B-mode, M-Mode, and color Doppler. Data analysis was carried out with Vevo Lab software (Visual Sonics, Fujifilm, Japan).

Software calculations derived from the LV-Trace tool for left ventricular function analysis are summarized in Table 1 and were performed in parasternal long-axis view. Left ventricular diameter and interventricular septum thickness were measured from M-Mode at the end of diastole. Early passive (E-wave) and late active filling (A-wave) profiles were quantified for diastolic function analysis.

Table 1 Left ventricular function assessment was performed using the Vevo Lab LV-Trace tool.

Parameter	Calculation
Ejection fraction [%]	EF=100*((LV Volume$_{Diastole}$-LV Volume$_{Systole}$)/LV$_{Diastole}$)
Cardiac Output [ml/min]	CO=HR* SV
Fractional shortening [%]	FS=100 * ((LVID;d – LVID;s) / LVID;d)
Stroke volume [µL]	SV= EDV- ESV
Leftventricular volume, diastole	LV,d= ((7.0 /(2.4 +LVID,s) * LVIDS, d^3)
Left ventricular volume, systole	LV,s= ((7.0 /(2.4 +LVID,s) * LVIDS, s^3)

3.3.3 Magnetic resonance imaging

For a comprehensive analysis of AS in the described model, MRI was performed by Prof. Ulrich Flögel in collaboration with the department of molecular cardiology. "*Data were recorded at a Bruker AVANCE^{III} 9.4T wide bore NMR spectrometer driven by ParaVision 5.1 (Bruker, Rheinstetten, Germany). Mice were anesthetized with 1.5 % isoflurane and kept at 37°C. The front paws and the left hind paw were attached to ECG electrodes (Klear-Trace; CAS Medical Systems, Branford), and respiration was monitored employing a pneumatic pillow positioned at the animal's back. Vital functions were acquired by an M1025 system (S.A. Instruments, Stony Brook, NY, USA) and used to synchronize data acquisition with cardiac and respiratory motion.* All mice were imaged four weeks after induction of AS. *For functional and morphometric analysis, high-resolution images of mouse hearts were acquired in short-axis orientation using an ECG- and respiratory-gated segmented cine fast gradient echo cine sequence with steady-state precession (FISP). Eight to ten contiguous slices were acquired to cover the entire heart. Routinely, 8-10 short axis slices were required for complete coverage of the left ventricle. For evaluation of functional parameters (e.g., EDV, ESV, EF.), ventricular demarcations in end-diastole and -systole were manually drawn with the ParaVision Region-of-Interest (ROI) tool (Bruker, Rheinstetten, Germany), which was also used for determination of the aortic indices described below. For analysis of the aortic valve, strain, and wall thickness, high-resolution*

cine loops were acquired at the atrio-ventricular level with the same parameters given above. Aortic valve opening was calculated from the maximal opening area in early systole related to the aorta's inner diameter in the end-diastole. Mean aortic wall thickness was estimated from planimetry of the vessel wall's inner- and outer borders in end-diastole. Here, both inner and outer areas were approximated by circles, and the difference between the two radii provides an averaged wall thickness of the aorta. Longitudinal slices orientated perpendicular to the atrio-ventricular level served to approximate the valve thickness by division of valve area and diameter of the aortic root. Aortic flow profiles were obtained by acquisition of velocity maps at the atrio-ventricular level. Flow profiles were analyzed by a software module developed in-house based on LabVIEW (National Instruments, Austin, TX), and 3D color map surface plots were generated with OriginPro (Originlab Corporation, Wellesley Hills, MA). Cardiac tissue characterization was carried out by T1 and T2 mapping. Besides global cardiac function, we also analyzed all data for regional alterations based on a midventricular slice to address adaptive local processes after induction of AS. To this end, we used an in-house developed software module based on LabVIEW (National Instruments, Austin, TX), which divided the left ventricle systematically into 200 equivalent sectors starting from the upper insertion point of the right ventricle as previously described (Bönner et al., 2014; Haberkorn et al., 2017)*."*

3.3.4 Flow-mediated dilation of the femoral artery

FMD is a non-invasive, ultrasound-based technique to measure endothelium-mediated vascular relaxation *in vivo*. Initially, the animal was anesthetized and fixed on the warmed examination table as described in 1.2. After fur removal of the left hind limb, a vascular occluder (5 mm, Harvard apparatus, USA) was positioned around the left hind limb, distal to the transducer. Femoral artery was visualized with the help of the MS-700 transducer of the Vevo 3100 Imaging System with manual adjustment of the transducer, ensuring proper imaging of the vessel wall in B-mode. Femoral arterial blood flow was verified by pulse wave Doppler at baseline. The cuff was then inflated to supra systolic pressure (250 mmHg), causing temporary occlusion of the vessel. The temporary flow arrest, was ensured by the abrogation of pulse wave Doppler signal. After five minutes of hind limb occlusion, the pressure was released to initiate a five-minute reperfusion phase. Images were taken at baseline and every 30 seconds in B-mode and pulse wave Doppler-mode.

The experimental setup is illustrated in Figure 9. To identify the extent of eNOS-dependent dilation in FMD studies, AS mice were subjected to intraperitoneal injection of eNOS inhibitor N^G-nitro-L-arginine methyl ester (L-NAME, 50 mg/kg body weight, sigma-aldrich, USA) in an additional experiment. The analysis was carried out with the software Brachial Analyzer for Research (Medical Imaging Applications, LLC, USA). Figures 4, 5, 6, 9 were created with biorender.com.

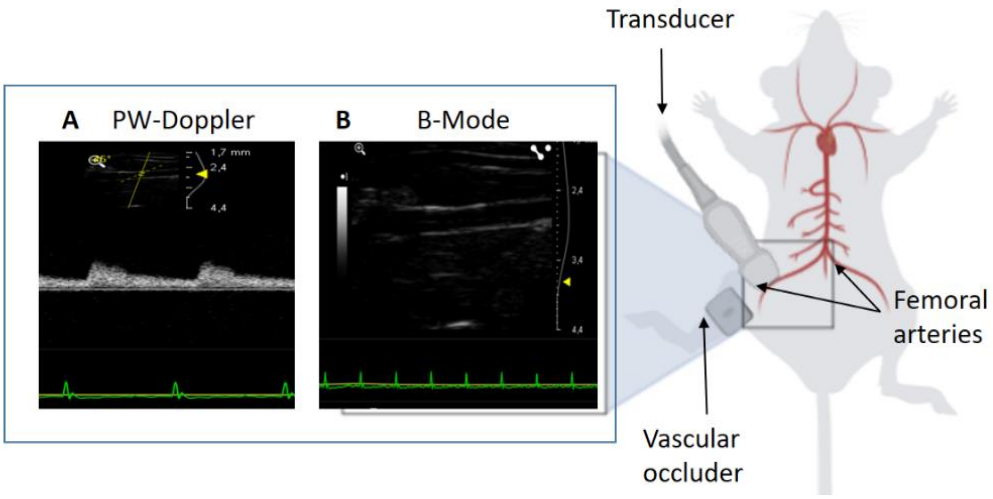

Figure 9 Illustration of Flow-mediated dilation in femoral artery measured by ultrasound
(A) Representative pulsed wave (PW) Doppler image of femoral arterial blood flow after cuff release (B) B-Mode image of femoral artery diameter after cuff release.

3.3.5 Flow-mediated dilation and haptoglobin administration

To test the effect of cell-free Hb scavenging by Hp, we administered haptoglobin during FMD measurement and assessed the potential regain of VSMCs relaxation response. Intravenous injection of Hp (phenotype 1-1, 40 µM/kg body weight, sigma-aldrich, USA) or vehicle was performed one minute before the start of the reperfusion phase, and FMD measurements were performed as described in 3.3.4. Hp solution was prepared in saline as a vehicle. Data analysis and diameter calculations were also performed as described above.

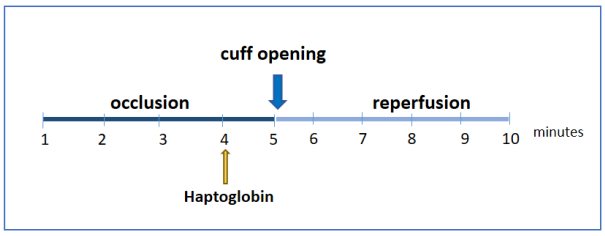

Figure 10 Representation of the time course of haptoglobin administration during flow-mediated dilation studies

3.3.6 Pulse wave velocity

Pulse wave velocity (PWV) was used to assess arterial vessel stiffness. The measurements were performed in accordance with an established protocol in our lab (Erkens et al., 2015). Briefly, the common carotid artery was visualized in the longitudinal section (B-mode). M-mode sequences were recorded in proximal and distal areas of the artery. The pulse wave velocity was calculated by determining the distance between the two measuring points and the time from the beginning of the R-wave of the ECG signal to the maximum diameter of the vessel wall at the end of the systole. PWV was calculated using the following formula:

Equation 1 Calculation of Pulse wave velocity:

$$PWV = \frac{distance\ \frac{T1}{T2}[mm]}{T\ distal[ms] - T\ proximal[ms]}$$

3.3.7 Pressure- volume loop measurements

Left ventricular pressure-volume relationship was carried out by catheterizing the LV by Millar catheter (1.2 F, and 4.5 mm electrode spacing, Transonic Systems Inc., USA). This technique enables simultaneous recording of left ventricular volume and pressure in real-time in an open-chest approach. Initially, thirty minutes before the procedure, analgesia was administered by subcutaneous injection of buprenorphine (0.1 mg/kg body weight). The animal was intubated with isoflurane inhalation and fixed in a supine position on the surgical table. Anesthesia was maintained by a murine respirator (micro ventilator, UNO, the Netherlands) with 2 % isoflurane (v/v) with oxygen-enriched room air. After ensuring the absence of pedal reflex, a lateral incision along the anterior axillary line was performed to expose the diaphragm. The diaphragm was cut with microscissors to expose the apex. With a 25 G cannula, the apex was punctured, and the catheter was inserted into the LV. When the signal was stable, pressure-volume loops were recorded for five minutes (Lab Chart 7, A.D. Instruments, New Zealand).

3.3.8 Blood pressure measurement

In order to measure blood pressure, animals were anesthetized as described in the previous section. After fixation on the surgical table, the common carotid artery was exposed by blunt dissection followed by temporary ligation of the vessel with a hemostat. After incision of the vessel, the catheter (SPR-829 Mikro-Tip® Millar, USA) was carefully inserted into the vessel by removing the hemostat simultaneously. The pressure was recorded for five minutes using the Lab Chart software. For calculations of mean arterial pressure, end-diastolic and

end-systolic pressure was used (MAP=2xEDP-ESP/3). Systemic vascular resistance was estimated by the simplified equation SVR≈MAP/CO. The venous pressure was neglected, as it is usually very low. Blood pressure measurements were performed with the generous support of Stefanie Becher.

3.4 In vitro studies

3.4.1 Aortic ring assay

We examined isolated aortic rings of mice that underwent wire-injury in an organ bath experiment (Harvard Apparatus, Cambridge, USA). For this purpose, the animal was anesthetized by intraperitoneal injection of a mixture of xylazine (10 mg/kg body weight) and ketamine (100 mg/kg body weight). The thoracic aorta was excised, cleaned from surrounding adipose tissue, and transferred into a petri dish containing KREBS-Hensleit buffer (NaCl 118 mM, KH_2PO_4 4.4 mM, KCl 5 mM, $MgSO_4$ 1.2 mM, $CaCl_2$ 1.6 mM, $NaHCO_3$ 25 mM, glucose), aerated with carbogen (5 % CO_2 / 95 % O_2). Aortic rings (2mm sized segments) were mounted on a wire into prewarmed (37 °C), aerated, buffer-containing chambers of the organ bath (Figure 11). During the one-hour equilibration period, the vessel was passively stretched to 1 g. Concentration-response curves were conducted as follows. First, the contractile response to 80 mM potassium chloride was obtained, followed by a 20 minutes washing phase. Intact rings were further subjected to increasing concentrations of phenylephrine (0.1 nM-10 µM). When the contractions reached a plateau, endothelium-dependent relaxation was obtained by cumulative addition of acetylcholine (0.1 nM-10 µM). To determine the extent of the eNOS-dependent vasodilation, the vessel was incubated with L-NAME (100 µM) for 20 minutes, and the concentration-response curves to phenylephrine and acetylcholine were repeated. Following a washing step, endothelium-independent vasodilation was carried out by cumulative addition of sodium nitroprusside (0.01 nM-10 µM) to the phenylephrine pre-contracted aortic rings. The presence of cyclooxygenase (COX) inhibitor indomethacin (10 mM) is indicated in the corresponding dose-response curves. The purpose of indomethacin was to block eNOS-independent reactions to acetylcholine, which also induce vasodilation response in the underlying smooth muscle cells, e.g., COX products (PGI_2).

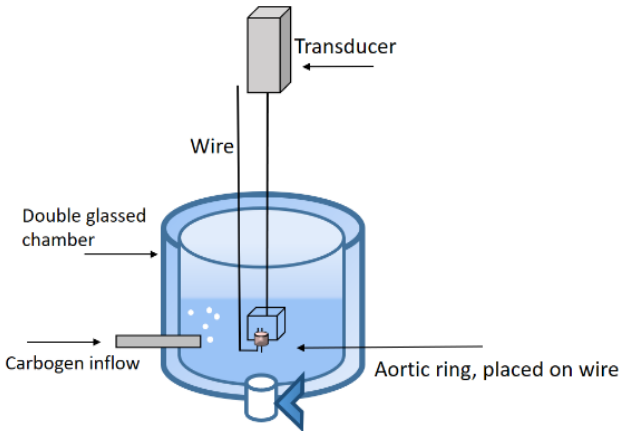

Figure 11 Schematic representation of aortic ring experiment

3.4.2 Myograph studies

The femoral artery was carefully dissected, freed from fat and surrounding connective tissue, and cut into 2 mm segments. For each mouse, two femoral arterial segments were mounted in the chambers of the Multi Myograph System, Model 620M (Danish Myo Technologies A/S, Hinnerup, Denmark). The chambers were filled with freshly prepared KREBS-Hensleit buffer (NaCl 118 mM, KH_2PO_4 4.4 mM, KCl 5 mM, $MgSO_4$ 1.2 mM, $CaCl_2$ 1.6 mM, $NaHCO_3$ 25 mM, glucose) and were continuously aerated with carbogen. The temperature of the chamber was maintained at 37 °C during the whole experiment. To ensure the integrity of the vascular endothelium, preparation and vessel mounting was performed under the microscope. Before starting each experiment, the segments were normalized using the DMT normalization module in the LabChart 8 software. The vascular function assessment was performed as described in 2.4.1.

3.4.3 Flow cytometry

The investigation of phosphatidylserine and CD71-expressing RBCs was performed by flow cytometry. Whole blood was diluted to 1:500, incubated with Annexin V (BD, cat# 51-65875X) and anti-CD71 antibody (Miltenyi Biotec, cat# 130-109-631) for 30 minutes in the dark. Flow cytometry was performed using BD FACS Verse Flow Cytometer (Becton Dickinson, USA).

3.4.4 Measurement of RBC deformability

The assessment of RBC deformability was performed using the laser optical rotational cell analyzer (Lorrca, RR Mechatronics, the Netherlands). The blood samples (25µl) were suspended in 5 ml of preheated polyvinylpyrrolidone solution (37 °C) (R.R.Mechatronics, the Netherlands). The red blood cell suspension was exposed to defined shear forces generated by two concentric cylinders. The deformation of the erythrocytes is expressed as elongation index EI=A-B/A+B, with A representing the vertical axis and B the horizontal axis (Hardeman et al., 1994).

3.4.5 Blood and organ taking

The blood and organs were taken after intraperitoneal injection of a mixture of xylazine (10 mg/kg body weight), ketamine (100 mg/kg body weight), and 200 µl heparin (25.000 I.E. /5 ml, Braun, Germany). A blood volume of approx. 1 ml was collected from the animal by cardiac puncture. The whole blood was either used for blood count, FACS analysis or centrifuged for 10 minutes at 800 g for further plasma collection and analysis. After opening the thorax and abdomen, the arterial and venous system was flushed with either ice-cold PBS or NEM/EDTA (10 mM/2 mM) solution for NOx analysis. Organs were carefully removed and snap-frozen in liquid nitrogen or processed for further histological analysis. All samples were stored at -80 °C until further analysis.

3.4.6 Blood count

The automated hematology device VET-Abc (scil animal care company GmbH, Germany), located in the central facility for animal research and scientific animal protection tasks (*ZETT*), was used for the blood count analysis. For analysis, a 10 µl EDTA blood sample was loaded in the suction nostril by enabling rodent full blood count parameter.

3.5 Analytical methods

3.5.1 Blood and tissue preparations for NOx analysis

To avoid NO_3^- and NO_2^- contamination, the labware was cleaned with ultra-pure water before usage. Blood was taken as described previously and diluted 1:10 (v/v) with a solution of 100 mM N-ethylmaleimide (NEM) and 20 mM ethylenediaminetetraacetic acid (EDTA) in PBS. For nitrite and RXNO measurement of tissue samples, organs were homogenized with NEM/EDTA buffer (100 mM/20 mM, PBS) on ice, with the help of TissueRuptor (Qiagen, the Netherlands). The three-fold volume of NEM/EDTA buffer was used according to the weight of the tissue. For the NO_3^- measurement in ENO-30, tissue samples were homogenized in methanol (2 ml/g tissue) and centrifuged for 10 minutes at 10,000 g (4 °C). Plasma samples were diluted with the same volume of methanol, vortexed for 10 seconds, and centrifuged for 10 minutes at 10,000 g (4 °C). After centrifugation, the supernatant was collected, and 10 µl of supernatant was injected into ENO-30.

3.5.2 Chemiluminescence detection (CLD)

To detect nitrite, nitrosamines, and nitrosothiols, the samples were measured using a chemiluminescence detector (CLD 88 e, Eco Physics GmbH, Germany), Figure 12. In a reaction chamber preheated to 60 °C and filled with a mixture of potassium iodide (45 mM) and iodine (10 mM) in 93 % acetic acid, samples were added via a septum using a 100 µl Hamilton syringe (Hamilton Company, USA). The NO in the samples will be released and passed through a cooling system in the chemiluminescence detector using helium as a carrier gas. NO reacts with ozone to form nitrogen dioxide with an excited electron. The quantum light emitted when the excited electron reaches the ground state was recorded by a photomultiplier. Before every measurement, a freshly prepared standard curve of nitrite (0-1200 nM) was measured. Samples were kept on ice, protected from light. For the determination of nitrite and RXNO, a 100 µl sample was added into the reaction chamber. To quantify RXNO, nitrite was eliminated by incubation with 5% sulfanilamide solution in 1 M HCl in a 1:10 ratio (v/v), and 300 µl of this sample was injected. The concentration of nitrite was calculated by substracting the area under the curve (AUC) generated by the signal of RXNO from the AUC generated by the untreated sample (sum of nitrite and RXNO). Data analysis was performed by eDAQ Powerchrome software (eDAQ, Poland).

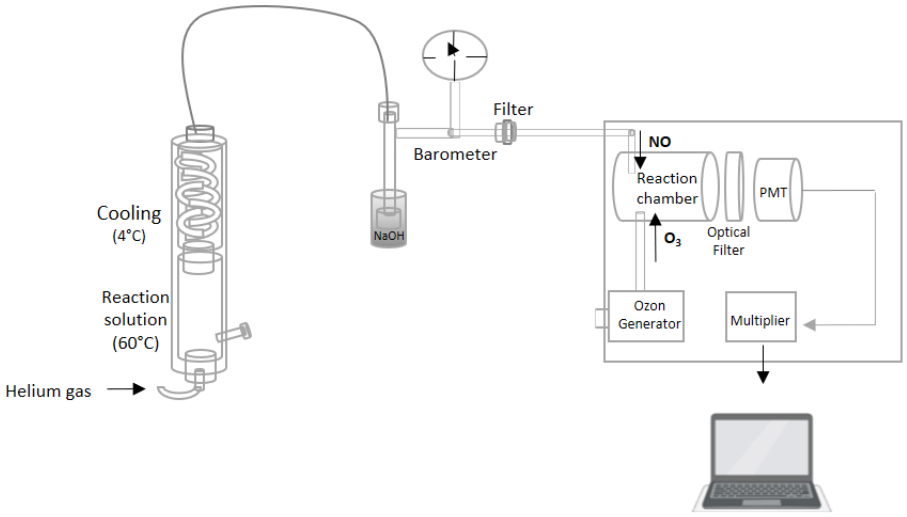

Figure 12 Illustration of complete set-up for measurement of nitrite/RXNO by CLD
PMT: photomultiplier.

3.5.3 Nitrate Measurement by high-performance liquid chromatography

The measurement of NO_3^- in plasma samples was carried out with the ENO-30 (AMUZA INC, USA). The measurement is based on the separation of NO_3^- and NO_2^- by high-performance liquid chromatography (HPLC), followed by the Griess reaction (Equation 2). The product of Griess reaction is a colored diazo compound that can be detected spectrophotometrically. In detail, the injected sample is filtered by the guard column (NO-PrePAK, EiCom, Ireland) and then enters the separation column (NO-PAK, EiCom, Ireland). Due to the higher affinity of NO_3^- to the polystyrol-polymer of the separation column, NO_3^- and NO_2^- are temporarily separated. This accounts for the different retention times of 4.5 minutes for NO_2^-, while NO_3^- will be eluted with a retention time of 8 minutes. After separation, the sample enters the reduction column, containing reduced copper and cadmium to reduce NO_3^- to NO_2^-. Before entering the reaction loop, samples are mixed with a reactor solution containing sulfanilamide and *N*-(1-naphthyl)ethylenediamine to form a red-colored diazo compound, which is measured by the detector at the wavelength of 540 nm. To determine AUC, peak analysis was performed with Clarity chromatography software 8.2.02.094 (DataApex, The Czech Republic).

Equation 2 Chemical equation of Griess reaction

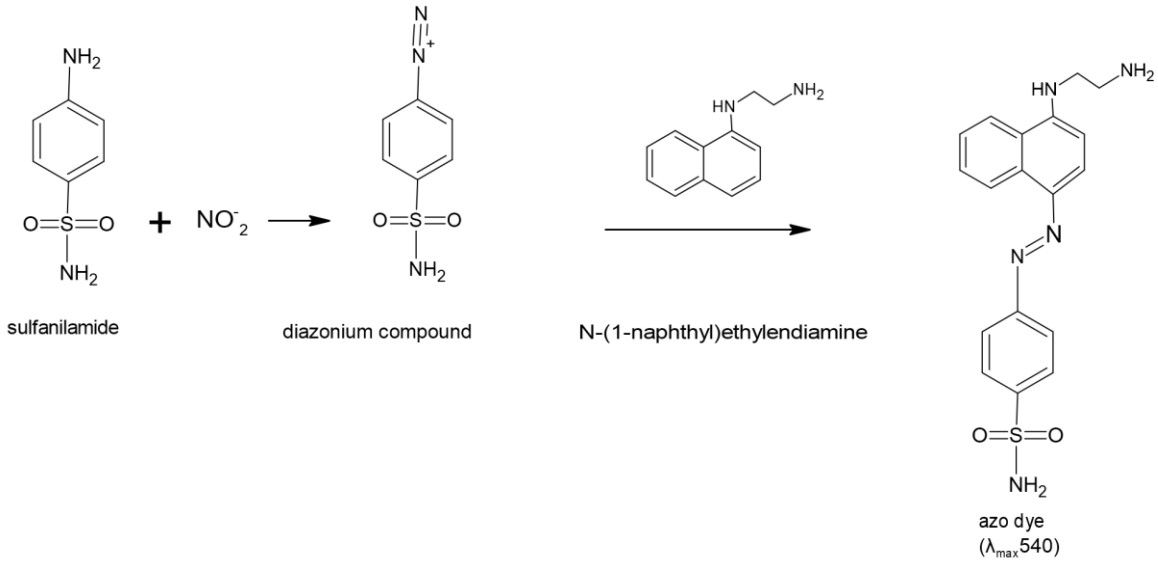

3.6 Molecular biochemical methods

3.6.1 Organ lysis and protein determination

The organs were transferred to a 2 ml Eppendorf tube and homogenized for 2 minutes at 30 Hz (Mixer Mill MM 400, RETSCH). Radioimmunoprecipitation assay buffer (RIPA) (150 mM NaCl, 5 mM EDTA, 50 mM Tris, 1 % NP-40 , 0.5 % sodium deoxycholate, 0.1 % SDS, protease and phosphatase inhibitors, Thermo Scientific™) was added and homogenized for another 2 minutes. The tissue was further lysed for 15 minutes in an ultrasonic bath. The samples were then centrifuged at 10,000 g for 15 minutes at 4 °C, and the supernatant was used for further analysis. Protein determination was performed by a colorimetric assay kit (D.C. Protein Assay, Bio-Rad Laboratories Inc., Hercules, USA), modified by the manufacturer to the Lowry method. Freshly prepared solutions of bovine serum albumin at a concentration of 0.0-2.0 mg/ml were used as standards. The samples were diluted in a ratio of 1:20 (v/v), and 5 µl sample and standard were transferred into a 96-well plate in duplicate. Next, 25 µl reaction solution A and 200 µl reaction solution B were added. After 15 minutes incubation in the dark, the protein concentration was determined at the wavelength 740 nm (FLUOstar Omega, BMG Labtech GmbH & CO. KG, Ortenberg, Germany).

3.6.2 Western-Blot

For SDS-page, samples were mixed with loading buffer (LDS sample buffer, NuPAGE™, Thermofisher) in a 1:4 ratio (v/v) and sample reducing agent (NuPAGE™, Thermofisher) in a 1:10 ratio, following a 10 minutes denaturation at 70 °C. An equal amount of protein was loaded and separated in 4-12 % Bis-Tris protein gels (Novex, NUPAGE™, ThermoFisher) at 150 mV for 60 minutes. The proteins were then transferred to a 0.2 µm nitrocellulose membrane (Amersham Prostra 0.2 GE Healthcare, Life Sciences, USA). To detect sample loading across the blot, the membrane was treated with a total protein stain for 5 minutes (Revert ™ 700, Total Protein Stain, LI-COR Biosciences-GmbH, Germany) at 700 nm. The membrane was then blocked in blocking buffer (Intercept Blocking Buffer TBS, LI-COR Biosciences GmbH, Germany) for 60 minutes at room temperature. According to the protein of interest, the primary antibodies were diluted in blocking buffer, 0.2 % TWEEN, as listed in Table 2 and incubated at 4 °C overnight. The next day, membranes were washed with TBS and incubated in accordance with the host-specific secondary antibody for 60 minutes at room temperature. Since secondary antibodies are light-sensitive, incubation was performed in the dark. After three more washing steps, membranes were detected at 700 nm or 800 nm in the Odyssey Fc Imaging System (LI-COR Biosciences GmbH, Bad Homburg, Germany).

Table 2 Primary antibodies for western blot analysis

Antigen	Host	Dilution	Company, cat-number
NOS III	**Mouse**	**1:500**	**BD Biosciences (#610296)**
AKT	**Rabbit**	**1:1000**	**Cell Signaling (#9272S)**
GUGY1B3	**Rabbit**	**1:1000**	**Abcam (#ab154841)**
Nitrotyrosine	**Mouse**	**1:1000**	**Santa Cruz (#sc-32757)**
GAPDH	**Rabbit**	**1:1000**	**Abcam (#ab9485)**

Table 3 Secondary antibodies for western blot analysis

Fluorescent labelled Antibody	Host	Dilution	Company Ordering n°
IRDye® 800CW anti -Rabbit	**Goat**	**1:10000**	**LI-COR Biosciences (#926-32211)**
IRDye® 680 RD anti-Mouse	**Goat**	**1:10000**	**LI-COR Biosciences (#926-68070)**

3.6.3 Analysis of mRNA expression levels

The quantification of mRNA expression of genes listed in table 4 was determined by real-time PCR using TaqMan® technology. RNA extraction was performed using KingFisher Duo Prime. Initially, thoracic aortas and femoral arteries were isolated as described in 3.1 and stored in the 10-fold volume of RNA stabilization solution (RNAlater, Thermo Fisher Scientific, USA) at minus 80 °C. Before tissue homogenization, samples were centrifuged, and RNA stabilizer solution was carefully removed. Samples were homogenized using Mixer Mill MM 400, RETSCH, in a pre-cooled container (4 °C). Next, a lysis buffer mix was added in a 10-fold volume corresponding to the tissue weight. Lysis buffer mix containing β-mercaptoethanol and RLT buffer (Qiagen, the Netherlands) in a 1:100 ratio. The lysates were transferred onto QIAshredder columns (Qiagen, the Netherlands) and centrifuged for 2 minutes at full speed at room temperature. Next, 200 µl of each sample lysate was transferred into a MagMax 96 Deep Well Plate (Thermo Fisher Scientific, USA), and the same volume of isopropanol was added to every sample. The plate was covered and shacked for 2 minutes at 900 rpm. In the next step, 30 µl of Binding Beads Mix (1:1 ratio of RNA Binding Beads and Lysis Enhancer) was added to each sample and shacked for another 5 minutes at 900 rpm. Before starting the extraction procedure, plate set-up was completed by adding elution buffer, wash solutions, and Turbo DNase Solution (MagMAX mirVana Total RNA Isolation Kit, Thermo Fisher Scientific, USA) in predesigned wells. After the RNA extraction was completed, purified samples were collected, and RNA concentration was measured using NanoDrop2000 spectrophotometer (DS-11 FX, DeNovix, USA). According to the manufacturer's protocol, reverse Transcription was performed with Super Script™ IV VILO™ Master Mix with ezDNase™ enzyme (Thermo Fisher Scientific, USA). Briefly, 100 ng RNA was mixed with 10 µl of the reaction mix, containing 10x ezDNase Buffer, ezDNase enzyme, nuclease-free water and incubated at 37 °C for 2 minutes. Afterward, 6 µl of nuclease-free water and 4 µl SuperScript™ IV VILO Master Mix or SuperScript™ IV VILO No R.T. Control was added, respectively. The samples were incubated for 10 minutes at 25 °C. Next, samples were incubated 50 °C for 10 minutes, followed by incubation for another 5 minutes 85 °C. After incubation steps, cDNA was used for preamplification with TaqMan® PreAmp Master Mix (Applied Biosystems, USA) following the manufacturers protocol. Finally, 5 ng of cDNA was used in a total reaction volume of 50 µl, containing TaqMan® PreAmp Master Mix (2x) and 20x TaqMan® Primer mix in a final dilution of 0.2x. GAPDH was used for internal standardization. Real-time PCR

was performed using Quant Studio 7 Flex System (Thermo Fisher Scientific, USA). Thermocycling conditions were set up as follow:

stage 1	**95.0 °C**	**20 s**
stage 2	**95.0 °C**	**1 s**
stage 3	**60.0 °C**	**20 s**

For relative quantification of mRNA expression, $\Delta\Delta C_T$ method (Livak & Schmittgen, 2001) was used. In this process, expression levels of the gene of interest were normalized to the housekeeping gene. The measurements were performed with the generous support of Hakima Ezzahoini.

Table 4 Genes and corresponding primers used for RT-PCR

Gene name	Primer	Amplicon Length
NOS3 (eNOS)	**Mm00435217_m1**	**71**
ICAM-1	**Mm00516023_m1**	**58**
VCAM-1	**Mm01320970_m1**	**71**
IL-6	**Mm00446190_m1**	**78**
IL-10	**Mm01288386_m1**	**136**
Tgfβ1	**Mm01178820_m1**	**59**
TNFα	**Mm00443260_g1**	**61**
Catalase	**Mm00437992_m1**	**64**
Superoxide dismutase 1	**Mm01344233_g1**	**71**
Glutathione reductase	**Mm00439154_m1**	**65**
Glutathione peroxidase 1	**Mm00656767_g1**	**134**
GAPDH	**Mm99999915_g1**	**109**

3.6.4 Measurement of free hemoglobin by enzyme-linked immunosorbent assay (ELISA)

Plasma cell-free Hb concentrations were measured using a commercially available ELISA kit (ab157715, abcam, United Kingdom). Briefly, 100 µl of standard (12.5-400 ng/ml) and sample were transferred into the 96- well plate and incubated for 60 minutes. After a washing step, 100 µl of the enzyme-antibody conjugate was added and incubated for 30 minutes in the dark. Afterwards, the microplate was again washed with washing buffer and 100 µl substrate solution was added and incubated for another 10 minutes. The reaction was terminated by adding 100 µl of stop solution. The absorption was measured immediately at the wavelength of 450 nm (FLUOstar Omega, BMG Labtech, Germany).

3.6.5 Glutathione Assay

To determine the glutathione (GSH) concentration in plasma and tissues, 10 mg of tissue was homogenized in 250 µL of ice-cold PBS (100 mM) and centrifuged at 14,000 g for 10 minutes at 4 °C. The supernatant was carefully separated and protein concentration was measured as described under 3.6.1. The remaining supernatant was mixed with an equal volume of 5 % 5-sulfo-salicylic acid solution for protein precipitation. Plasma samples were treated in the same way. The mixture was incubated for 10 minutes and centrifuged at 14,000 g for 10 minutes at 4 °C. The supernatant was removed from the protein pellet and diluted with assay buffer (1:2.5). GSH standards were prepared in concentrations 0.195-25 µM. To check for a complete conversion of oxidized glutathione (GSSG) to GSH, a control preparation was run simultaneously. The standards, samples, and control were transferred into the black half-area plate as duplicates and incubated with 25 µl of reagent solution for 15 minutes. The fluorescence signal corresponding to free GSH concentration was measured emission and excitation wavelengths at 510 nm and 390 nm, respectively. During this step, a non-fluorescent molecule binds to the free thiol group of GSH and releases a fluorescence product. To yield free GSH, samples were incubated with the reaction mixture for 15 minutes, reducing GSSG. All fluorescence readings were carried out with fluorescence microplate reader FLUOstar Omega (BMG Labtech, Germany). The procedures were performed using Glutathione Fluorescent Detection Kit (Arbor Assays, USA).

3.7 Histological analysis

The heart was cryopreserved in a water-soluble embedding medium (Tissue Tek® OTC™ Compound, Sakura Finetek Europe B.V., Germany) before 6 µm-thickness sectionings using a microtome and fixed on adhesive microscope slides. The slides were later fixed with cold formaldehyde (4 %, buffered, pH 6.9) for 10 minutes.

3.7.1 Haematoxylin-Eosin Staining

Tissue sections were thawed, rehydrated and transferred to a hematoxylin solution according to Gill II for 30 seconds. Afterward, slides were rinsed under running tap water for 10 minutes. The slides were then incubated in a solution of Eosin G for 1 minute. The excess color was removed through 3 washes in distilled water, following dehydration in 70 %, 96 %, and absolute ethanol for 15 seconds. Slides were cleared in Roticlear® and capped with ROTI®Histokitt (Carl Roth, Germany).

3.8 Statistical Analysis

Statistical analysis and graphical illustrations were performed using GraphPad Prism 6.01 (Graphpad Prism Inc., La Jolla, California, USA). If not stated otherwise in figure legends, data are presented as mean ± standard error of the mean (SEM) of *n* individual samples. Two-sided Student's t-test using Tukey's multiple comparisons test was carried out for comparison of two groups. For more than two groups, one-way analysis of variances (ANOVA) or two-way ANOVA followed by Tukey's or Sidak's post hoc test. Data were considered statistically significant with a p-value ≤ 0.05. Significance level further stated as $*p \leq 0.05$, $**p \leq 0.01$, p $***\leq 0.001$, p $****\leq 0.0001$.

4 Results

4.1 Characterization of cardiac function in a murine model of aortic valve stenosis

4.1.1 Echocardiographic analysis

The aim of this thesis was to investigate local and systemic consequences of AS in a wire-induced murine AS model. For this purpose, we first performed a comprehensive characterization of the wire-injury model of AS regarding cardiac function and valvular morphology. The consequences of AS on RBC integrity and vascular endothelial function will be presented in the next chapters.

To evaluate AS in mice, we have employed parameters used for diagnosis in humans in our mouse model. Therefore, the main parameters describing the severity and progression of AS are peak velocities, mean gradient, and peak pressure gradient. Moreover, we assessed the left ventricular systolic and diastolic function longitudinally by assessment of parameters listed in Table **5**. To differentiate between pressure and volume overload in the model, we further separated the data regarding the presence of aortic regurgitation (AR) after four weeks (Figure 13). Consequently, mice with concomitant aortic regurgitation (AS+AR) were defined as a separate group and excluded from further evaluation. Assessment of AR was carried out by color Doppler and pulse wave Doppler. Importantly, we defined a minimum of 1.5-fold increase in peak velocity compared to baseline as relevant AS. The characterization of the model was done as follows: First, we performed an intraindividual analysis to understand the changes based on the echocardiography data before and four weeks after injury in the same mice. Afterwards, the interindividual analysis was done comparing age-matched sham animals after four weeks.

Manipulation of the aortic valve by wire-injury induces relevant AS four weeks after surgical procedure indicated by a significant increase in peak velocity, mean pressure gradients and peak pressure gradients compared to baseline conditions (Table 5).

Table 5 Left ventricular function parameters and aortic blood flow velocities assessed by high resolution ultrasound under baseline conditions and after four weeks after the induction of aortic valve stenosis. n=28. IVS,d: interventricular septum thickness, diastole, LVID,d: left ventricular diameter, E/A: ratio between peak velocities of the early (E) and late (A) ventricular filling.

	unit	Baseline	Four weeks	*p*-value
Peak Velocity	mm/s	1283 ± 38.95	2462 ± 111.4	***< 0.0001****
Mean Gradient	mmHg	1.7 ± 0.2	5.5 ± 0.5	***< 0.0001****
Peak Gradient	mmHg	6.8 ± 0.5	21.0 ± 1.7	***< 0.0001****
Heart Rate	bpm	420.7 ± 11.2	460.1 ± 14.8	***0.004****
Endsystolic Volume	µl	24.1 ± 1.3	27.5 ± 1.7	0.0634
Enddiastolic Volume	µl	58.9 ± 2.4	62.7 ± 3.3	0.2118
Stroke Volume	µl	34.9 ± 1.3	35.2 ± 1.7	0.8144
Ejection Fraction	%	59.0 ± 0.8	57.1 ± 0.8	0.053
Fractional Shortening	%	14.9 ± 0.8	13.8 ± 0.9	0.3466
Cardiac Output	µl/min	14.7 ± 0.6	15.7 ± 0.6	0.0581
IVS,d	mm	1.0 ± 0.1	1.0 ± 0,1	***0.001****
LVID,d	mm	3.7 ± 0.1	4.0 ± 0.1	***0.0495****
E/A	a.u.	1.7 ± 0.1	1.5 ± 0.1	0.0522
Isovolumic Contraction Time	ms	15.8 ± 0.9	16.1 ± 1.3	0.8693
Isovolumic Relaxation Time	ms	16.5 ± 0.9	14.8 ± 1.1	0.161

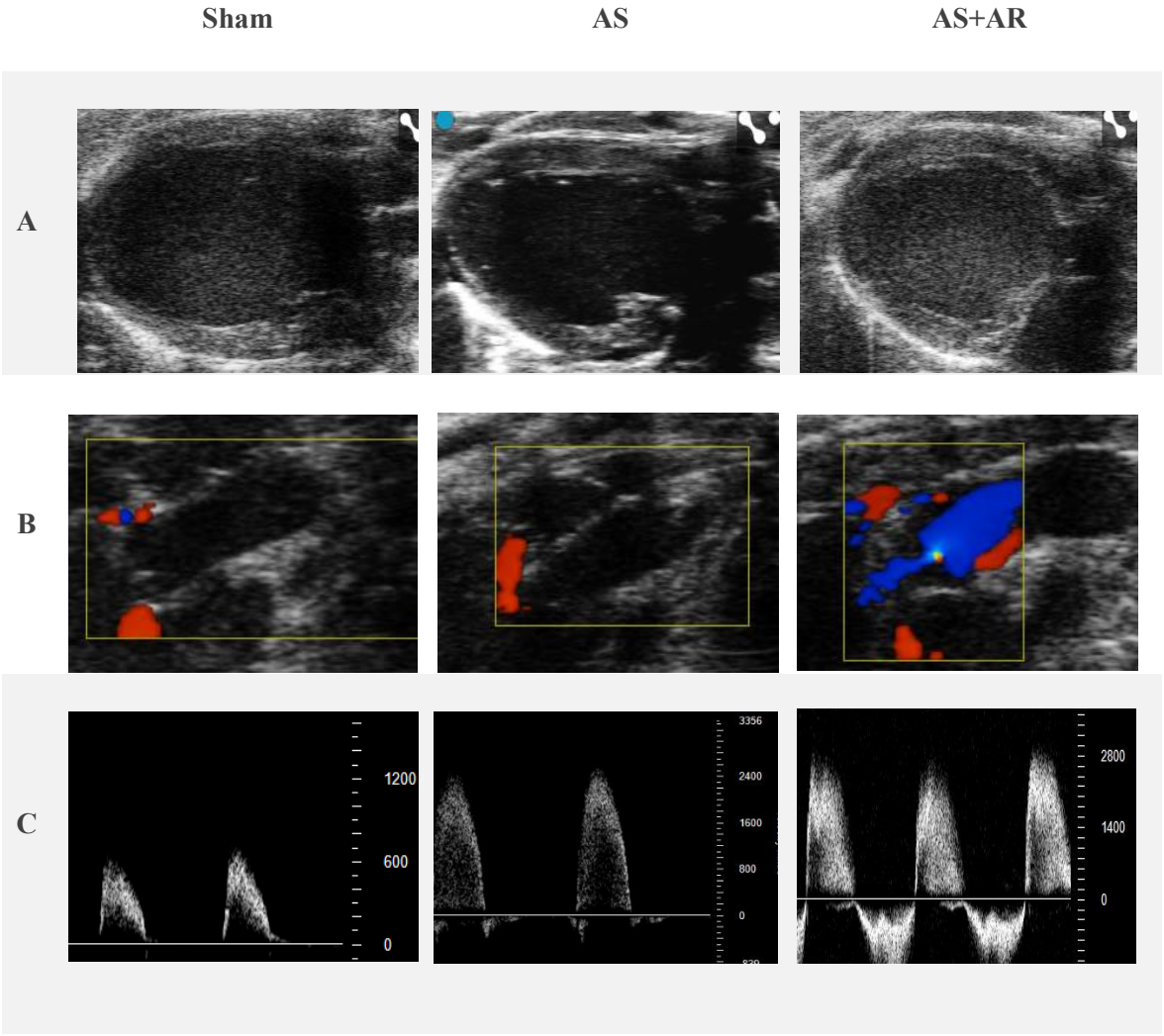

Figure 13 Representative echocardiographic images
Images illustrating echocardiographic assessment of sham mice, mice with aortic valve stenosis (AS) and mice with concomitant aortic regurgitation (AR + AS), four weeks after wire-injury or sham surgery, respectively. (A) Parasternal long-axis view (PSLA) demonstrated myocardial hypertrophy in AS animals vs. left ventricular dilation in mice with concomitant regurgitation (AS+AR). (B) Two-dimensional color Doppler depicted regurgitation jet during diastole in AS+AR mice. The direction of blood flow away from the transducer is indicated by color-coding as blue or blood flow towards the transducer as red. (C) Peak flow velocities indicated an increase in flow velocity in AS mice, while the additional presence of regurgitation was clear by negative flow velocity values.

To conduct interindividual analysis, the control group consisted of age-matched animals, which underwent sham surgery. Compared with sham mice, the relative increase in aortic peak velocity was 2.1 ± 0.1 fold higher in mice with AS. Mean pressure gradient was 4.8 ± 0.67 fold increased, with a 4.04 ± 0.35 fold increase in peak pressure gradient (Figure 14). Left ventricular function analysis demonstrated a preserved left ventricular function (Figure 15). Compensatory adaptions due to pressure overload were observed by analyzing interventricular septum thickness (IVSd) and left ventricular diameter (LVIDd) (Figure 15). Interventricular septal thickness in diastole was significantly increased (sham 0.96 ± 0.11 mm vs. AS 1.02 ± 0.12 mm, $p<0.05$), suggesting concentric hypertrophy of the LV (Figure 15).

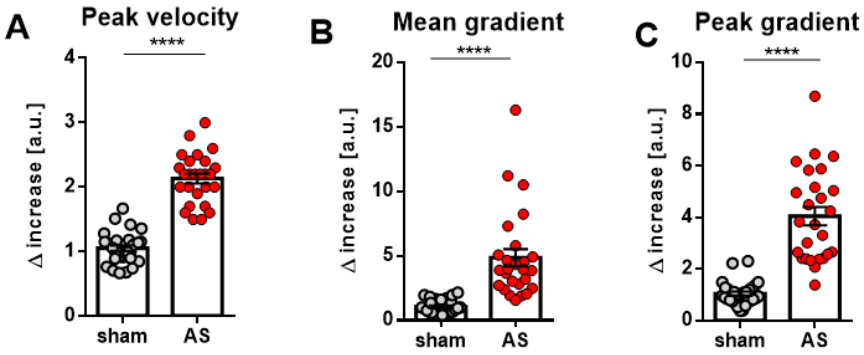

Figure 14 Relative increase in aortic blood flow velocity, mean and peak gradients in sham mice and mice with aortic valve stenosis, four weeks after wire-injury
Aortic blood flow velocities and pressure gradients were assessed using pulse-wave Doppler in the ascending aorta of sham and mice with aortic valve stenosis (AS). Relative increase of (A) peak velocity, (B) peak gradient and (C) mean gradient were calculated as fold-change from baseline conditions in each group. Unpaired t-test, ****$p<0.0001$. Data are shown as mean ± SEM, sham n=31, AS n=26.

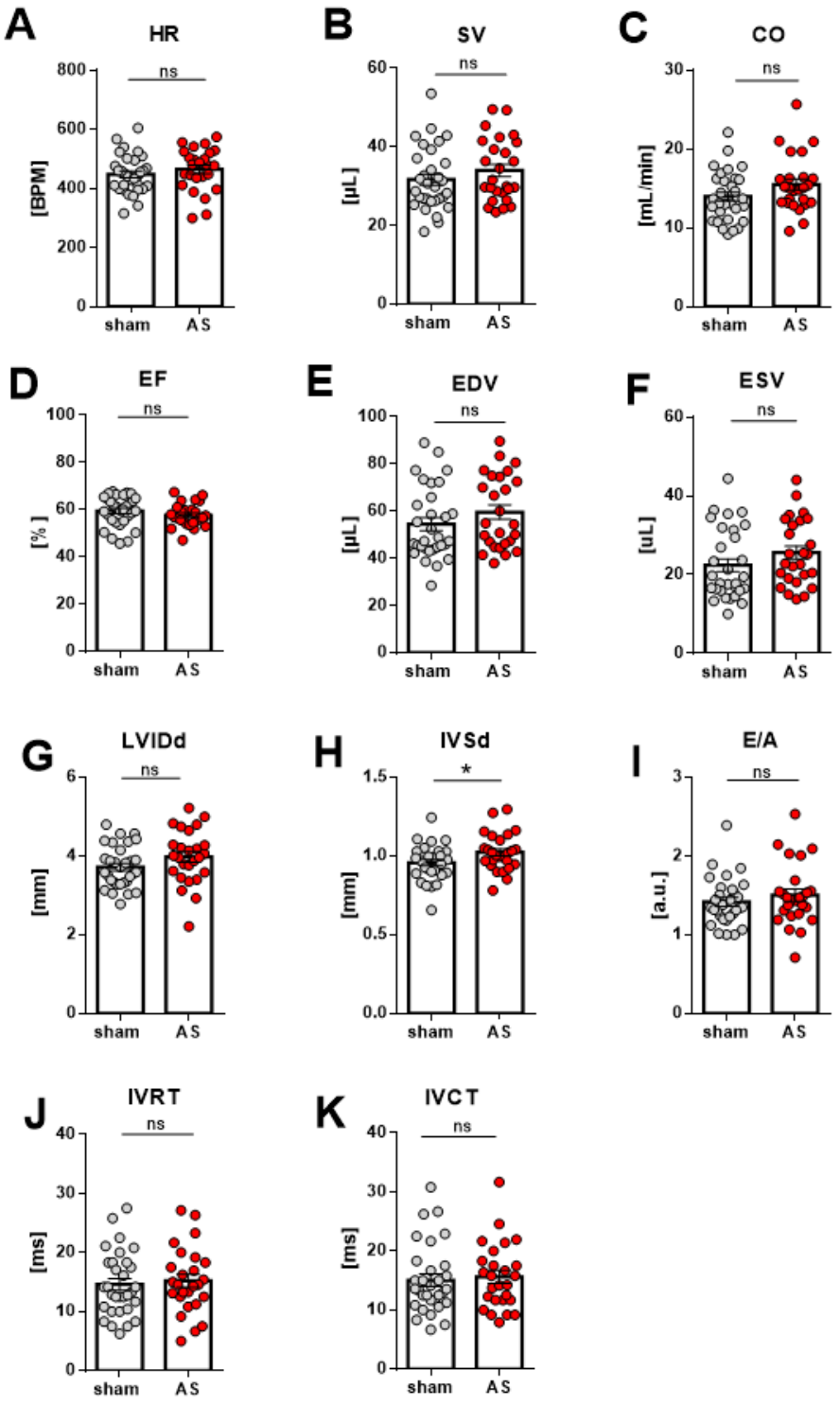

Figure 15 Cardiac function analysis in sham mice and mice with aortic valve stenosis.
Left ventricular functional parameters were assessed by echocardiography four weeks after induction of aortic valve stenosis (AS) or sham surgery, respectively. Heart rate (HR), stroke volume (SV), cardiac output (CO), ejection fraction (EF), end-diastolic volume (EDV), end-systolic volume (ESV), left ventricular diameter in diastole (LVIDd), interventricular septum thickness in diastole (IVSd), the ratio of passive and active diastolic filling (E/A), isovolumic relaxation time (IVRT) and isovolumic contraction time (IVCT). Unpaired t-test, *p<0.05. Data are shown as mean ± SEM, sham n=31, AS n=26.

As stated previously, we also identified mice with AS and concomitant AR. The majority of mice, which underwent wire-injury, showed no operative effects, e.g. destruction of the aortic valve. Nevertheless, 33.33% of the total cohort were observed with heart failure, indicated by concomitant AR. The volume overload accounted for an enhanced ventricular filling during diastole, evoked a significant increase in end-systolic volume (sham: 22.4 ± 8.9 µl vs. AS+AR: 50.2 ± 22.6 µl, p=0.0005) and as a consequence significant increase in left ventricular diameter (sham: 3.7 ± 0.5 mm vs. AS+AR: 4.8 ± 0.6 mm, p<0.0001). Moreover end-systolic volume was significantly increased (sham: 54.6 ± 15.3 µl vs. AS+AR: 79.2 ± 28.0 µl, p<0.0001), while there was a significant decrease in ejection fraction (EF) (sham: 59.5 ± 6.4 % vs. AS+AR: 37.7 ± 9.3 %, p=0.0001), see Figure 16.

One should consider that under these circumstances, the net blood flow into the aorta was decreased due to regurgitation. In humans, effective stroke volume in the aorta can be quantified by assessment of the sum of the area of the left ventricular outflow tract (LVOT) and the velocity time integral (VTI) of LVOT. In murine echocardiography, the assessment of this area is extremely challenging, aggravating a precise evaluation of this parameter. Likewise, the assessment of the regurgitation fraction was not realizable, as it requires exact quantification of the regurgitation volume. We were able to evaluate the presence of AR by the size of the regurgitation jet by color- Doppler approach. Therefore, the effective stroke volume in mice with AS+AR was not quantifiable.

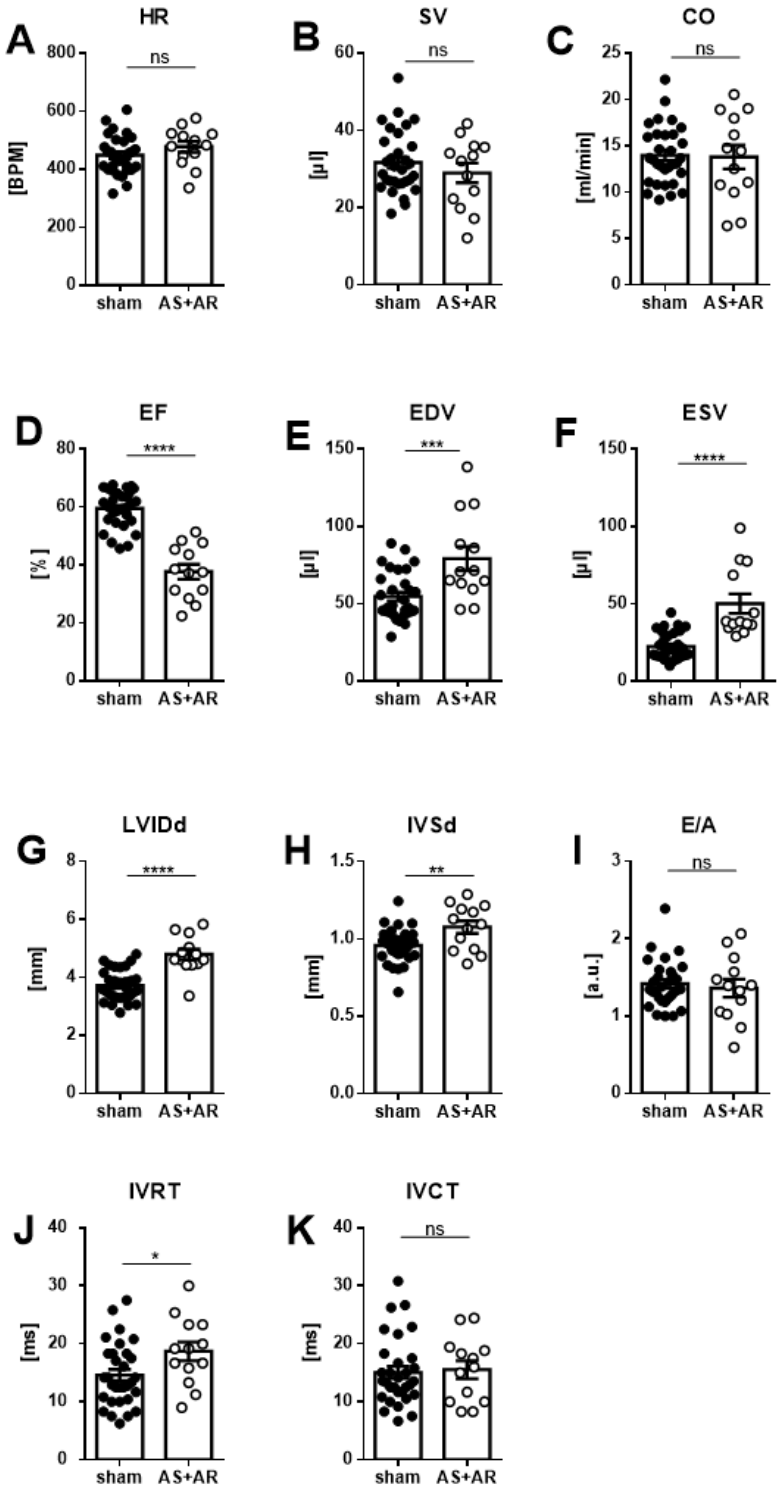

Figure 16 Cardiac function analysis in mice with concomitant aortic regurgitation
Left ventricular functional parameters were assessed using echocardiography. Panels (A-K): Heart rate (HR), stroke volume (SV), cardiac output (CO), ejection fraction (EF), end-diastolic volume (EDV), end-systolic volume (ESV), left ventricular diameter in diastole (LVIDd), interventricular septum thickness in diastole (IVSd), ratio of passive and active diastolic filling (E/A), isovolumic relaxation time (IVRT) and isovolumic contraction time (IVCT). Aortic valve stenosis (AS), aortic regurgitation (AR). Unpaired t-test, p*<0.05, p**<0.01, p***<0.001, ****p<0.0001. Data are shown as mean ± SEM, sham n=31, AS+AR=13.

For longitudinal assessment of the model, we set a further endpoint after three months post-induction of AS. The data demonstrate no further increase in peak velocities (four weeks AS: 2698 ± 182.6 mm/s vs. three months AS: 2700 ± 255.6 mm/s) or pressure gradients (four weeks AS: 30.80 ± 4.24 mmHg vs. three months AS: 32.99 ± 6.10 mmHg) compared to four weeks. Likewise, left ventricular function showed no significant differences compared to four weeks. A summary of the data is represented in Table 6.

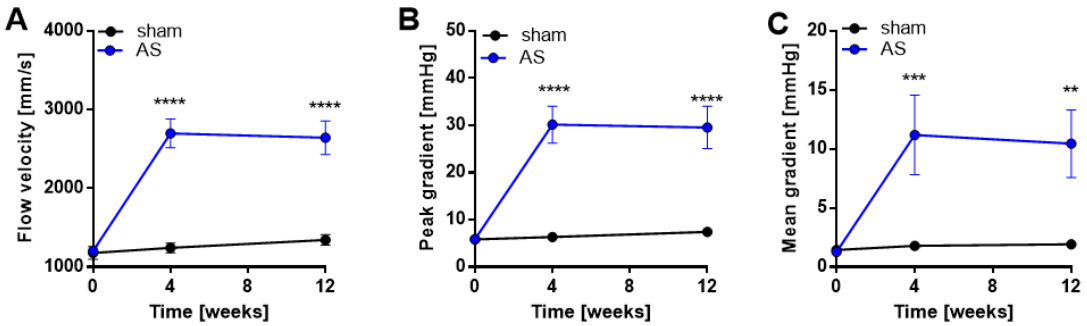

Figure 17 Analysis of flow velocities and pressure gradients revealed no further increase three months after wire-injury.
Aortic blood flow velocities and pressure gradients were assessed using pulse-wave Doppler in the ascending aorta of sham and mice with aortic valve stenosis (AS), panels (A-C). Two-way ANOVA, Sidak's multiple comparison test, **p<0.01, ***p<0.001, ****p<0.0001. Data are shown as mean ± SEM, sham n=12, AS n=10.

Table 6 Left ventricular function parameters and aortic blood flow velocities assessed in sham and mice with aortic valve stenosis three months after surgery. sham n=12, AS n=10. IVS,d: interventricular septum thickness, diastole, LVID,d: left ventricular diameter, E/A: ratio between peak velocities of the early (E) and late (A) ventricular filling.

	unit	Three months sham	Three months AS	*p*-value
Peak Velocity	mm/s	1344.0 ± 67.3	2643.0 ± 212.6	***<0.0001****
Mean Gradient	mmHg	1.9 ± 0.3	10.5 ± 2.9	***0.0062****
Peak Gradient	mmHg	7.4 ± 0.7	29.6 ± 4.5	***<0.0001****
Heart Rate	bpm	440.2 ± 19.3	437.4 ± 19.9	0,9225
Endsystolic Volume	µl	27.7 ± 2.9	43.1 ± 8.2	0,0629
Enddiastolic Volume	µl	64.4 ± 4.8	85.7 ± 11.2	0,0694
Stroke Volume	µl	36.7 ± 2.1	42.6 ± 3.8	0,1622
Ejection Fraction	%	57.7 ± 1.6	51.9 ± 2.8	0,0750
Fractional Shortening	%	11.7 ± 1.0	12.3 ± 1.1	0,7161
Cardiac Outout	µl/min	16.2 ± 1.3	18.8 ± 2.2	0,2982
IVS,d	mm	1.2 ± 0.1	1,6 ± 0.1	***0.0035****
LVID,d	mm	3.4 ± 0.1	4,3 ± 0.2	***0.0036****
E/A	a.u.	1.4 ± 0.1	1,4 ± 0.1	0,9133
Isovolumic Contraction Time	ms	13.8 ± 1.5	15.5 ± 1.6	0,7554
Isovolumic Relaxation Time	ms	14.6 ± 1.4	17.9 ± 1.9	0,1742

4.1.2 Magnetic resonance imaging

In a clinical setting, echocardiography is the standard tool for diagnosis and assessment of AS. We adapted this technique to assess the wire-injury model of AS. Nevertheless, murine echocardiographic analysis of stenotic valves was challenging regarding the precise assessment of the aortic valve orifice area. In comparison, MRI allows this precise assessment of morphological changes of the valve, myocardial texture analysis via T1 and T2 mapping, as well as analysis of flow patterns in the aorta ascendens.

4.1.3 Wire-injury induced restricted, asymmetric aortic valve opening and valve thickening

In comparison to sham mice, AS animals showed a restricted, asymmetric opening of the aortic valve (Figure 18A). Planimetry of the aortic valve revealed a significant decrease in aortic valve opening area compared to sham and control animals, normalized to the total supravalvular aortic area assessed in end-diastole (sham: 80.1 ± 8.6 %, control: 77.8 ± 6.3 % vs. AS: 60.2 ± 9.8 %, p=0.0006, p=0.0010), see Figure 18. Besides, long-axis slices, perpendicular to the aortic valve, there is significant valve thickening, validated by analysis of total leaflet area (sham: 0.12 ± 0.01%, control: 0.12 ± 0.01 % vs. AS: 0.17 ± 0.01 %, p<0.0001 , p=0.0001) (Figure 18).

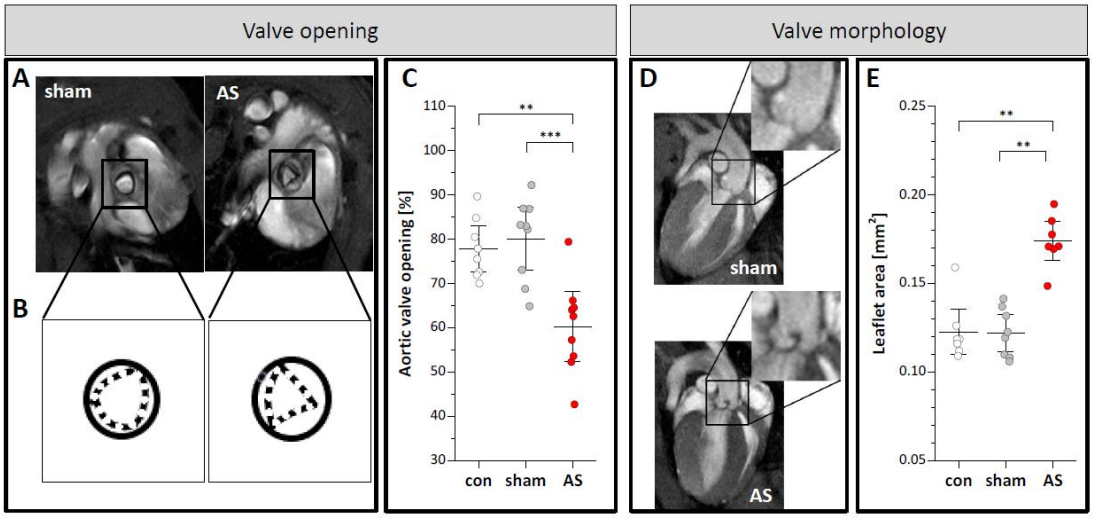

Figure 18 Aortic valve morphology after wire-injury
Assessment of valve morphology and valve orifice area by magnetic resonance imaging in untreated control mice (con), sham animals and mice with aortic valve stenosis (AS), four weeks after wire-injury. (A-C) The aortic valve opening area normalized to the total supravalvular aortic area. (D-E) Aortic valve thickening was observed by analysis of the total leaflet area. Unpaired t-test **p<0.01, ***p<0.001. Data are shown as mean ± SD, n=7-9. Figures were taken from the original publication (Quast et al., 2022).

Figure 19 illustrates differences in aortic valve area and flow profiles of sham and mice with AS. In line with echocardiographic analysis, peak flow velocities were significantly increased in AS mice (sham: 117.3 ± 17.4 cm/s, control: 117.0 ± 81.5 cm/s. vs. AS: 204.8 ± 38.4 cm/s, p=0.0001, p=0.0001). Furthermore, MRI-derived velocity maps allowed reconstructing for three-dimensional surface plot above the valve. In contrast to the bell-shaped flow profile of sham mice, stenotic flow profiles were featured asymmetric and turbulent (Figure 19 A-B).

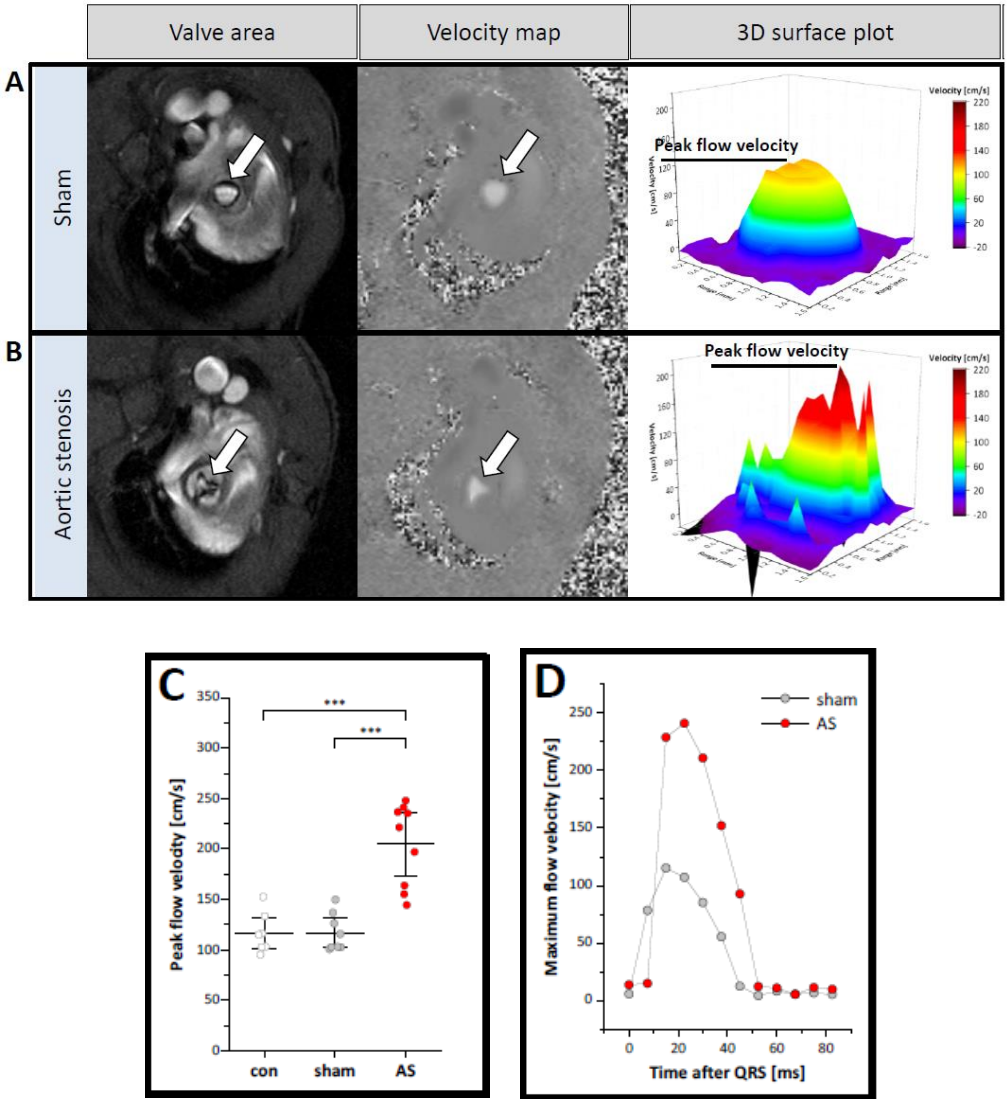

Figure 19 Magnetic resonance imaging of aortic valve area and flow profiles
Effects of wire-injury on valvular function and blood flow were assessed by magnetic resonance imaging in untreated control mice (con), sham animals and mice with aortic valve stenosis (AS) after four weeks. Illustrations of aortic valve area, 2D velocity maps and 3D plots in (A) sham and (B) mice with AS. 3D surface plot presents the blood flow velocities over the vessel cross-sections. (C) Peak velocities and (D) representative peak velocities in sham and AS animals over one cardiac cycle. ***p< 0.001, unpaired t-test. Data are shown as mean ± SD, n=7-9. Figures were taken from the original publication (Quast et al., 2022).

In addition to the assessment of peak flow velocities, 3D flow profiles were used to identify mice with concomitant AR, representing mixed vitium. While in echocardiography, AR was identified by color- Doppler and pulse wave-Doppler, MRI allowed for detection of a regurgitation jet during diastole by 3D reversed flow profiles with negative velocity values. Therefore mice with combined vitium were characterized by increased peak velocity with concomitant presence of regurgitation jet (Figure 20).

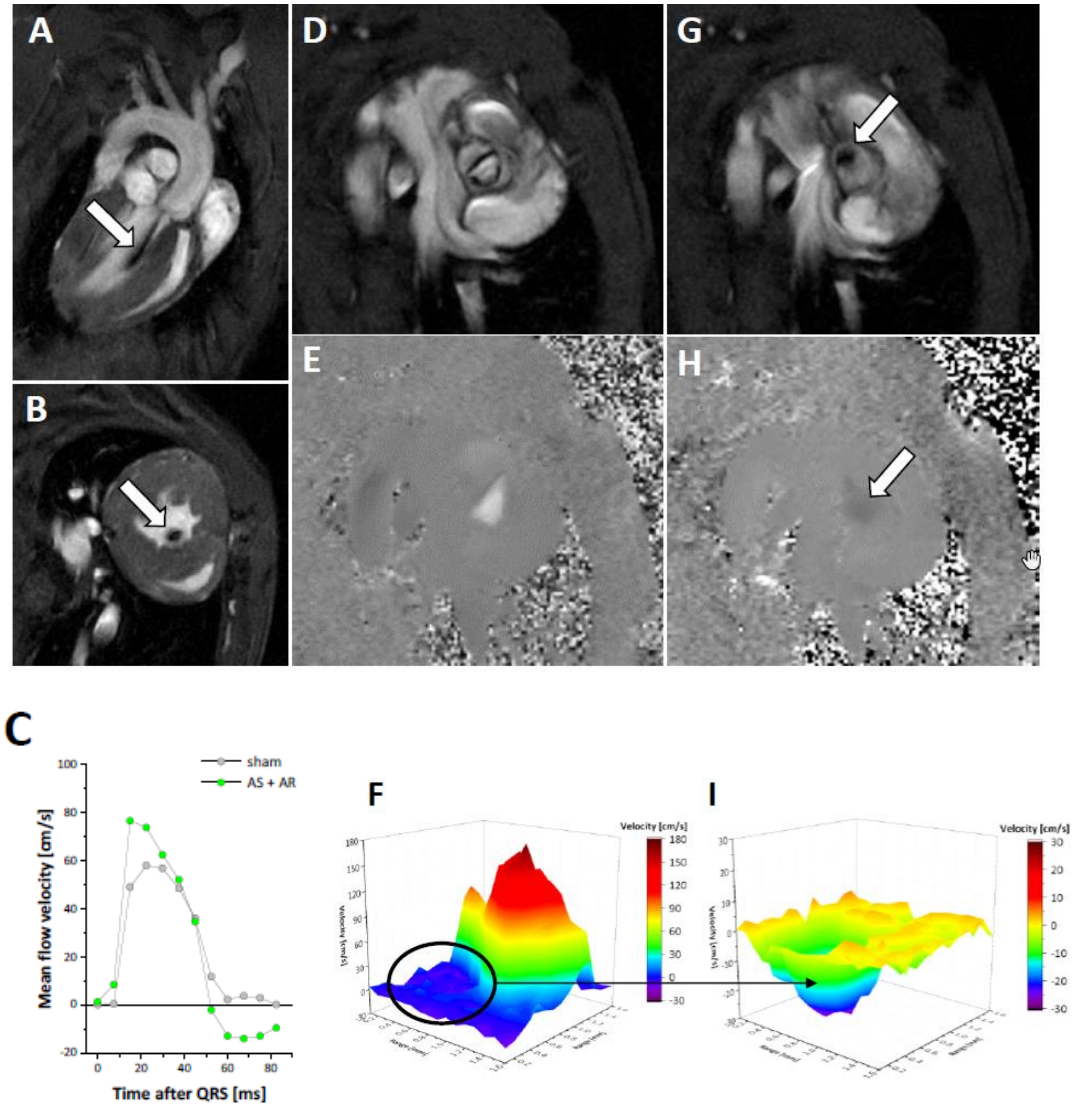

Figure 20 Assessment of aortic regurgitation by magnetic resonance imaging
The evaluation of aortic regurgitation was carried out by assessment of backward flow at the beginning of diastole in mice with aortic valve stenosis (AS) and concomitant aortic regurgitation (AR). (A-B) Illustrations of aortic regurgitation jet in long and short slices. Arrows indicating black regurgitation jet. (C) Blood flow analysis over one cardiac cycle revealed negative flow during diastole. (D-G) Backward flow at valvular level in short axis slices, the arrow indicates backflow. (E-H) 2-D velocity maps with the arrow indicate the location of backward flow corresponding to the anatomical map. (F-I) Blood flow velocity is presented as 3D velocity maps. Figures were taken from the original publication (Quast et al., 2022).

Functional alterations of the ascending aorta, due to AS and subsequent turbulent flow was identified by circumferential strain analysis, illustrated in Figure 21. Subsequently, in mice with AS, circumferential strain was significantly increased (sham: 0.16 ± 0.05 %, control: 0.14 ± 0.06 % vs. AS: 0.23 ± 0.07 %, p= 0.0325, p= 0.0153). Moreover, significant increase in aortic wall thickness at the level of aortic valve was observed in AS mice (sham: 0.13 ± 0.01 mm, control: 0.13 ± 0.01 mm vs. AS: 0.16 ± 0.02 mm, p= 0.0003, p= 0.0015) (Figure 21 I). Comparing aortic diameter during systole, we observed significant increase in outer aortic diameter in AS animals compared to sham and control animals (sham: 2.36 ± 0.12 mm, control: 2.36 ± 0.13 mm vs. AS: 2.49 ± 0.11 mm, p= 0.0331, p =0.0494) (Figure 21G).

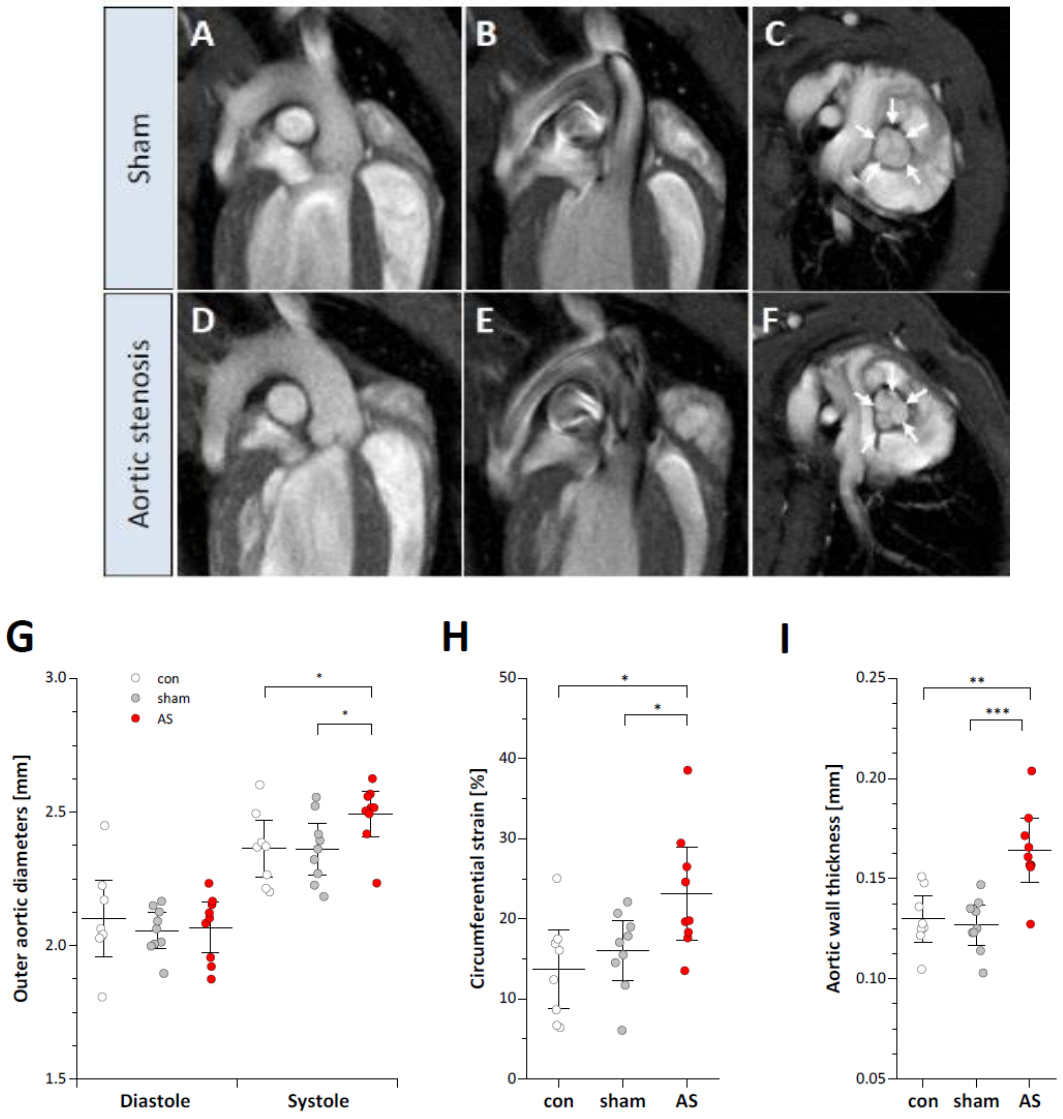

Figure 21 Aortic wall function and morphology
Assessment of aortic wall function and morphology by magnetic resonance imaging in untreated control mice (con), sham animals, and mice with aortic valve stenosis (AS), four weeks after wire-injury. Representative short and long-axis slices and flow conditions in the ascending aorta in sham (A-C) and (D-F) AS mice. White arrows indicate aortic wall thickening on valvular level in AS animals. (G) Outer aortic diameter, (H) circumferential strain of the aortic root, (I) aortic wall thickness measured on aortic valve level. *p<0.05, ** p<0.01, *** p<0.001, control vs. AS, sham vs. AS, unpaired t-test. Data are shown as mean ± SD, n=7-9. Figures were taken from the original publication (Quast et al., 2022).

Furthermore, left ventricular function analysis was performed by short-axis cine loops. Stroke volume (SV), cardiac output (CO), and heart rate (HR) were unchanged, while the LV's hypertrophic changes were indicated by increased diastolic wall thickness (sham: 0.95 ± 0.04 mm, control: 0.95 ± 0.06 mm vs. AS: 1.02 ± 0.05 mm, p=0.0046, p=0.0174).

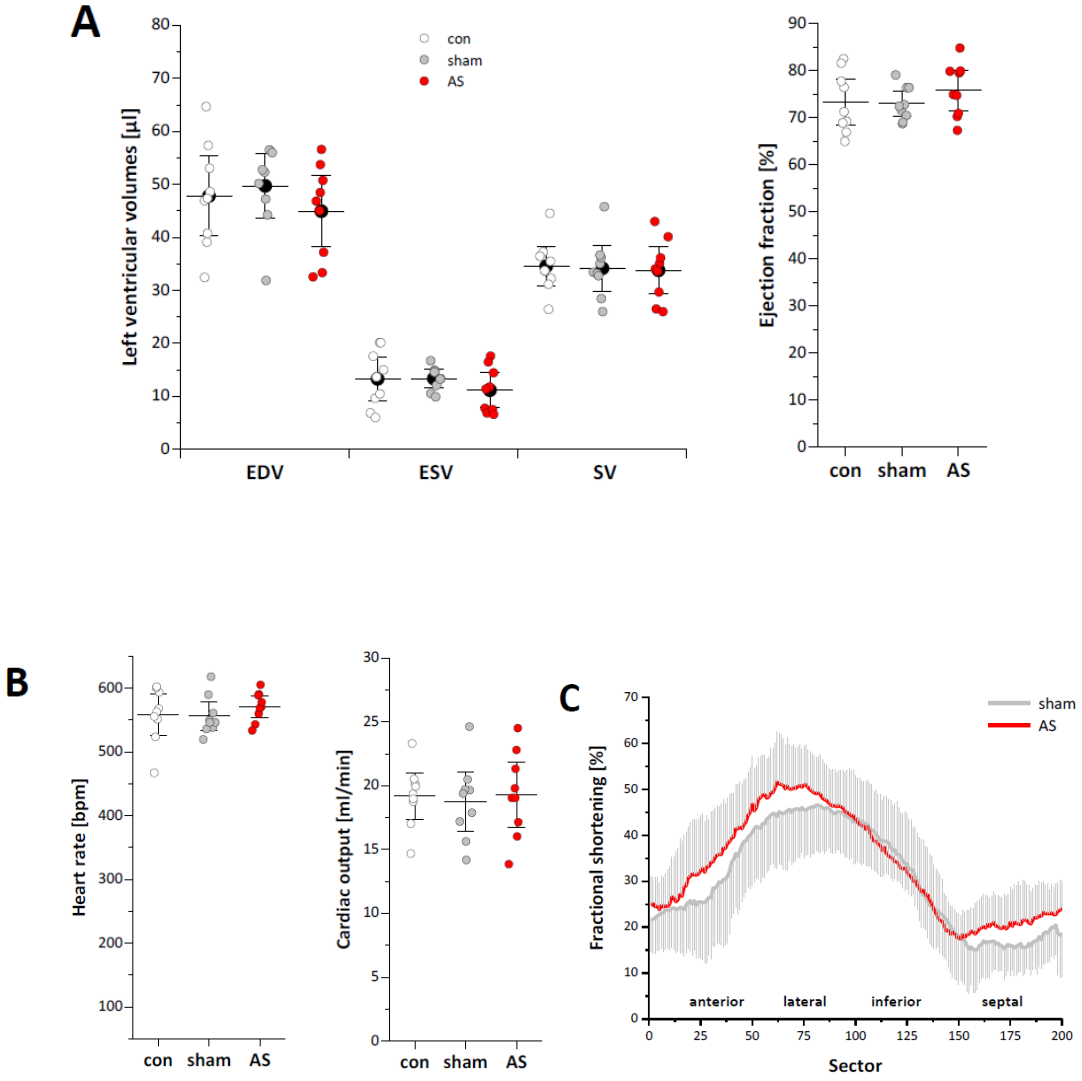

Figure 22 Mice with aortic valve stenosis showed preserved left ventricular function
Magnetic resonance imaging analysis of left ventricular functional parameters in control (con), sham and mice with aortic valve stenosis (AS). (A) Stroke volume (SV), end-diastolic volume (EDV), end-systolic volume (ESV), ejection fraction and (B) heart rate and cardiac output. (C) Sectorial analysis of fractional shortening. p<0.05, unpaired t-test, control vs. AS, sham vs. AS. Data are shown as mean ± SD, n=7-9. Figures were taken from the original publication (Quast et al., 2022).

Cardiac tissue characterization by T1 and T2 mapping revealed significantly reduced values for both parameters in AS (Figure 23). This demonstrates the absence of myocardial edema at this time point (Myocardial T1: sham: 981.23 ± 88.04 ms, control: 989.17 ± 103.27 ms vs. AS: 790.85 ± 135.77 ms, Myocardial T2: sham: 19.36 ± 0.91 ms, control: 19.64 ± 1.72 ms vs. AS: 16.82 ± 2.14 ms, p= 0.0082, p= 0.0128).

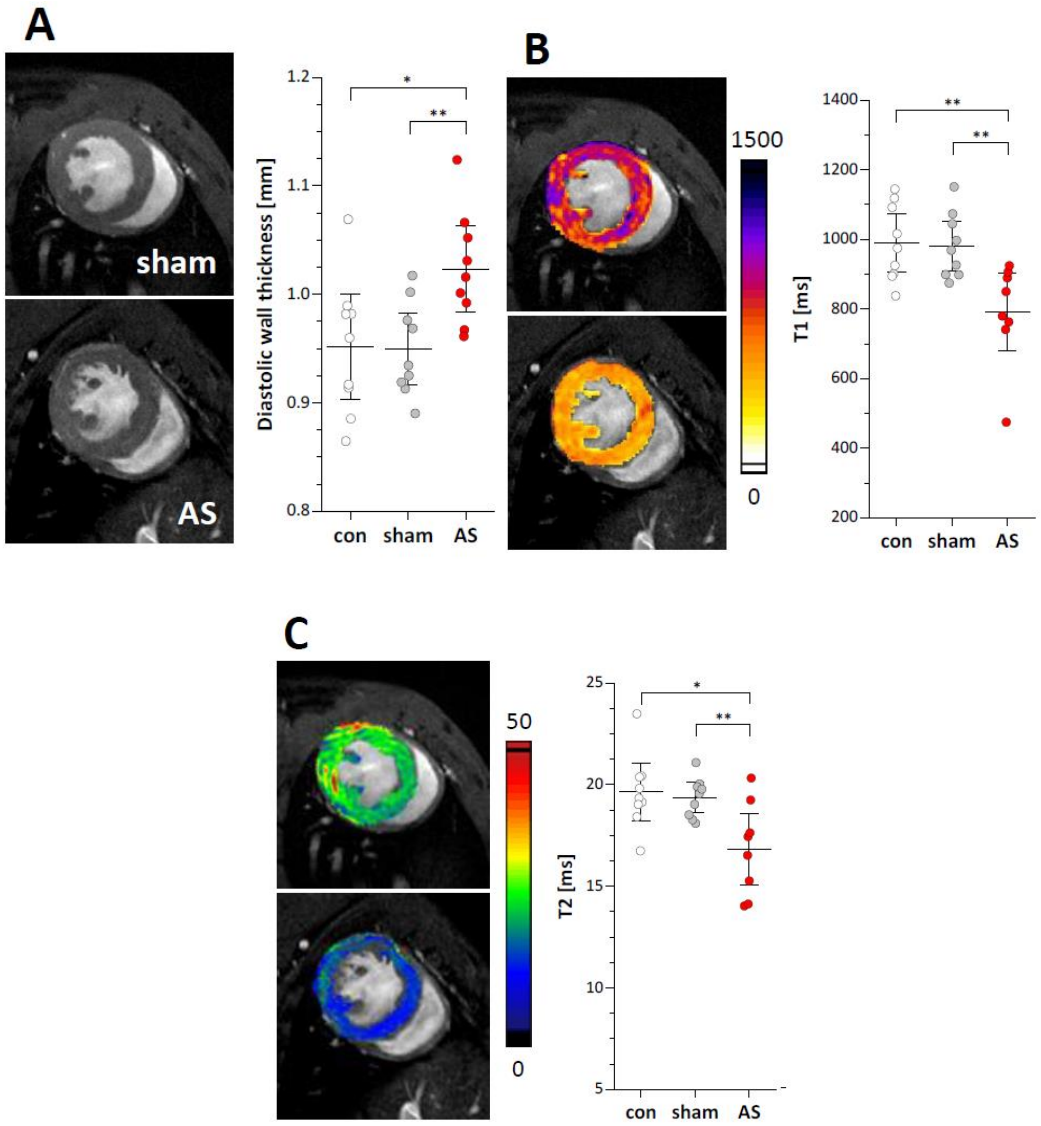

Figure 23 Assessment of structural adaptions to aortic valve stenosis.
Magnetic resonance imaging analysis was used to assess the left ventricular diastolic wall thickness (short axes) (A). Ventricular texture was assessed by T1 and T2 mapping in control (con), sham and mice with aortic valve stenosis (AS) (B-C). *p<0.05, **p<0.01, unpaired t-test, control vs. AS, sham vs. AS. Data are shown as mean ± SD, n=7-9. Figures were taken from the original publication (Quast et al., 2022).

4.1.4 Pressure- volume loop analysis revealed left ventricular pressure overload in AS animals

Since echocardiography and MRI were used to assess changes in valvular, aortic, and left ventricular function, we used pressure-volume loop analysis to confirm pressure load of the LV. Of note, the measurement was performed from the apical side of the heart in an open-chest approach. Four weeks after wire-injury, mice showed a significant increase in left ventricular end-systolic pressure (sham: 93.25 ± 5.07 mmHg vs. AS: 124.90 ± 6.78 mmHg, p=0.0109) and end-diastolic pressure (sham: 23.00 ± 1.68 mmHg vs. AS: 30.78 ± 1.97 mmHg, p=0.0264). Moreover, a significant increase in maximal pressure rise (max dP/dt) was observed (sham: 4005.0 ± 448.4 mmHg/s vs. AS: 6448.0 ± 727.0 mmHg/s, p=0.0428). Stroke volume and heart rate did not differ significantly (Figure 24).

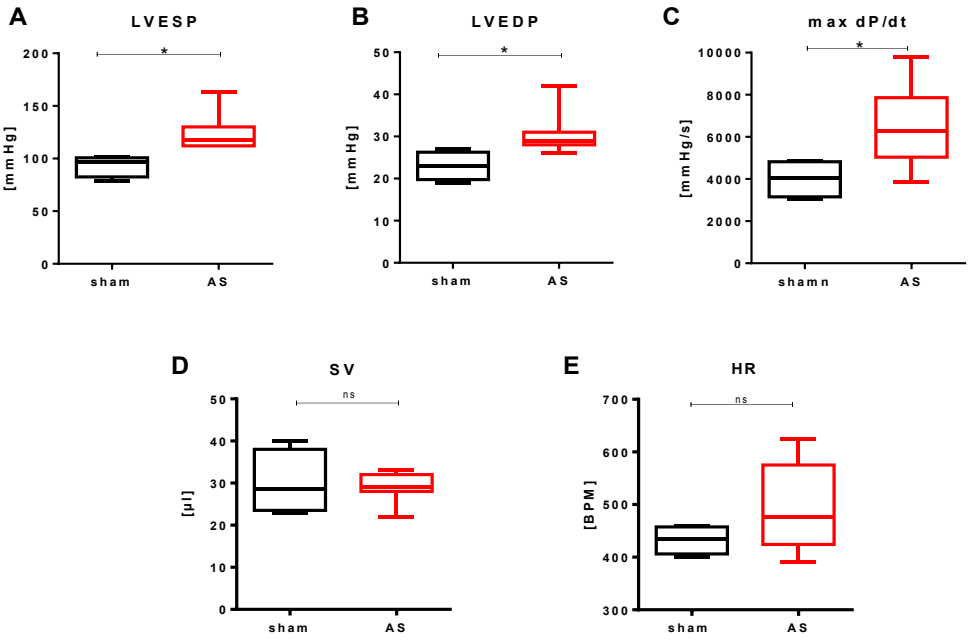

Figure 24 Pressure volume relationship in stenotic mice after wire-injury
Pressure volume analysis was performed by left ventricular catheterization from the apical side in an open chest approach. (A) Left ventricular end-systolic pressure (LVESP), (B) left ventricular end-diastolic pressure (LVEDP) and (C) maximal pressure rise during isovolumetric contraction (dP/dtmax), (D) stroke volume (SV) and (E) heart rate (HR). Presented as box-plot. *p<0.05, unpaired t-test, sham n=4, AS n=7.

4.2 Wire-injury induced significant aortic valve thickening

To analyze morphological changes after wire-injury, aortic valves tissue sections were stained and imaged. Hematoxylin- Eosin staining showed significant leaflet thickening in mice with AS after four weeks (sham: 39.40 ± 4.64 µm vs. AS: 103.80 ± 19.86 µm, p=0.0007) and after three months (sham: 53.32 ± 2.61 µm vs. AS: 120.60 ± 20.15, p=0.0468 µm) compared to age-matched sham animals (Figure 25).

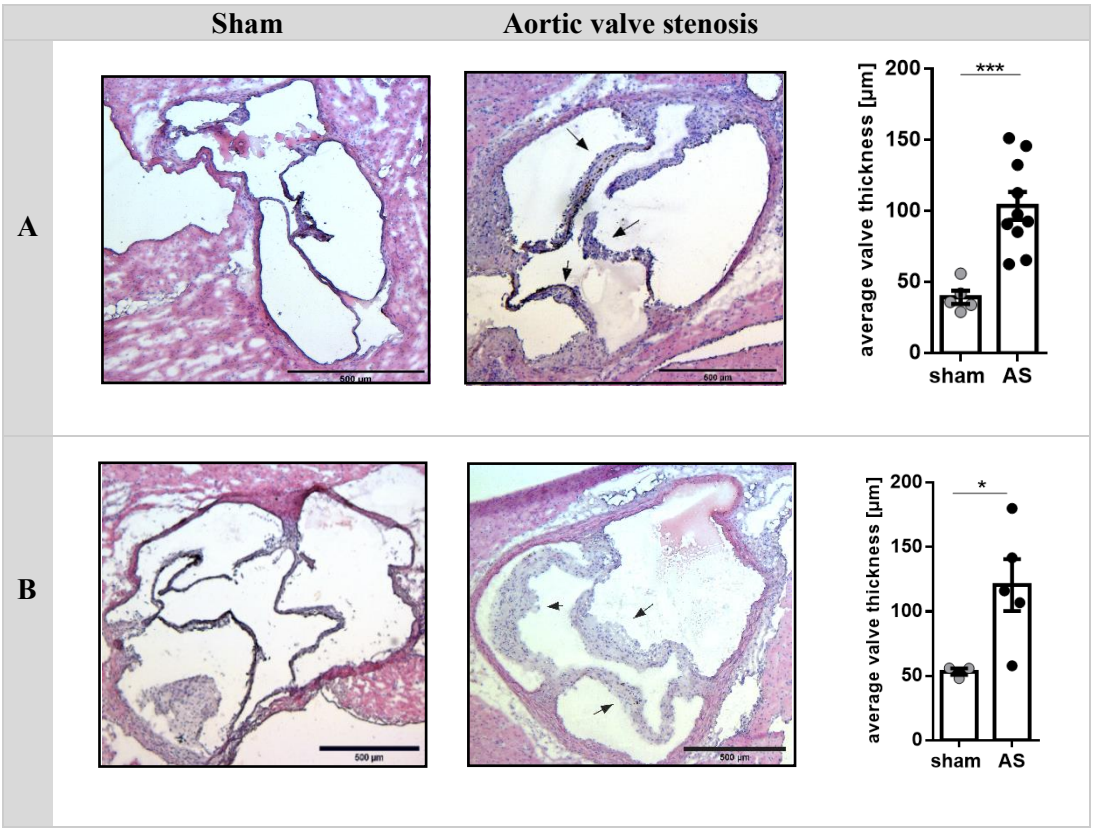

Figure 25 Histological analysis and quantification of aortic valves after wire-injury
Hematoxylin-eosin (HE) staining of aortic valve cross-sections were used to analyze aortic valve thickening after wire-injury. Representative HE images of aortic valve's cross-sections of sham and mice with aortic valve stenosis (AS) after (A) four weeks and after (B) three months after wire-injury. The average thickness was quantified at the maximal leaflet width of each valvular leaflet. **p<0.01, sham vs. AS, unpaired t-test. Data are shown as mean ± SEM, sham n=3-5, AS n=5-10.
Scale bar=500 µm.

Our previously published data, described mild, moderate and severe wire-injury and its valvular consequences illustrated in Figure 26 (Niepmann et al., 2019). Von Kossa staining revealed significant calcium depositions in mice with severe AS. Significant infiltration of CD68 positive macrophages into valvular leaflets was evident in stenotic valves in comparison to sham mice (Figure 26 B, F). Moreover, Sirius-Red staining showed fibrotic changes in moderate and severe stenosis (Figure 26 C, G). Taken together, manipulation of the aortic valve by wire-injury induced relevant AS, which was demonstrated by a significant increase in aortic peak velocities, pressure gradients, restricted valve opening and turbulent blood flow in the ascending aorta. Left ventricular function analysis showed mild myocardial hypertrophy as an adaptive response to pressure overload. Moreover, histological analysis of the aortic valve revealed fibrotic and inflammatory changes of the aortic valve leaflets.

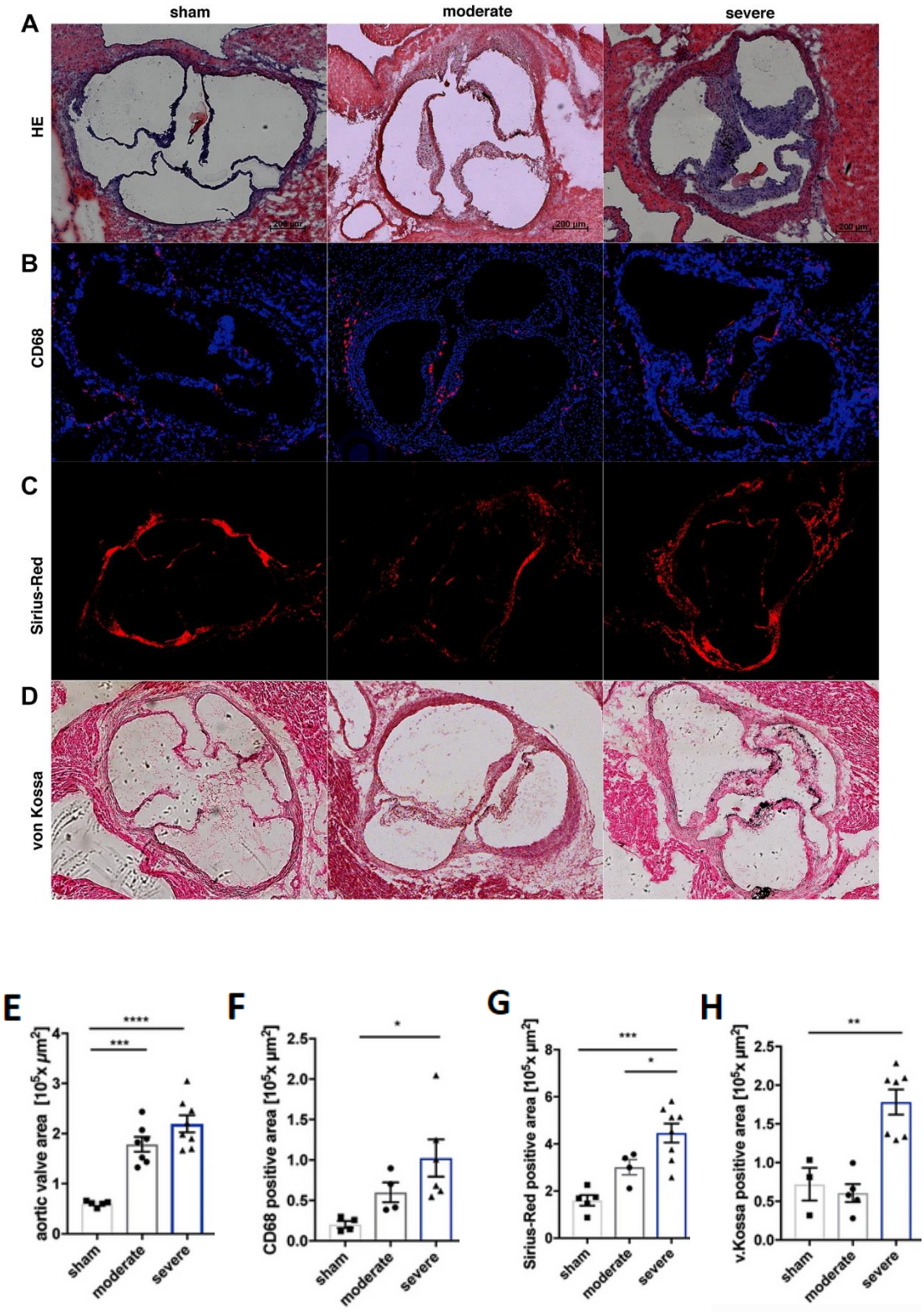

Figure 26 Histological changes of the aortic valve after wire- injury.
Representative histological images of aortic valve cross-sections after wire-injury or sham surgery, respectively. (A) Hematoxylin-eosin staining, (B) immunofluorescence anti- CD68 staining, (C) Sirius- Red staining and (D) von Kossa staining. (E-F) Quantitative analysis of positive valve area. Figures were taken from the original publication (Niepmann et al., 2019).

4.3 Aortic valve stenosis in global eNOS KO mice

Several studies have demonstrated that valvular endothelium-derived NO plays a critical role in the disease progression of AS (Richards et al., 2013b) and that eNOS KO mice are more prone to fibrotic alterations of the aortic valve (El Accaoui et al., 2014). Based on these studies, we hypothesized that progression of AS induced by wire-injury is faster and more severe in eNOS KO mice than in WT mice. Thus, the characterization of AS in eNOS KO mice was integrated into the first aim of this thesis. FMD studies were performed to verify loss of endothelium-derived NO in global eNOS KO mice (maximal change in vessel diameter WT: 22.15 ± 1.27 % vs. eNOS KO: 4.16 ± 1.10 % $p<0.0001$). Examination of blood pressure confirmed significant increase in diastolic blood pressure (WT: 55.00 ± 3.51 mmHg vs. eNOS KO: 72.00 ± 1.00 mmHg, $p=0.0096$) and systolic blood pressure (WT: 82.0 ± 3.1 mmHg vs. eNOS KO: 107.7 ± 0.3 mmHg, $p=0.0011$), with a decrease in heart rate (WT: 474.0 ± 30.5 bpm vs. eNOS KO: 371.3 ± 12.00 bpm, $p=0.0352$). Next, we analyzed whether the progression of AS was accelerated compared to WT mice. Surprisingly, there were no significant differences between eNOS KO mice and WT mice regarding peak velocities (WT: 216 ± 92.75 mm/s vs. eNOS KO: 2161.0 ± 119.5 mm/s), peak pressure gradients (WT: 16.8 ± 2.7 mmHg vs. eNOS KO: 16.2 ± 1.5 mmHg), or mean pressure gradients (WT: 5.8 ± 1.6 mmHg vs. eNOS KO: 5.6 ± 1.1 mmHg) after four weeks of induction of AS (Figure 27).

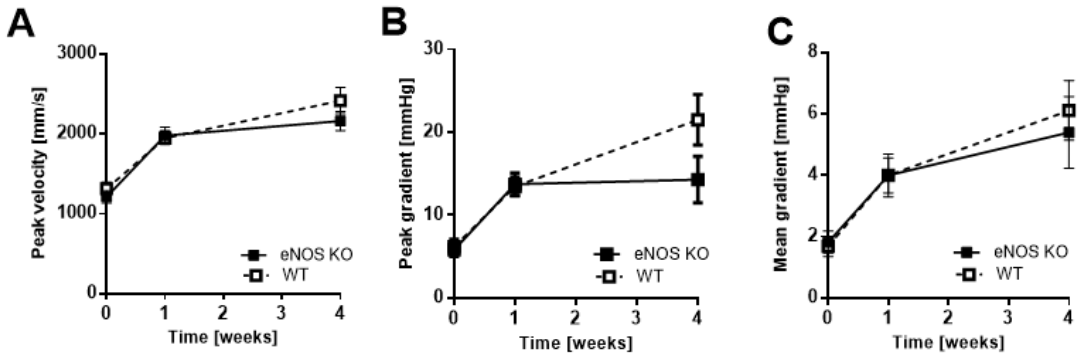

Figure 27 Progression of aortic valve stenosis was similar in eNOS KO and WT mice
The course of (A) flow velocities, (B) peak gradient and (C) mean gradient were assessed in wild type (WT) and global eNOS KO mice four weeks post wire-injury using high- resolution ultrasound in the ascending aorta. Two-way ANOVA, Sidak's multiple comparisons test. Data are shown as mean ± SEM, WT n=5, eNOS KO n=5.

Moreover, cardiac function analysis showed significantly greater interventricular septum sickness (WT: 0.9 ± 0.1 mm vs. eNOS KO: 1.3 ± 0.1 mm), as well as greater isovolumic relaxation time (WT: 8.2 ± 2.7 ms vs. eNOS KO: 18.2 ± 1.7 ms) in eNOS KO mice which underwent wire- injury.

Table 7 Left ventricular function parameters and aortic blood flow velocities assessed in WT and eNOS KO mice with aortic valve stenosis four weeks post wire-injury. WT n=5, eNOS KO n=5. IVS,d: interventricular septum thickness, diastole, LVID,d: left ventricular diameter, E/A: ratio between peak velocities of the early (E) and late (A) ventricular filling.

	unit	WT			eNOS KO			*p*-value
Peak Velocity	mm/s	2166	±	92.8	2161	±	119,5	0,9728
Mean Gradient	mmHg	5.8	±	1.6	5.6	±	1.1	0,9006
Peak Gradient	mmHg	16.8	±	2.7	16.2	±	1.5	0,8674
Heart Rate	bpm	502.4	±	18.0	397.5	±	15.1	***0,0021****
Endsystolic Volume	µl	20.1	±	0.8	15.1	±	3.0	0,1378
Enddiastolic Volume	µl	46.2	±	1.5	42.0	±	6.8	0,5586
Stroke Volume	µl	26.2	±	1.2	26.9	±	4.0	0,8695
Ejection Fraction	%	56.5	±	1.4	64.8	±	1.6	***0,005****
Fractional Shortening	%	13.3	±	2.4	15.5	±	1.9	0,5184
Cardiac Output	µl/min	13.2	±	1.0	10.5	±	1.4	0,1491
IVS, d	mm	0.9	±	0.1	1.3	±	0.1	***0,0031****
LVID,d	mm	3.6	±	0.2	3.4	±	0.24	0,5824
E/A	a.u.	1.4	±	0.1	1.7	±	0.2	0,0895
Isovolumic Contraction Time	ms	10.7	±	3.0	15.8	±	1.6	0,164
Isovolumic Relaxation Time	ms	8.2	±	2.7	18.2	±	1.7	***0,0132****

4.4 Aortic valve stenosis altered red blood cell integrity and increased levels of cell-free hemoglobin

The second aim of this study was to investigate whether wire-induced AS affects RBC integrity and thus induces release of cell-free Hb. Since cell-free Hb is known to be a potent scavenger of NO and may be involved in systemic endothelial dysfunction, we evaluated levels of free Hb in plasma samples. First, blood count analysis was performed to check for potential changes with special regard to total Hb and RBC indices. Blood count did not show any significant changes regarding RBC characteristics four weeks after wire-injury compared to sham animals (Figure 28). Interestingly, AS mice showed a significantly lower platelet number than sham animals (sham: 1508.9 ± 50.0 10^3/mm vs. AS: 1231.7 ± 98.2 10^3/mm, =0.0292). All other parameters remained unchanged (Table 8).

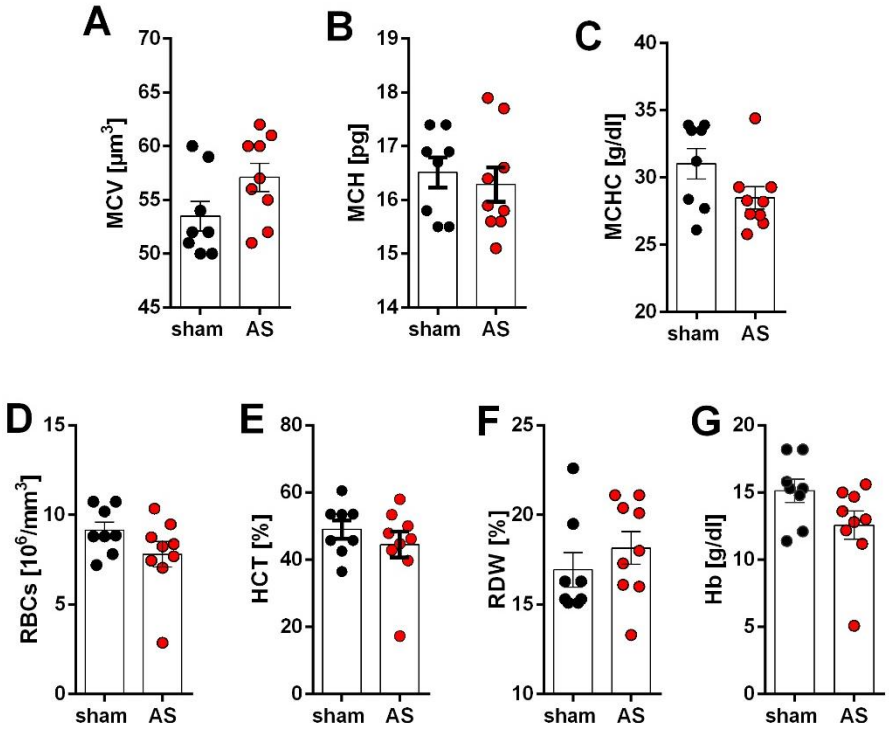

Figure 28 Aortic valve stenosis did not induce serious hemolytic damage
Blood count performed using the vet abc™ animal blood counter four weeks after wire-injury. MCV: mean corpuscular volume (B) MCH: mean corpuscular hemoglobin (C) MCHC: mean corpuscular hemoglobin concentration (D) RBCs: red blood cells, (E) HCT: hematocrit, (F) RDW: red cell distribution width, (G) Hb: hemoglobin. Data shown as mean ± SEM. AS n=9, sham n=8

Table 8 Blood count performed using the vet abc™ animal blood counter. Comparisons between sham and stenotic mice, four weeks after wire-injury. WBC: white blood cells, PLT: platelets MPV: mean platelet volume. Data shown as mean ± SEM. AS n=9, sham n=8

	unit	sham	AS	*p*-value
WBC	$10^3/mm^3$	3.1 ± 0.5	3.0 ± 0.5	0.92
PLT	$10^3/mm$	1508.9 ± 50.	1231.7 ± 98.2	***0.0292**
MPV	μm^3	6.0 ± 0.1	6.2 ± 0.08	0.08
Lymphocytes	%	77.4 ± 2.7	89.9 ± 14.2	0.41
Monocytes	%	4.9 ± 0.2	4.4 ± 0.4	0.25
Granulocytes	%	17.7 ± 2.6	18.3 ± 3.2	0.88

To further check RBCs integrity, we performed FACS analysis of Annexin V and CD71+ positive erythrocytes. Aging, as well as hemolytic conditions, were shown to induce translocation of membrane phosphatidylserine from the intracellular to the extracellular surface (Boas et al., 1998). Annexin V is a high-affinity binding protein to phosphatidylserine. Moreover, the soluble transferrin receptor 1 (CD71) is present on erythroid progenitor cells and reticulocytes due to their high demand for iron. In mice with AS, we observed a significant increase in Annexin V positive RBCs compared to sham mice (sham: 0.16 ± 0.01 % vs. AS: 0.92 ± 0.17 %, p=0.018 (Figure 29). The amount of CD71+ positive cells did not change significantly (Figure 29 B). Importantly, the analysis of plasma cell-free Hb levels revealed a 2.3-fold increase in AS animals compared to sham mice (sham: 9.07 ± 2.01 mg/ml vs. AS: 21.09 ± 1.92 mg/ml, p=0.0018). To further evaluate whether reduced RBC integrity leads to red blood cell functional changes in our model of AS, RBCs deformability was investigated. There were no changes regarding red blood cell deformability between sham and AS animals after four weeks (Figure 29). Maximal elongation (EI_{max}) was similar in both experimental groups (sham: 0.57 ± 0.008 vs. AS: 0.57 ± 0.003). Likewise, shear forces to reach half-maximal elongation ($SS_{1/2}$) did not differ (Figure 29). Of note, the increase in plasma cell-free Hb did not substantially differ between four weeks and three months (2.3-fold vs. 1.8-fold increase).

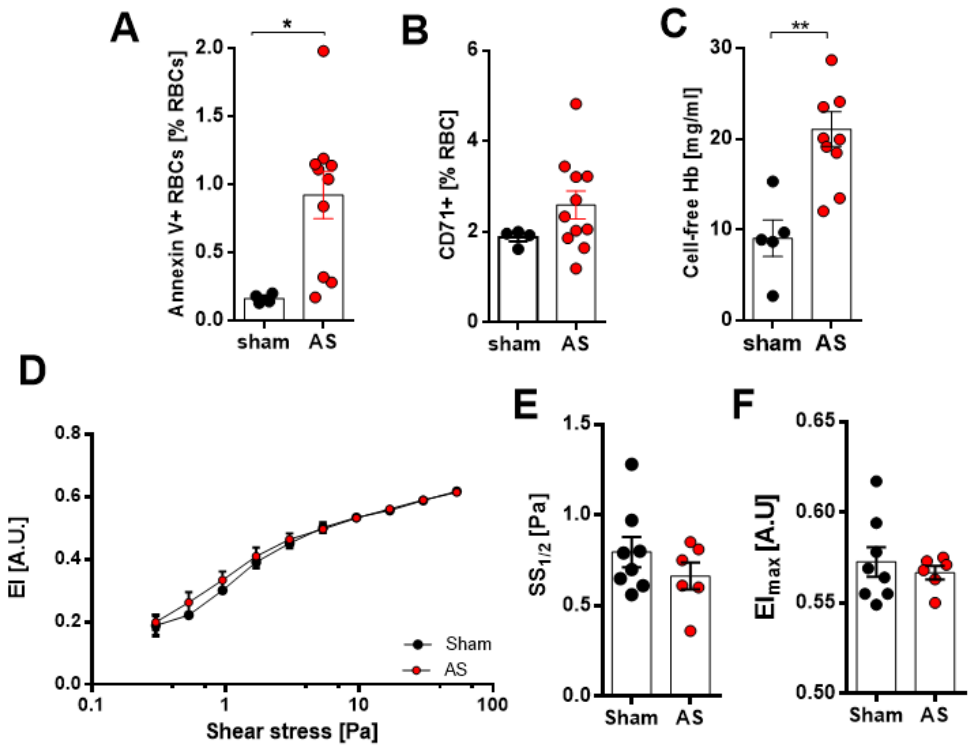

Figure 29 Cell-free haemoglobin was increased in aortic valve stenosis, whereas red blood cell deformability was preserved

The amount of Annexin V (A) and CD71 (B) positive red blood cells (RBCs) were analyzed by flow cytometry. (C) Cell-free hemoglobin was measured in plasma of sham and mice with aortic valve stenosis (AS) by enzyme-linked immunosorbent assay. RBCs deformability was studied by ektacytometry under increasing shear stress in a laser-assisted optical rotational cell analyzer (LORCA). (D) The deformability was expressed as elongation index (EI), describing the ratio between the horizontal and vertical axis of the red blood cells during deformation from the biconcave to the ellipsoid shape. (E) Half-maximal deformability ($SS_{1/2}$) and (F) maximal deformability (EI_{max}). Statistics were performed by one-way ANOVA, Sidak's multiple comparisons test, and unpaired t-test. Data shown as mean ± SEM, n=6-11 *p<0.05, *p<0.01.

4.5 Nitric oxide metabolism

The well-known deoxygenation reaction describes the reaction of NO with oxyHb under the formation of and Hb(Fe^{3+}) and NO_3^-. To further investigate the findings of altered RBC integrity with respect to dysregulation of NO metabolism, we investigate the concentrations of NO metabolites' NO_2^-, NO_3^- , RXNO in tissue and plasma four weeks after wire-injury. The data showed no significant differences in NO_2^- concentrations in the heart (sham: 2173 ± 14.03 nM vs. 2182 ± 20.11 nM) and aorta (sham: 41.93 ± 8.10 nM vs. AS: 5.31 ± 3.92), whereas in liver a decrease (tendency) in NO_2^- concentration was observed in mice with AS (sham: 608.8 ± 251.4 nM vs. AS: 338.7 ± 114.0 nM). The RXNO concentrations in analysed tissues were not significantly different between sham and stenotic mice (Figure 30 C-D). Plasma analysis found no differences in NO_2^- (sham: 376.1 ± 110.9 nM vs. AS: 369.6 ± 112.3 nM) or RXNO concentrations (sham: 3.38 ± 2.02 nM vs. AS: 4.31 ± 1.01 nM) between the experimental groups. Moreover, NO_3^- concentrations tend to increase in the plasma of AS mice (sham: 11.4 ± 2.49 µM vs. AS: 15.98 ± 2.41 µM). The data are summarized in Figure 30.

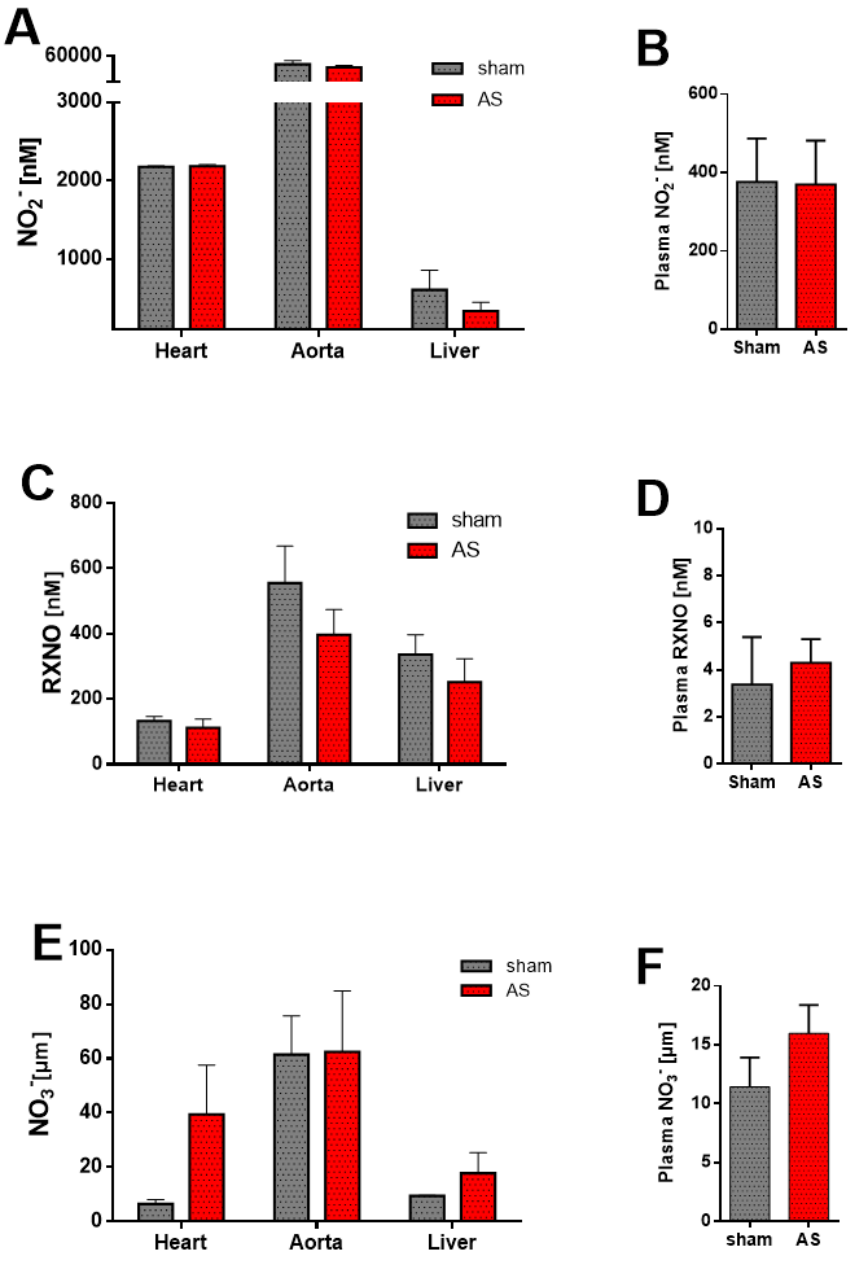

Figure 30 Effects of aortic valve stenosis on nitrate, nitrite and RXNO concentrations in plasma and tissues.
Concentrations of nitrite (NO_2^-), nitrate (NO_3^-) and nitrosation products (RXNO) were assessed by chemiluminescence detection or high performance liquid chromatography (ENO-30), four weeks after wire-injury or sham surgery, respectively. (A-B) Concentrations of nitrite, (C-D) RXNO and (E-F) nitrate were investigated in heart, aorta, liver and plasma of sham mice and mice with aortic valve stenosis (AS). Unpaired t-test. Data shown as mean ± SEM, plasma n=12, heart n=3-5, aorta n=4, liver n=3-5.

4.6 Flow-mediated dilation studies revealed endothelial dysfunctional phenotype in stenotic mice

This work aimed to investigate the hypothesis that turbulent blood flow conditions in AS induce mechanical damage to RBCs with increase in cell-free Hb, thus leading to scavenging of NO and therefore reduction of NO bioavailability. The results described in the previous sections found clear support for an altered RBC integrity with concomitant increase in cell-free Hb. Therefore, according to the third aim of this study, we investigated in the following section the systemic effects of wire-induced AS on peripheral endothelial function *in vivo*, by measuring FMD in the left femoral artery.

To conduct an intraindividual analysis, we initially assessed FMD under baseline conditions and repeated the measurements four weeks after surgery in the same mice. Afterwards, we compared the FMD data from sham animals with AS animals to obtain an interindividual analysis after four weeks. Changes in diameter and flow velocities were continuously recorded. We observed significant impairment of FMD in mice with AS, four weeks after wire-injury compared to baseline conditions (maximal change in vessel diameter: baseline 22.15 ± 1.27 % vs. four-weeks 14.4 ± 1.08 %, p=0.0019, Figure 31A-C) and compared to age- matched sham animals after four weeks (maximal change in vessel diameter: sham 18.93 ± 1.57 % vs. AS 14.00 ± 0.68 %, p=0.0085, Figure 31 G-I). In contrast, no changes in FMD were observed in sham animals between baseline conditions and four weeks after sham surgery (Figure 31 D-F). Interestingly, the analysis did not show differences in flow velocities after vessel occlusion in sham and AS animals (Figure 31).

To confirm that the impaired FMD is eNOS-dependent, we applied the competitive eNOS inhibitor L-NAME 30 minutes prior to FMD measurement. The inhibitor L-NAME abolished vasodilator response after reperfusion in sham (maximal change in vessel diameter: sham 18.93 ± 1.57 % vs. sham+ L-NAME 4.66 ± 4.05 %, p=0.0024) and AS animals (maximal change in vessel diameter: AS 14.00 ± 0.68 % vs. AS+L-NAME 3.61 ± 1.84 %, p<0.0001), referring to Figure 31 G-I. In line with these findings, blood flow velocities were significantly decreased during the reperfusion phase, compared to blood flow velocities in the absence of L-NAME.

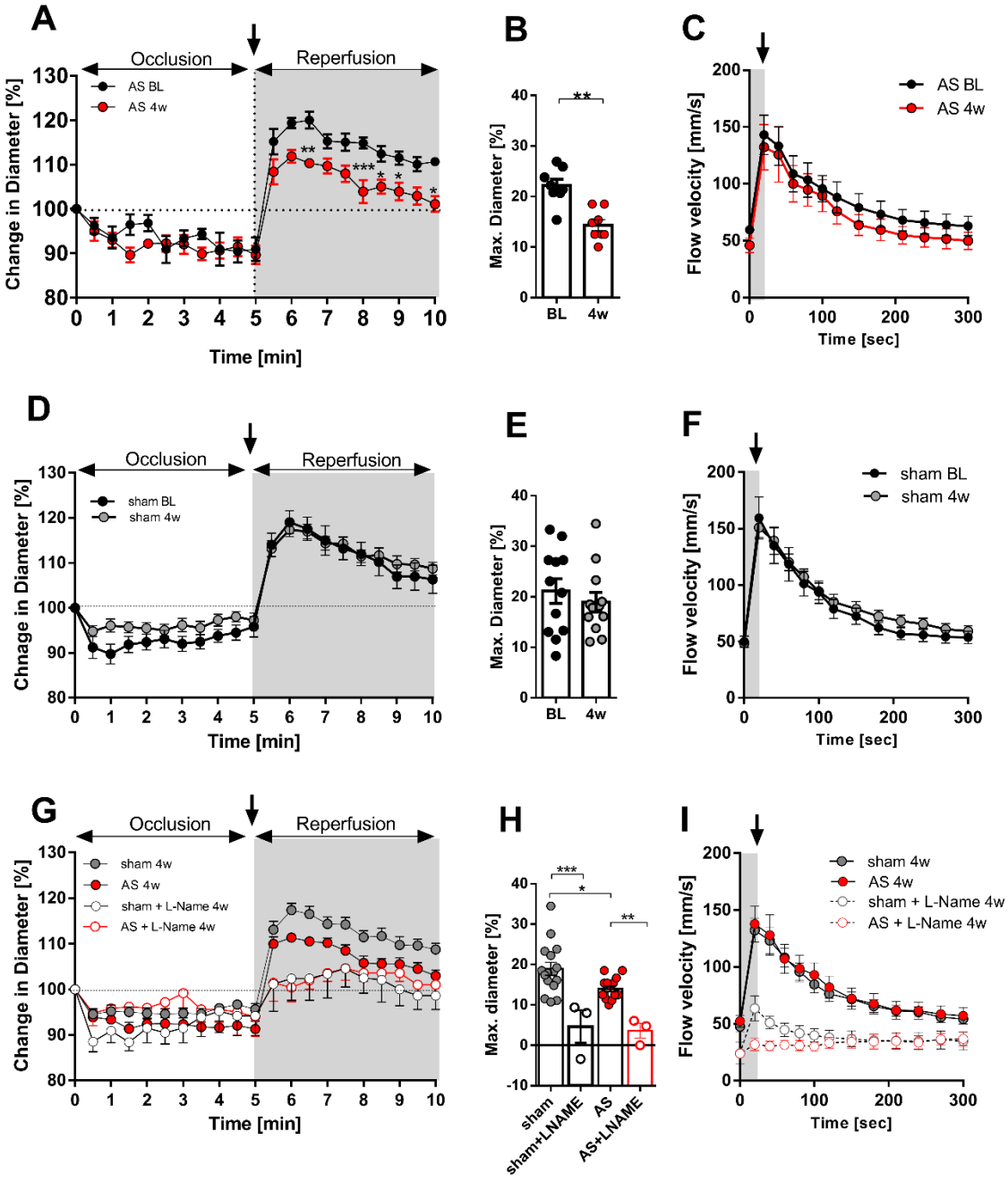

Figure 31 Aortic valve stenosis was accompanied by impaired flow-mediated dilation
Endothelial function was studied by flow mediated dilation (FMD) in the left femoral artery after five minutes hindlimb occlusion. Change in vessel diameter and blood flow velocity during reperfusion phase was compared before (baseline conditions) and four weeks (4w) after induction of aortic valve stenosis (AS) (A-C) or sham surgery (D-F) and after four weeks following treatment with N^G-nitro-L-arginine methyl ester (L-NAME**).** Arrows indicating cuff opening. Statistics performed by paired t-test and two-way ANOVA, Sidak's multiple comparisons test, p*<0.05, p**<0.01, p***<0.001. Data shown as mean ± SEM. AS n=8-15, sham n=16,AS+L-NAME n=3, sham+L-NAME n=3

A further marked decline of FMD was observed in mice three months after induction of AS (maximal change in vessel diameter: sham 17.25 ± 2.15 % vs. AS 6.18 ± 1.68 %, p=0.0007, Figure 32). However, the analysis of recorded flow velocities tend to be decreased in mice that underwent wire-injury (Figure 32C).

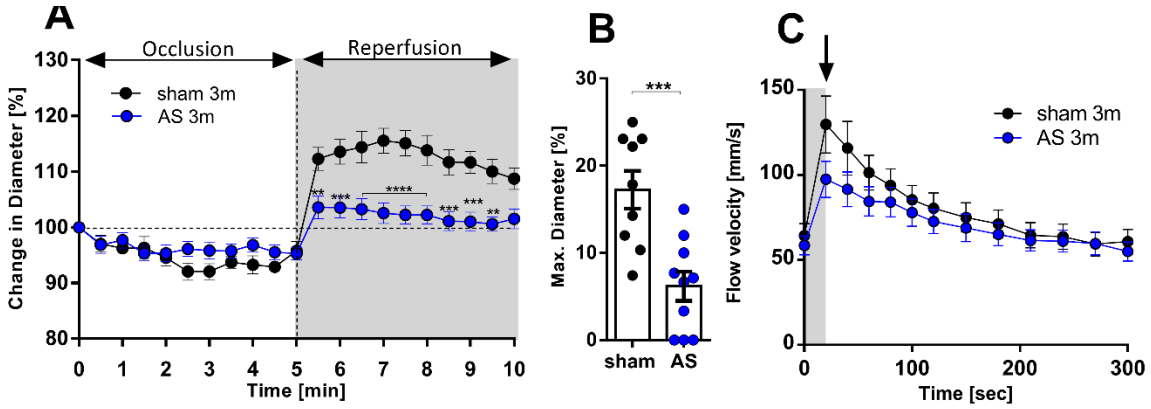

Figure 32 Flow- mediated dilation was further impaired in stenotic mice three months after wire-injury.
Endothelial function was studied by flow mediated dilation (FMD) in left femoral artery after five minutes hindlimb occlusion. Change in vessel diameter and blood flow velocities during the reperfusion phase was compared between sham mice and mice with aortic valve stenosis (AS), three months (3m) after wire-injury or sham surgery, respectively. Arrow indicating cuff opening. Statistics performed by paired t-test and two-way ANOVA, Sidak's multiple comparisons test. p**<0.01, p***<0.001, p****<0.0001. Data shown as mean ± SEM, n=9-10.

The assessment of baseline femoral artery diameter did not differ between the different groups (Figure 33). Moreover, we measured pulse-wave velocity (PWV) as a function of arterial stiffness. PWV did not significantly change in sham and AS mice after four weeks, but was significantly increased in mice three months after wire-injury (sham: 0.95 ± 0.06 mm/ms vs. AS: 1.64 ± 0.36 mm/ms, p=0.0135). Comparing these data between four weeks and three months old AS animals, there was a further significant increase in PWV (four weeks AS: 0.58 ± 0.12 mm/ms vs. three months AS: 1.64 ± 0.36 mm/ms, p=0.002).

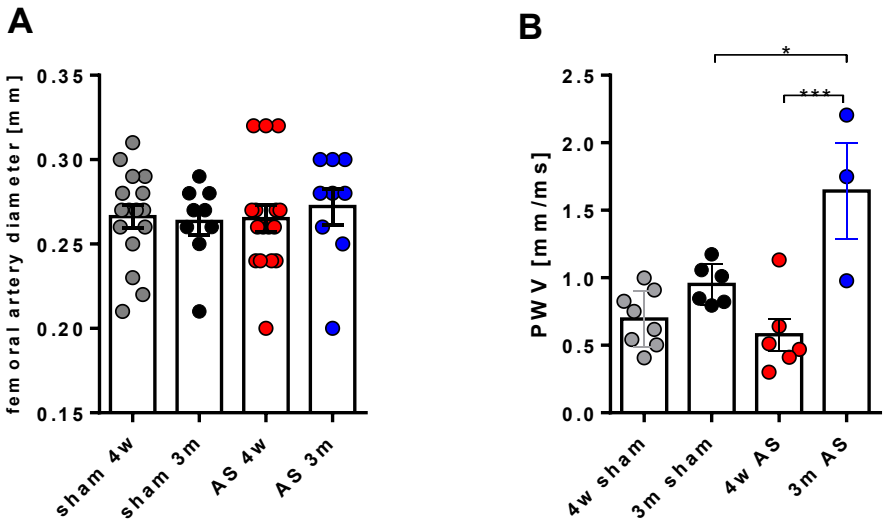

Figure 33 Arterial Stiffness increased in age-dependent manner in animals with aortic valve stenosis
(A) Baseline femoral artery diameter was assessed by high resolution ultrasound before cuff occlusion during flow- mediated dilation studies. (B) Arterial vessel stiffness was carried out by measurement of the pulse-wave velocity (PWV) in the common carotid artery. Data were assessed after four weeks (4w) and after three months (3m) in sham mice and mice with aortic valve stenosis (AS). Statistics performed by pearson correlation, one-way ANOVA, Sidak's multiple comparisons test. $p<0.05$, ***$p<0.001$. Data shown as mean ± SEM, n=3-16.

In summary, *in vivo* analysis of endothelial function revealed an endothelial dysfunctional phenotype in mice with AS. Impairment of FMD showed further deterioration with increasing age of AS animals and concomitant increase in vascular stiffness.

4.7 Haptoglobin improved endothelial flow- mediated dilation in aortic valve stenosis

To investigate whether the increase in cell-free Hb limits NO induced VSMCs relaxation due to scavenging of NO, we performed a regain of function experiment with Hp, the physiological scavenger of cell-free Hb. We found that administration of Hp resulted in significant increase in maximal vessel diameter during the first minute of reperfusion phase in AS animals compared to untreated AS mice (AS: 13.99 ± 0.68 % vs. AS+Hp: 18.97 ± 3.53 %, $p=0.0407$), while there were no differences between untreated AS mice and vehicle control. Interestingly, flow velocities during reperfusion showed no significant differences in all groups (Figure 34 C.)

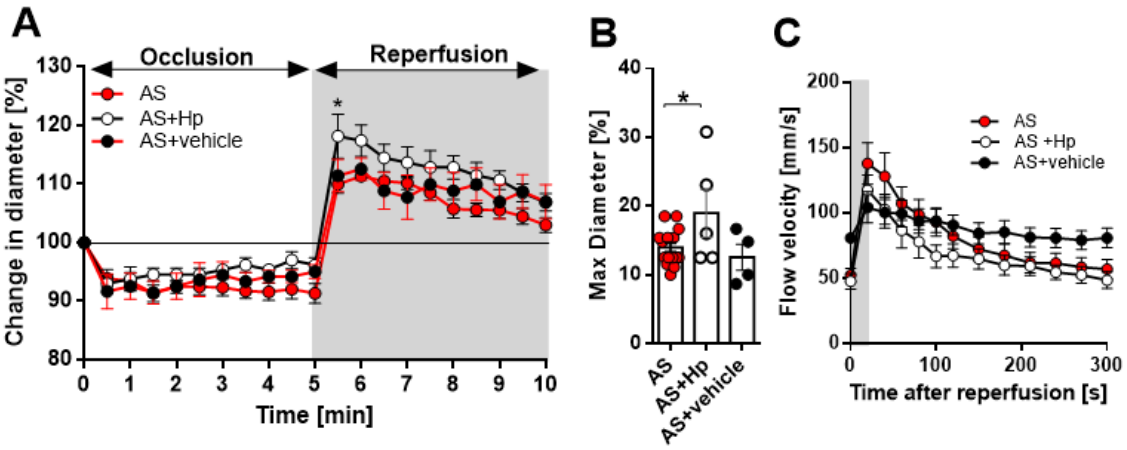

Figure 34 Haptoglobin improved flow-mediated dilation in mice with aortic valve stenosis
Femoral artery endothelial function was assessed by flow-mediated dilation (FMD) after five minutes occlusion of the left hind limb, four weeks after wire-injury. (A-C) Changes in vessel diameter and blood flow velocities during the reperfusion phase were compared between mice with aortic valve stenosis (AS), AS mice treated with haptoglobin (AS+ Hp) and AS mice treated with vehicle (AS+ vehicle). Statistics performed by paired t-test and two-way ANOVA, Sidak's multiple comparisons test.*p<0.05. Data shown as mean ± SEM. AS n=15, AS+ Hp n=5, AS+ vehicle n=4.

Moreover, assessment of blood pressure did not show any differences between sham and AS mice. Calculation of mean arterial pressure and systemic vascular resistance revealed no changes (Figure 35).

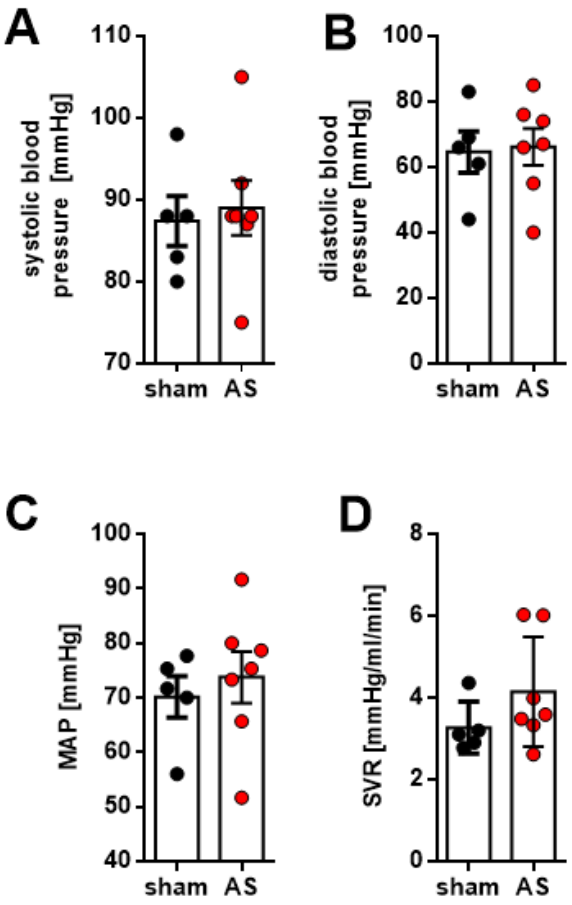

Figure 35 Mean arterial pressure and systemic vasculare resistance were unchanged in mice with aortic valve stenosis.
Pressure at end systole (A) and diastole (B), (C) mean arterial pressure (MAP) and (D) systemic vascular resistance (SVR) were assessed by invasive catheterization of the ascending aorta of sham and mice with aortic valve stenosis (AS), four weeks after wire-injury. Statistics performed by unpaired t-test. Data shown as mean ± SEM, n=5-7.

4.8 Ex vivo femoral artery vasodilator and vasoconstrictor function was preserved in aortic valve stenosis

To investigate whether AS also affect receptor-induced endothelium-dependent relaxation responses, segments of femoral arteries were subjected to vascular reactivity studies in an organ bath setting. First, vasoconstriction response to phenylephrine were analyzed. Sensitivity and maximal constriction to phenylephrine were comparable in sham and mice with AS after four weeks, as well as after three months after wire-injury (E_{max}: after four weeks: sham: 93.7 ± 15.1 % vs. AS: 88.2 ± 12.1 %, Figure 36 A, after three months: sham: 100.9 ± 4.3 % vs. AS: 94.8 ± 15.8 %, Figure 36 D). Acetylcholine-induced maximal relaxing responses were similar between two experimental groups at both time points (E_{max}: after four weeks: sham: 98.7 ± 3.2 % vs. AS: 101.4 ± 1.1 %, Figure 36 B, after three months: sham: 102.9 ± 1.6 % vs. AS: 99.97 ± 1.2 %, Figure 36 E). Experiments were performed in the presence of COX inhibitor indomethacin.

In order to identify the amount of eNOS- dependent dilation in femoral artery, segments were incubated with eNOS inhibitor L-NAME, as described previously. After four weeks, acetylcholine-induced maximal relaxation responses were attenuated but happened to a similar extent in sham and AS mice (sham: 78.2 ± 5.6 % vs. AS: 81.73 ± 5.8 %). Similar results were observed after three months: L-NAME decreased maximal relaxation response to acetylcholine to a similar extent in sham and AS animals (sham: 68.1 ± 8.5 % vs. AS: 53.4 ± 9.4 %). As shown in Figure 36A, C maximal constriction responses to phenylephrine remained unaffected by L-NAME in all groups. Furthermore, the sensitivity of femoral arterial segments to phenylephrine and acetylcholine were comparable in AS and sham animals at both time points (four weeks vs. three months, Table 9). In addition, endothelium-independent response to NO donor SNP and thus the sensitivity of vascular smooth muscle cells, revealed no differences between the two experimental groups after four weeks (E_{max}: sham: 100.9 ± 1.1 % vs. AS: 101.9 ± 2.4 %, $LogEC_{50}$ sham:-6.966 M vs. AS:-7.023 M) and three months (E_{max}: sham: 106.9 ± 2.9 % vs. AS: 93.5 ± 12.6 %, $LogEC_{50}$ sham: -7.032 M vs. AS: -7.043) (Figure 36 C, F)

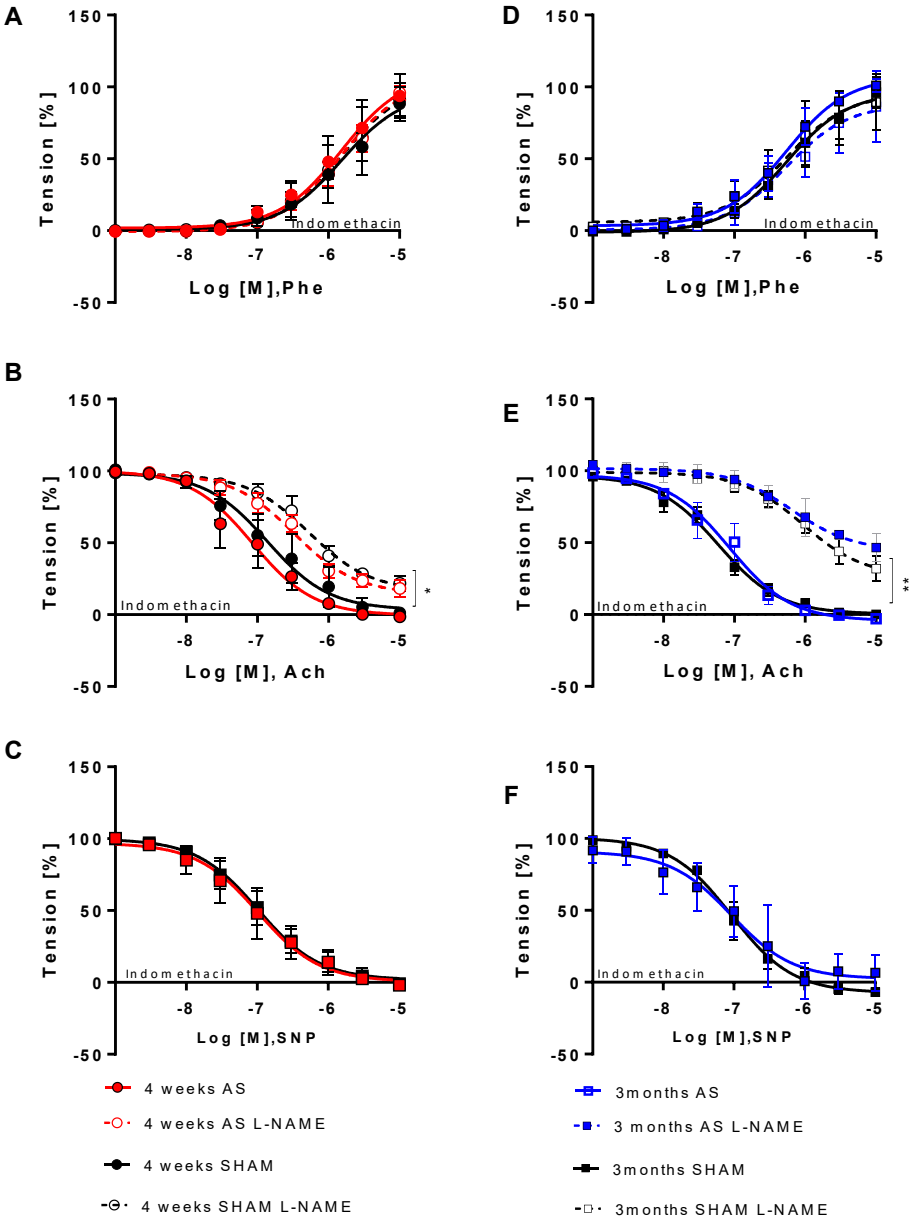

Figure 36 Femoral artery vascular function was preserved in aortic valve stenosis
Phenylephrine (Phe) induced contractile responses. Acetylcholine (Ach) and sodium nitroprusside (SNP) induced relaxing responses in isolated segments of femoral arteries of sham mice and mice with aortic valve stenosis (AS) after four weeks (A, B, C red and black circles) and three months (D, E, F blue and black squares) in the presence of indomethacin and N^{G}-nitro-L-arginine methyl ester (L-NAME). *p<0.05, **p<0.01. Statistics performed using unpaired t-test of maximal responses. Data are shown as mean ± SEM, four weeks sham n=4, four weeks AS n=4, three months sham n=7, three months AS n=3.

Table 9 LogEC50 values were calculated from the corresponding dose response curves in the presence of eNOS inhibitor N^G-nitro-L-arginine methyl ester (L-NAME). ACH: acetylcholine, Phe: phenylephrine, AS: aortic valve stenosis

Four weeks	**AS**	**sham**	***p*-value**
Ach	-7.073	-6.862	*ns*
Ach+ L-NAME	-6.483	-6.275	*ns*
p-value	***0.0032***	***0.0119***	
Phe	-5.970	-5.744	*ns*
Phe+ L-NAME	-5.713	-5.825	*ns*
p-value	*ns*	*ns*	
Three months	**AS**	**sham**	***p*-value**
Ach	-7.069	-7.226	*ns*
Ach+ L-NAME	-6.194	-6.034	*ns*
p-value	***0.0013***	***<0.0001***	
Phe	-6.340	-6.175	*ns*
Phe+ L-NAME	-6.196	-6.440	*ns*
p-value	*ns*	*ns*	

Interestingly, the amount of eNOS-dependent dilation, calculated as delta of the area under the curve (AUC) from acetylcholine induced relaxing responses in the presence and absence of L-NAME, changed in femoral artery segments in an age-dependent manner. Four weeks after wire-injury, eNOS- dependent dilation represented 24.52 % (sham) and 25.69 % (AS) of total dilation response (AUC sham: 67.3 ± 21.8 a.u. vs. AS: 74.1 ± 37.6 a.u.). In contrast, eNOS-dependent dilation in the three months group represented 45.07 % in sham and 45.93 % in AS animals (AUC sham: 144.0 ± 14.0 a.u. vs. AS: 156.4 ± 29.8 a.u.).

4.9 Aortic endothelial function was altered in mice with aortic valve stenosis

The mechanisms underlying vascular reactivity differ between the different types of arteries in the vascular bed. To further delineate between local structural and functional adaptions versus systemically relevant effects in AS, potential changes in endothelial function were investigated by *ex*- vivo studies in isolated aortic rings of sham and AS animals.

The first set of experiments investigated vascular reactivity in isolated aortic rings of animals four weeks after wire-injury. Initially, contractile reactivity was characterized by the cumulative addition of phenylephrine. Maximal contraction and sensitivity were similar in the absence (Figure 37 A) and presence (Figure 37 B) of cyclooxygenase inhibitor indomethacin in sham and AS mice. Exclusively the incubation with eNOS inhibitor L-NAME showed a mild increase in maximal contractile response in AS mice compared to sham animals (Figure 37 C). However, the sensitivity (EC_{50}) to phenylephrine was comparable in both experimental groups (Table 10).

Table 10 LogEC50 values were calculated from the corresponding dose-response curves in the absence of pharmacological inhibitors, in the presence of indomethacin and eNOS inhibitor NG-nitro-L-arginine methyl ester (L-NAME) after four weeks.
Ach: acetylcholine, Phe: phenylephrine, AS: aortic valve stenosis

Phe	**AS**	**sham**	***p*-value**
Absence of inhibitors	-6.585	-7.084	*ns*
Indomethacin	-7.027	-6.689	*ns*
L-NAME + Indomethacin	-7.282	-6.784	*ns*
Ach			
Absence of inhibitors	-7.537	-7.465	*ns*
Indomethacin	-7.186	-7.097	*ns*
L-NAME + Indomethacin	*n.a.*	*n.a.*	*n.a.*

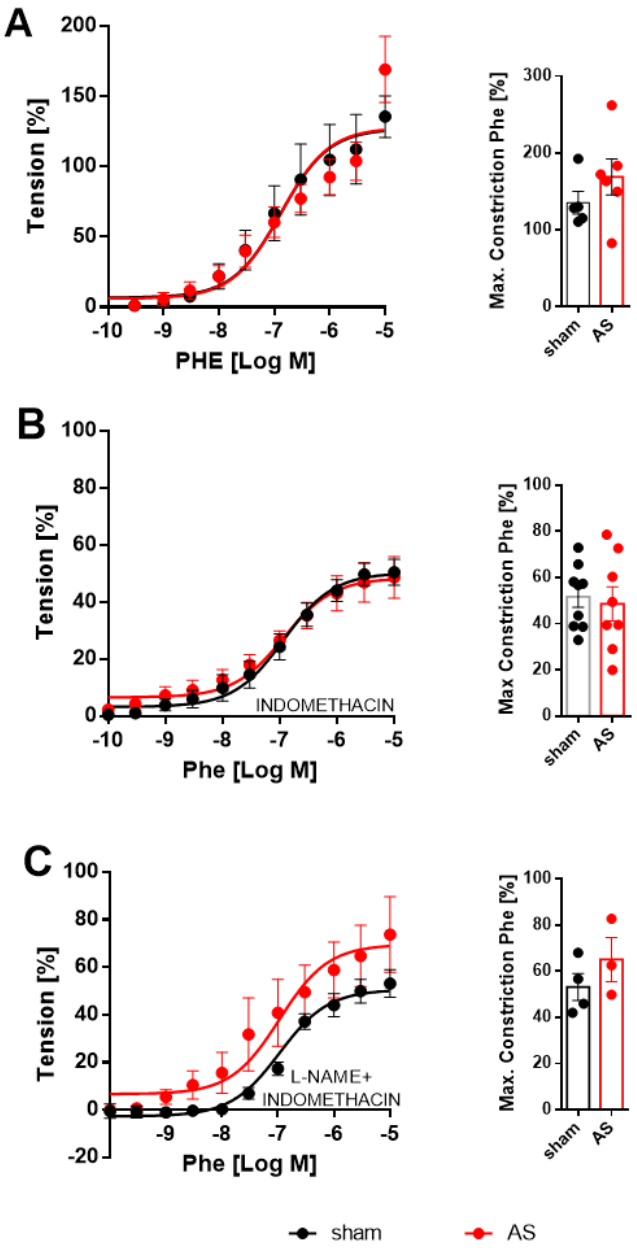

Figure 37 Effects of aortic valve stenosis on phenylephrine-induced contractile response, four weeks after wire-injury.
Phenylephrine induced contractile responses in isolated aortic segments from sham and mice with AS. (A) In the absence of pharmacological inhibitors. (B) In the presence of indomethacin. (C) In the presence of indomethacin and N^G-nitro-L-arginine methyl ester (L-NAME). Unpaired t-test. Data are shown as mean ± SEM, n=3-9. AS: aortic valve stenosis.

Next, phenylephrine pre-contracted aortic rings were subjected to cumulative addition of acetylcholine, which revealed significantly decreased maximal relaxing response in AS mice in the presence of indomethacin (sham: 75.87 ± 0.04 % vs. AS: 59.39 ± 5.00 %, p=0.0061, Figure 38 B). However, maximal relaxing response in the absence of pharmacological inhibitors (Figure 38 A) was decreased without reaching statistical significance.

Incubation with L-NAME abolished vasodilator response to acetylcholine to the same extent in sham and AS mice, indicating complete eNOS dependent relaxation in the aorta of the two groups. Additionally, both experimental groups showed similar sensitivity to acetylcholine (Table 11).

Moreover, sensitivity ($LogEC_{50}$ sham: -7.92 M vs. AS:-8.09 M) and maximal relaxation response (E_{max}: sham: 102.80 ± 2.27 % vs. AS: 107.10 ± 4.64 %) to endothelium-independent NO donor SNP was not affected (Figure 39).

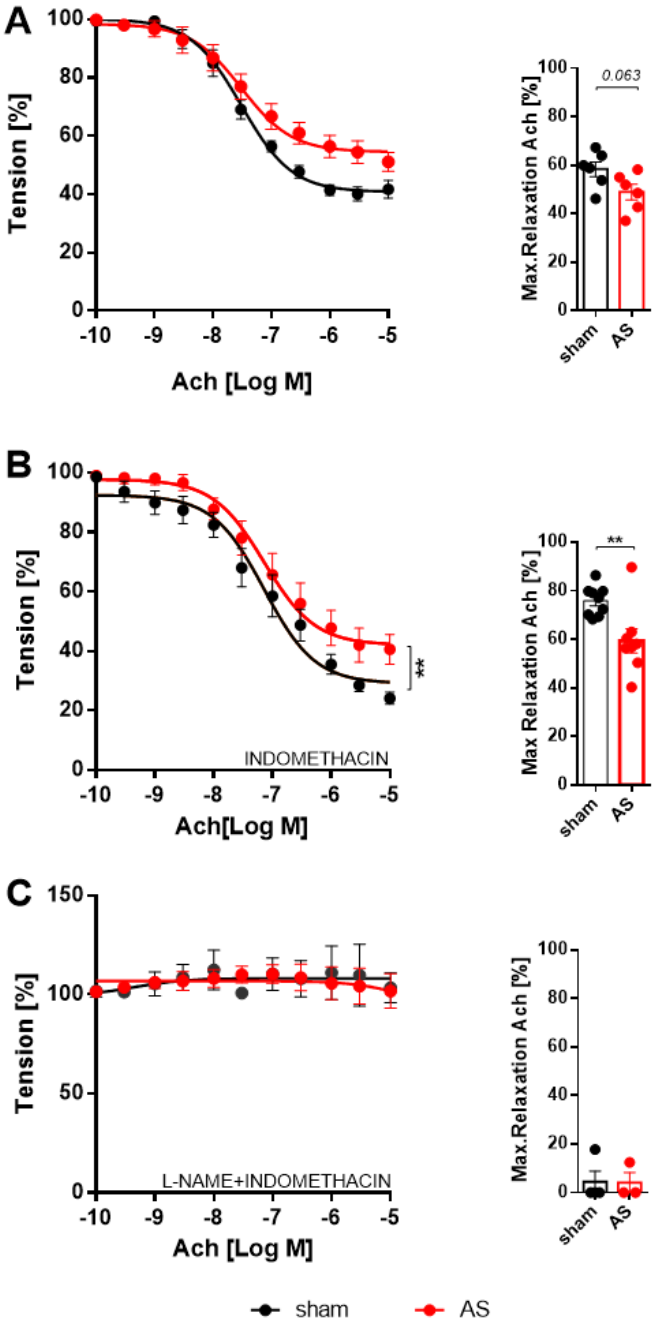

Figure 38 Impaired aortic endothelium-dependent relaxation in mice with aortic valve stenosis, four weeks after wire-injury
Acetylcholine induced relaxation responses in isolated aortic segments of sham and mice with AS. (A) In the absence of pharmacological inhibitors. (B) In the presence of indomethacin. (C) In the presence of indomethacin and N^G-nitro-L-arginine methyl ester (L-NAME). **p<0.001. Unpaired t-test. Data are shown as mean ± SEM, n=3-9. AS: aortic valve stenosis

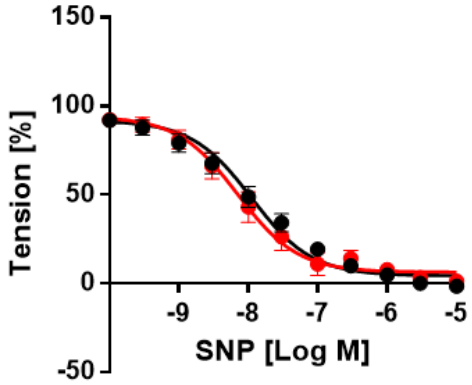

Figure 39 Endothelium-independent relaxation was preserved in aorta of mice with aortic valve stenosis, four weeks after wire-injury
Sodium nitroprusside (SNP) induced relaxation responses in isolated aortic segments of sham and mice with aortic valve stenosis. n=3-9. AS: aortic valve stenosis.

To evaluate the effect of age on *ex vivo* vascular reactivity in AS animals, experiments were repeated in aortic rings of AS animals three months after wire-injury. The phenylephrine-induced maximal contractile response was significantly enhanced in AS animals in the absence of indomethacin (control: 92.32 ± 17.17 % vs. AS: 200.00 ± 45.83 %, p=0.047, Figure 40 A). Interestingly, the maximal contractile response tends to increase in mice with AS in comparison to sham mice in the presence of indomethacin (sham: 30.09 ± 6.70 % vs. AS: 45.19 ± 5.18 %, p=0.1122, Figure 40 B). In addition, maximal contractile response after L-NAME treatment was similar in sham and AS animals (Figure 40 C).

Table 11 LogEC$_{50}$ values were calculated from the corresponding dose-response curves in the absence of pharmacological inhibitors, in the presence of indomethacin and eNOS inhibitor NG-nitro-L-arginine methyl ester (L-NAME) after three months.
Ach: acetylcholine, Phe: phenylephrine, ctrl: control (healthy WT), AS: aortic valve stenosis

Phe	AS	sham/ctrl	*p*-value
Absence of inhibitors	-5.526	-6.473	*ns*
Indomethacin	-7.735	-7.403	*ns*
L-NAME + Indomethacin	-7.055	-6.965	*ns*
Ach			
Absence of inhibitors	-6.907	-7.472	*ns*
Indomethacin	-6.733	-6.956	*ns*
L-NAME + Indomethacin	*n.a.*	*n.a.*	*n.a.*

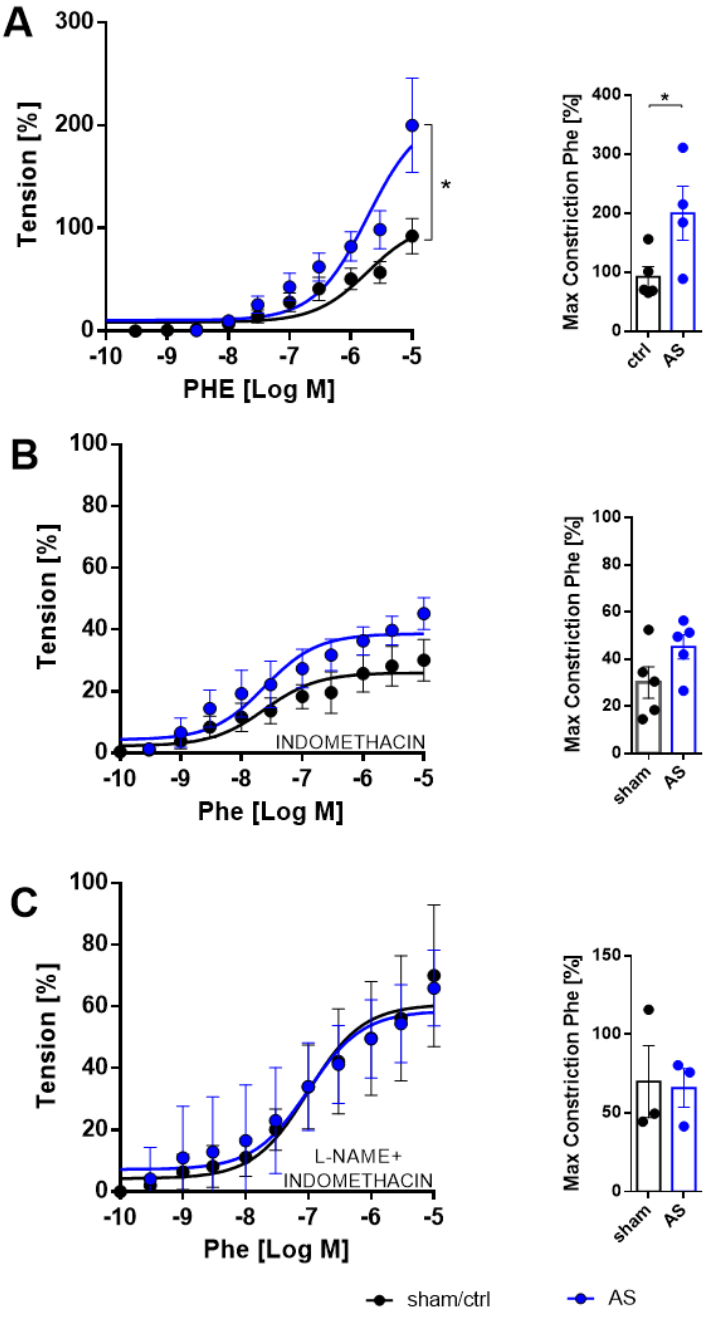

Figure 40 Effects of aortic valve stenosis on phenylephrine-induced contractile response, three months after wire-injury.
Phenylephrine induced contractile responses in isolated aortic segments from sham and mice with AS. (A) In the absence of pharmacological inhibitors. (B) In the presence of indomethacin. (C) In the presence of indomethacin and NGnitro-L-arginine methyl ester (L-NAME). *p<0.05. Unpaired t-test. Data are shown as mean ± SEM, n=3-5. AS: aortic valve stenosis.

We then obtained relaxing responses to acetylcholine in sham and AS mice, three months after wire-injury. Maximal relaxation response was decreased by tendency in the absence (control: 55.56 ± 5.85 % vs. AS: 40.10 ± 5.41 %, *p*= 0.1001, Figure 41) and presence of indomethacin (sham: 76.04 ± 6.22 % vs. AS: 61.03 ± 3.42 %, *p*=0.0673, Figure 41 B). In the presence of L-NAME, relaxation response to acetylcholine was completely abolished in the two experimental groups. However, there were no substantial changes in EC_{50} values between sham and AS mice in any of these experimental conditions (Table 11). In addition, phenylephrine pre-contracted aortic rings were treated with NO donor sodium nitroprusside to determine endothelium-independent relaxation. Maximal relaxation response and sensitivity were similar in sham and AS mice to endothelium- independent NO donor SNP was not affected (E_{max}: sham: 104.30 ± 4.84 % vs. AS: 98.32 ± 2.03 %, $LogEC_{50}$ sham: -7.179 M vs. AS:-7.252 M) (Figure 42).

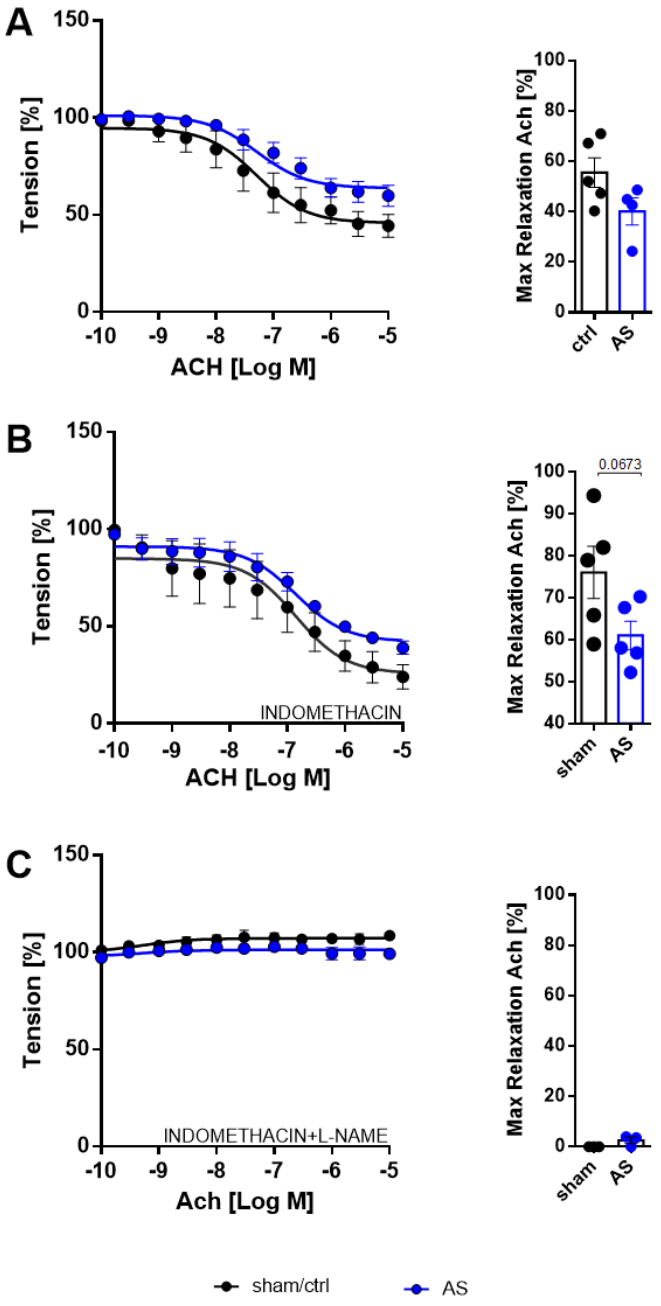

Figure 41 Impaired aortic endothelium-dependent relaxation in mice with aortic valve stenosis, three months after wire-injury
Acetylcholine induced relaxation responses in isolated aortic segments from sham and mice with AS. (A) In the absence of pharmacological inhibitors. (B) In the presence of indomethacin. (C) In the presence of indomethacin and N^G-nitro-L-arginine methyl ester (L-NAME). Unpaired t-test. Data are shown as mean ± SEM, n=3-5. AS: aortic valve stenosis.

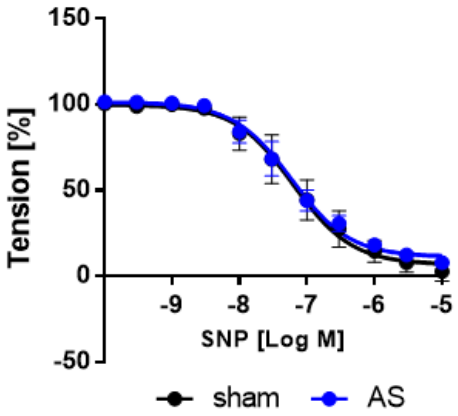

Figure 42 Endothelium-independent relaxation was preserved in aorta of mice with aortic valve stenosis, 3 months after wire-injury
Sodium nitroprusside (SNP) induced relaxation responses in isolated aortic segments of sham and mice with aortic valve stenosis, n=3-5. AS: aortic valve stenosis

To summarize, we observed impaired acetylcholine-induced relaxation responses in mice with AS. Addition of pharmacological inhibitor indomethacin unmasked the acetylcholine-induced release of COX products. The incubation with eNOS inhibitor L-NAME completely abolished relaxation response to acetylcholine, indicating NO as the major factor in endothelium-dependent relaxation in the aortic vessel in our model. Relaxation response to acetylcholine in older mice tends to be decreased, while we observed a markedly stronger response to the phenylephrine-induced contraction in the absence of indomethacin in these animals. Endothelium-independent relaxation responses to NO donor SNP showed no alterations in sham or AS animals at both time points. No changes were found in EC_{50} values in all groups, indicating unaltered sensitivity to the pharmacological substances.

4.10 Aortic eNOS expression was altered in animals with aortic valve stenosis

To investigate whether the decrease in endothelium-dependent relaxation in AS animals results in modified expression of key enzymes of NO-dependent relaxation, immunoblotting was used to analyze expression levels of total eNOS, AKT, and sGcβ1 in aortic tissue of sham and AS animals. The total eNOS expression was significantly up-regulated by 4.12 ± 0.60-fold in AS mice compared to sham mice (Figure 43 B). There was no difference in expression levels of sGCβ1 or total AKT (Figure 43 C, D).

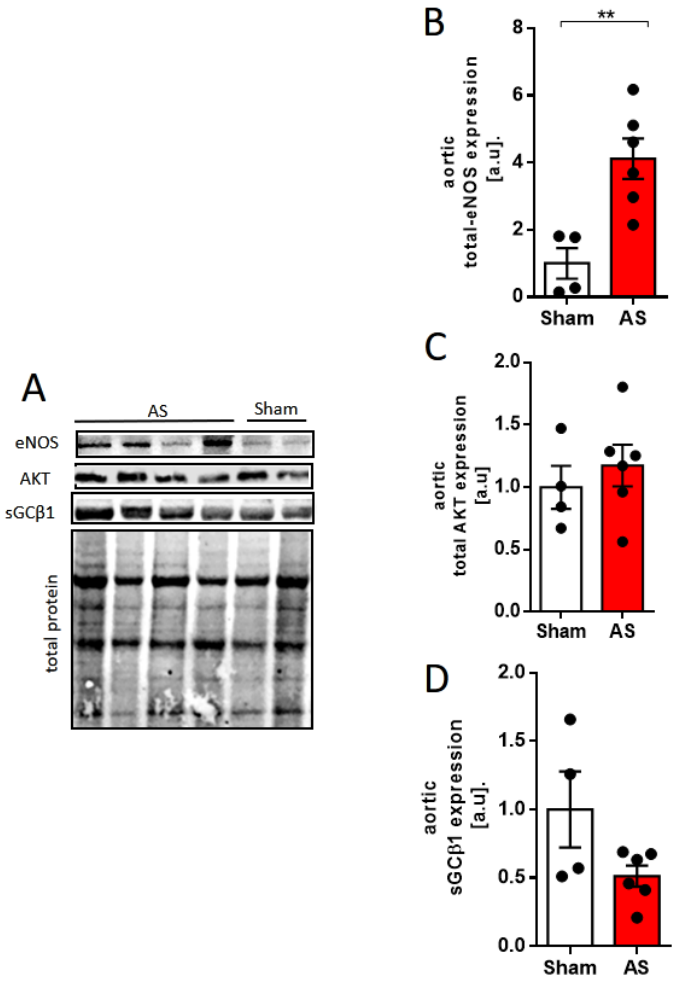

Figure 43 Aortic eNOS expression was enhanced in mice with aortic valve stenosis
Immunoblotting was used to assess protein expression levels in aortic lysates of sham mice and mice with aortic valve stenosis (AS). (A) Representative western blots of (B) total eNOS expression (C) total AKT and (D) sGCβ1 expression. ** $p<0.05$. Unpaired t-test. The values were normalized to the mean value of controls. Data shown as mean ± SEM, n=4-6.

In order to analyze if changes in eNOS expression at protein level were also present at the mRNA expression level, quantification of *Nos3* gene expression in the aorta was performed using real-time PCR. In contrast to western blot results, mRNA expression of *Nos3* did not differ between sham and stenotic mice (Figure 44).

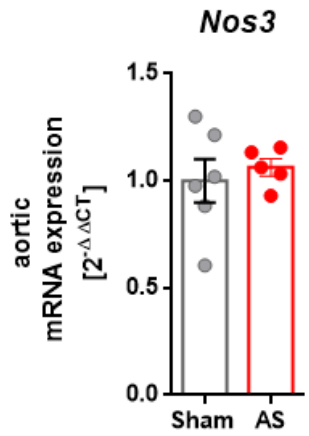

Figure 44 Aortic mRNA expression levels remained unchanged between sham and mice with aortic valve stenosis.
Relative mRNA expression levels of endothelial nitric oxide synthase (NOS3) were assessed in aortic lysates four weeks after wire-injury or sham surgery, respectively. Data were evaluated using RT-PCR. The value of each gene was normalized to the mean of controls. Statistical analysis was performed using unpaired t-test. Data shown as mean ± SEM, n=5-6. AS: aortic valve stenosis.

It is known that EC activation by proinflammatory cytokines could precede endothelial dysfunction. Therefore, markers for EC activation *Icam1, Vcam1*, as well as inflammatory markers such as *Il6, Tnfα, Il10,* and *TGfβ* were analyzed in AS and sham mice.

Analysis of relative expression of *Icam1* and *Vcam1* at mRNA level showed no significant differences in stenotic mice compared to sham mice (Figure 45 A, B). *Il6* and *Tnfα*, proinflammatory cytokines known to be involved in EC activation and leucocyte adhesion, showed no relevant alterations (Figure 31 C, D). There were no statistically significant differences observed in expression levels of *Il10* or *TGfβ* (Figure 45 E, F).

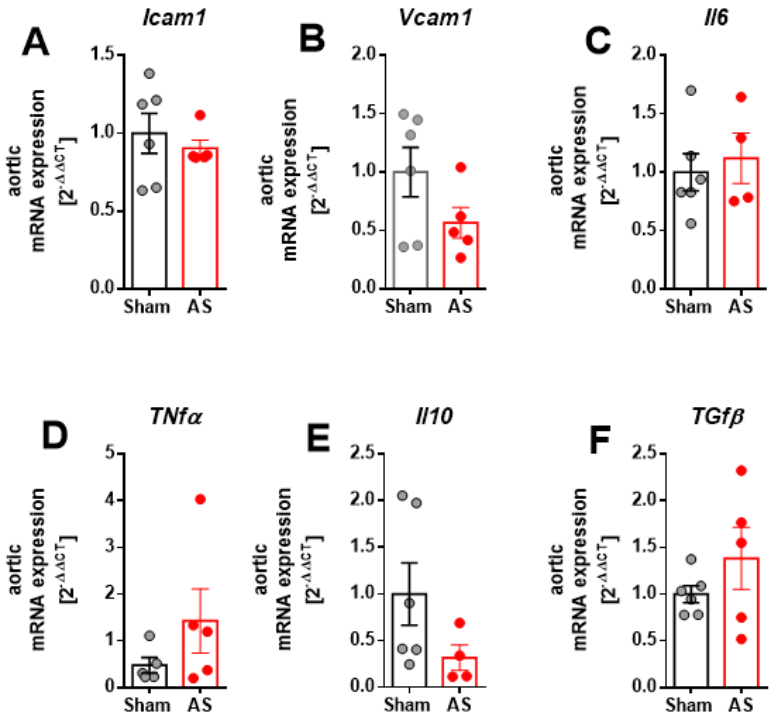

Figure 45 Quantification of aortic mRNA expression levels of genes involved in endothelial cell activation.
Relative mRNA expression levels of (A-B) adhesion molecules *Icam1*, *Vcam1* and (C-F) *Il6, TNfα, Il10* and *TGfβ*. The value of each gene was normalized to the mean of controls. Statistical analysis was performed by unpaired t-test. Data shown as mean ± SEM, n=5-6. AS: aortic valve stenosis.

Taken together, the presented data revealed that aortic eNOS protein expression levels showed an upregulation in AS animals. Further analysis of the aortic vessel showed no changes in mRNA expression levels of enzymes involved in EC activation.

4.11 Wire-induced AS altered antioxidant capacity in aortic vessel

To evaluate changes in antioxidant capacity in mice suffering from AS, analysis of GSH and GSSG were performed in plasma, heart and aortas four weeks after wire-injury. The GSH/GSSG ratio was significantly decreased to 0.76 ± 0.21-fold in aortic tissue from AS animals (Figure 46). The GSH/GSSG ratio was not significantly altered in plasma. However, there was a trend towards a lower GSH/GSSG ratio in the heart.

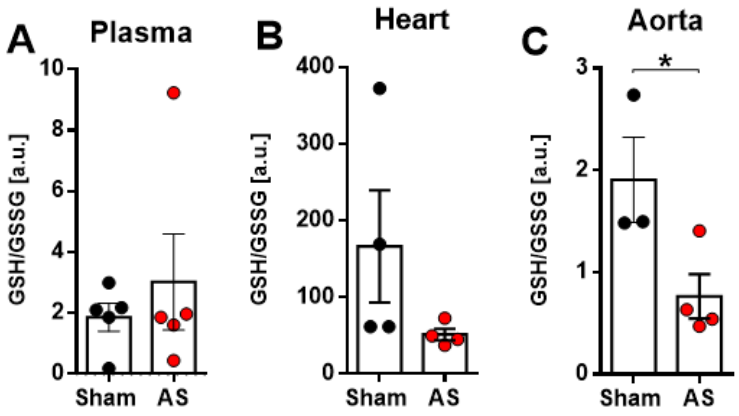

Figure 46 Aortic GSH/GSSG ratio was increased in stenotic mice
Levels of reduced glutathione (GSH) and oxidized glutathione (GSSG) were determined in plasma, heart and aortic tissue of sham and mice with aortic valve stenosis (AS), four weeks after wire-injury or sham surgery, respectively (A-C). Values are expressed as ratio of GSH to GSSG. *p<0.05, unpaired t-test. Data shown as mean ± SEM, n=3-4.

Interestingly, mRNA expression levels of enzymes involved in the antioxidant defense remained unchanged, apart from catalase, which was increased to 1.2 ± 0.1-fold in aortic tissue of AS mice (Figure 47).

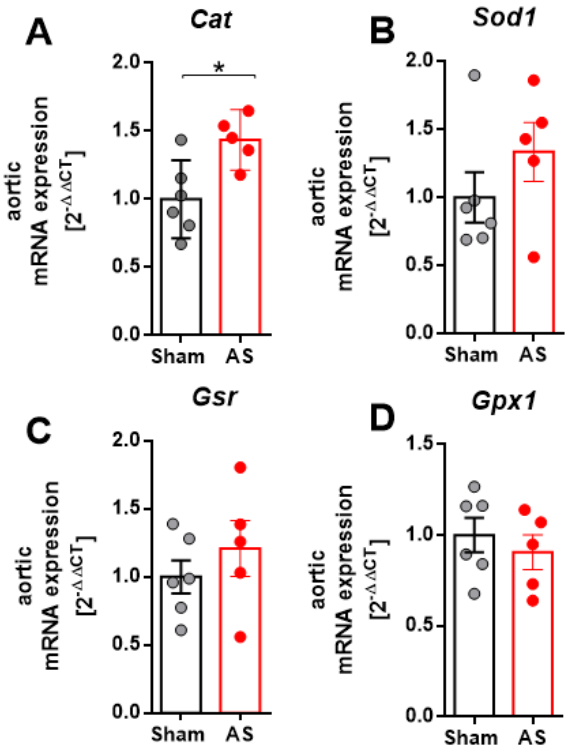

Figure 47 Changes of catalase expression levels in aortic tissue of AS animals
RT-PCR was used to assess relative mRNA expression levels of enzymes involved in antioxidant defence in aortic tissue of sham mice and mice with aortic valve stenosis (AS). Relative expression of (A) catalse (*Cat*), (B) superoxide dismutase 1 (*Sod1*), (C) glutathione reductase (*Gsr*) and (D) glutathione peroxidase 1 (*Gpx1*). The value of each gene was normalized to mean of controls. *p<0.05, unpaired t-test. Data shown as mean ± SEM, n= 5-6.

Vascular oxidative stress was further assessed by checking expression levels of 3-Nitrotyrosine in aortas, a marker for $ONOO^-$. Four weeks after wire-injury, there was no significant difference in expression levels of 3-Nitrotyrosine between sham and mice with AS (Figure 48).

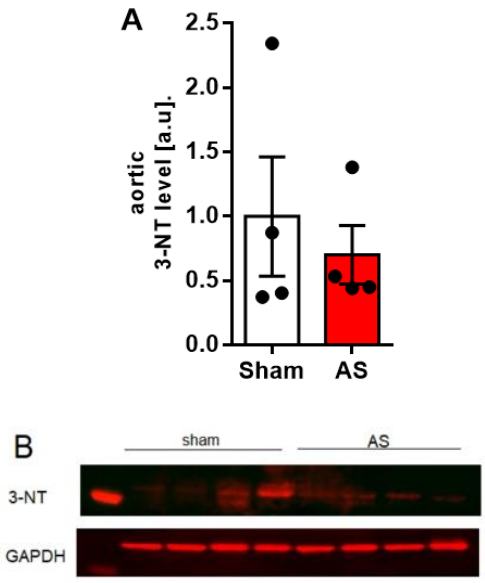

Figure 48 3-Nitrotyrosine levels were unaltered in aorta
Western Blot analysis of aortic tissue lysate from sham mice and aortic valve stenosis (AS) mice. (A) For quantification, levels of 3-Nitrotyrosine (3-NT) were normalized to the mean value of controls (B) Representative western blots. Unpaired t-test. Data shown as mean ± SEM, n=4.

To sum up, we observed decreased ratio of GSH/GSSG in aorta, but no significant changes in heart and plasma. Further analysis revealed increased expression of catalase in aorta. At this stage, we did not observe changes in nitrotyrosine levels in aorta.

5 Discussion

This work aimed to characterize the model of wire-induced AS and its effect on NO-dependent vascular endothelial function irrespective of confounding comorbidities being present in humans. We raised the hypothesis that turbulent blood flow in AS disrupts NO bioavailability, which is essential for the homeostasis of systemic endothelial function. To explore our hypothesis, the following aims were investigated: 1.) Characterization of the wire-injury model regarding turbulent blood flow alterations in the ascending aorta, left ventricular function adaptions and morphological changes of the aortic valve 2.) Investigation of the role of AS on RBC integrity. 3.) Analysis of the systemic consequences of AS on NO-dependent vascular endothelial functional properties in the aorta and femoral artery with regard to eNOS function.

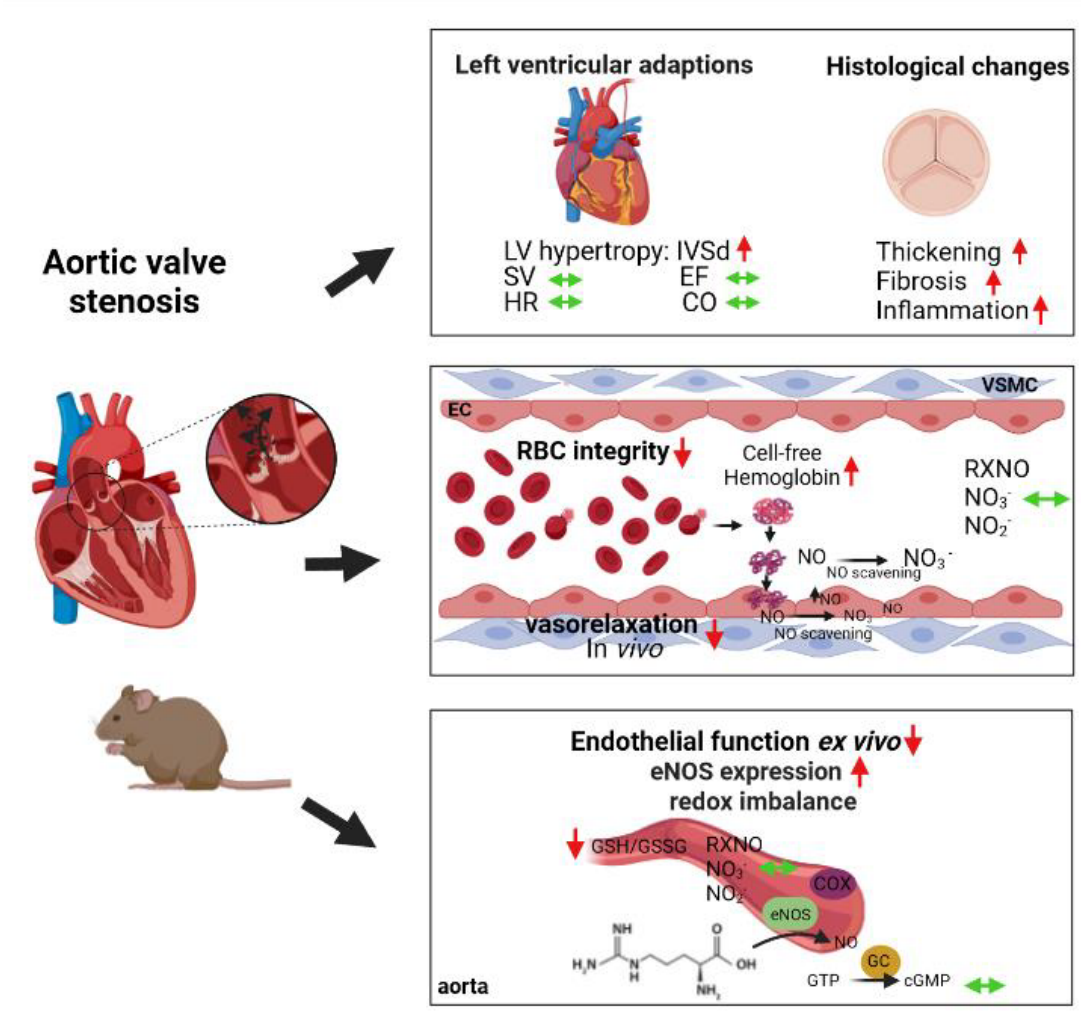

Figure 49 Overview Findings
The experimental model of aortic valve stenosis (AS) based on wire-injury, were characterised with a significant increase in aortic peak velocities, pressure gradients, restricted valve opening and turbulent blood flow in the ascending aorta. Left ventricular function was preserved, but the myocardium was identified with significant hypertrophy. Histological analysis of the aortic valve revealed thickening of the aortic valve cusps, fibrosis and infiltration of macrophages. 2.) AS significantly increased plasma levels of cell-free hemoglobin and the amount of Annexin V positive RBCs four weeks after wire-injury. Plasma nitrate, nitrite and RXNO remained unaltered. Femoral arterial flow-mediated dilation was significantly impaired. 3.) Aortic endothelium-depdendent relaxation was decreased in mice with AS. Further, aortic eNOS expression was enhanced, while a reduction of aortic GSH/GSSG ratio was observed. CO: cardiac output, COX: cyclooxygenase, cGMP: cyclic guanosine monophosphate, EF: ejection fraction, EC: endothelial cell, eNOS: endothelial nitric oxide synthase, GC: guanylate cyclase, GSH: glutathione, GSSG: oxidized glutathione (glutathione disulfide), GTP: guanosine triphosphate, Hb: hemoglobin, HR: heart rate, LV: left ventricle, NO: nitric oxide, RXNO: sum of nitrosothiols and nitrosoamines, VSMC: vascular smooth muscle cell.

The major findings of this study are following:

1. Manipulation of the aortic valve by wire-injury caused relevant aortic valve stenosis with narrowed aortic valve area, fibrotic valve thickening, turbulent blood flow conditions in the ascending aorta, and left ventricular hypertrophy.
2. Mice suffering from aortic valve stenosis showed altered red blood cell integrity with a concomitant increase in cell-free hemoglobin, but preserved RBCs deformability. The levels of NO metabolites remained unaltered.
3. Mice suffering from aortic valve stenosis showed imapired FMD responses.
   In addition, *ex-vivo* NO-dependent endothelial relaxation response was impaired in the aorta with concomitant increase in aortic eNOS expression.

5.1 Wire-injury induced morphological and functional adaptions of the aortic valve

A murine model was employed based on wire-injury of the aortic valve to investigate the characteristics of experimental AS and its effects on vascular endothelial function. To this end, it was essential to use a mouse model, which features human pathophysiology regarding valve morphology and turbulent blood flow in the ascending aorta. Previously characterized mouse models of AS are mainly based on diet-induced, genetically modified animals or a combination of both (Sider et al., 2011). In 2006 Weiss et al. introduced a mouse model of calcific AS in genetically hypercholesterolemic mice. In their study, low-density lipoprotein receptor-deficient apolipoprotein B-100-only (*LDLr $^{-/-}$ApoB$^{100/100}$)* mice were fed a chow diet for 17 to 22 months to study calcific AS. Likewise, Tanaka and colleagues investigated the age-associated valvular degeneration in an apolipoprotein E (*Apoe$^{-/-}$)* mouse model (Tanaka et al., 2005). Even though these models demonstrated sclerotic, calcific, or inflammatory changes in the aortic valve, the number of mice developing significant hemodynamic stenosis were relatively low (<2% in *Apoe$^{-/-}$* and <30% in *LDLr $^{-/-}$ApoB$^{100/100}$* mice), and require a long study period of up to 24 months, considered challenging because of the necessity of long study periods. In addition, in these mouse models, a detailed consideration of systemic consequences attributable only to AS is challenging, as diet and genetic intervention lead to globally relevant changes in the metabolism.

Honda et al. (2014) established a new approach for experimental AS, which is based on mechanical injury of the aortic valve. Their approach was supported by the response- to-tissue injury theory, a widely accepted theory in developing valve diseases. This is of particular interest considering the growing number of studies leading to a reconsideration of AS initiation as an active cellular mechanism through endothelial alterations (Rajamannan et al., 2011). With their experimental approach, Honda and colleagues showed that mechanical manipulation of the aortic valve leads to fibro-proliferative, osteochondrogenic and inflammatory changes, and hemodynamically significant stenosis (Honda et al., 2014). In addition, they focused on valvular consequences investigated by markers related to osteochondrogenic signaling (BMP-2, Sox9, Runx2), inflammation (Mac3, TNFα, TGFβ, IL-1β), and oxidative stress (DHE, p-22phox).

We used the wire-injury model with a modified protocol regarding the number of rotations to induce moderate AS. In contrast to the original published protocol, we increased the number of rotations from 50 to 100 and pushed the wire back and forward 50 times instead of 20 times with a straight wire. This protocol adjustment resulted in a reproducible induction of moderate AS evidenced by a significant increase in maximal peak velocity, mean and maximal pressure gradients validated by echocardiography (Niepmann et al., 2019).

In the initial model, Honda et al. demonstrated that flow velocities and pressure gradients increased up to 16 weeks after surgery. However, in our model, no further increase in flow velocities or pressure gradients between four weeks and three months after surgery were observed. One possible explanation might be the different methodological approach regarding the spring wire diameter used during surgery, which likely induced greater endothelial injury of the valvular tissue (0.36 mm vs. 0.14 mm). Moreover, we separated the groups based on the characteristic of pure AS or AS mice with concomitant AR, assessed by color Doppler. In contrast, Honda et al. did not report about the number of mice suffering from concomitant AR during the serial echocardiographic assessment.

In our modified wire-injury model, we were able to show that the degree of injury can define the severity of AS. This graded injury can induce a mild, moderate and severe AS. For induction of severe AS, the coronary wire was used with a 15° angled tip and rotated up to 200 times. Of note, the severity of injury showed a positive correlation with the incidence of AR, which accounts for a greater number of mice with mixed vitium when they underwent severe wire-injury. The adjustment of wire-injury allows the investigation of different disease severities, which is essential regarding the unperceived development of AS and fatal

outcome once symptoms occur. Overall these findings are in accordance with the original publication (Honda et al., 2014), validating wire-injury as a promising experimental model for AS. Furthermore, taking into consideration the limitations of diet and genetic manipulation based AS models, surgically induced AS could be used to study disease progression in the presence of comorbidities such as diabetes, hypertension, renal dysfunction etc., to name a few of the most abundant comorbidities found in patients with AS (Rezzoug et al., 2015; Salinger et al., 2018, Rudolph et al., 2020).

In addition, it was demonstrated that WT mice that underwent wire-injury showed preserved left ventricular systolic and diastolic function. The restricted valve opening area induced an increase in pressure gradient and triggered mild hypertrophic adaption of LV to chronic pressure overload. As a consequence, increased diastolic wall thickness of the myocardium was observed. These data are consistent with the results of left ventricular catheterization, indicating a significant increase in maximum pressure rise.

In addition to the evaluation of aortic flow and valvular alterations, MRI was used to assess fibrotic changes in the myocardium non-invasively in our AS model. The finding of reduced T1 and T2 times substantiate the absence of myocardial edema and fibrosis. Interestingly, in humans, myocardial interstitial fibrosis, described as the transition from myocardial hypertrophy to heart failure, was described to correlate with severity of AS, indicated by an increase in T1 (Bohbot et al., 2020; Everett et al., 2018) and might predict prognosis (Dweck et al., 2011; Park et al., 2021). However, this might be attributable to different stages of the disease and to different acquisition periods. Patients suffering from AS show considerable variations in the degree of hypertrophy and fibrosis, which can also be attributed to comorbidities (Dweck et al., 2012; Kupari et al., 2005). Therefore future research should consider comorbidities and differences in disease stages to further evaluate myocardial tissue texture in murine AS.

5.2 Wire-injury-based AS showed narrowed aortic valve orifice with fibrotic valve thickening and turbulent blood flow conditions in the ascending aorta

Echocardiography is the standard diagnostic tool in serial AS evaluation in humans. However, accurate echocardiographic assessment of murine valve morphology is challenging due to the small size of the murine valve. The additional MRI assessment of the wire-injury model allows for a higher informative value regarding valve morphology and valve function. MRI analysis of our AS model demonstrated an impaired valve opening and valve thickening due to valvular remodeling. Furthermore, in line with previous studies, it was shown that MRI is a reliable tool to quantify narrowing and valvular functional impairment in a murine model of AS in *LDLr*$^{-/-}$*ApoB*$^{100/100}$ mice (Weisell et al., 2019). They and others extensively studied the pathological changes in murine aortic valves during stenotic thickening (Aikawa et al., 2007; Miller et al., 2010). The fibrotic changes of the valve, assessed during MRI, were further evidenced by histological evaluation. The histological analysis of the valve shows significant fibrotic thickening and inflammation in AS animals. These data are consistent with the findings of Honda et al. (2014). In addition they observed increased oxidative stress and the involvement of Sox9, Runx2, BPM-2 in osteochondrogenic remodeling.

Furthermore, studies have demonstrated the crucial role of NO in aortic valve sclerosis (T. C. Lee et al., 2000; Richards et al., 2013a). In line with this concept, eNOS-deficient mice were identified with accelerated profibrotic activity of VICs and an increase in the prevalence of bicuspid aortic valves that were more prone to calcification (El Accaoui et al., 2014). In addition, we previously showed the spontaneous development of AS in twelve-month-old global eNOS-deficient mice accompanied by aggravated cardiac function and shorter lifespan (*unpublished data*). Nevertheless, these observations were limited to old mice, not young eNOS KO animals. Surprisingly, eNOS-deficient mice did not show significantly faster AS progression compared to WT mice four weeks post-wire-injury. Our findings imply that the NO-dependent mechanism, accelerating valvular fibrosis in trileaflet aortic valves, becomes more relevant with aging. Aging is long known to be the leading risk factor for AS in humans (Coffey et al., 2016). Therefore, future research will be focussed to investigate wire-injury-based induced AS progression in older WT and eNOS KO mice.

Overall these findings are consistent with research from human aortic valves, showing that fibrosis, inflammation, and calcification are the key aspects of valvular pathology (Lerman et al., 2015). Subsequently, these changes lead to a significant increase in maximal peak velocities and asymmetric turbulent blood flow conditions in the ascending aorta.

It was shown that these turbulent flow conditions determine structural and functional changes in the ascending aorta, indicated by significantly increased circumferential strain in AS animals, which is associated with increased aortic wall thickness. Several studies focused on consequences of structural remodeling in the aorta due to modified hemodynamic environment in AS, e.g., increase in aortic rigidity and its consequences for LV function (Rosca et al., 2011), aortic dilation, and rise of WSS in the ascending aorta (Suwa et al., 2020; van Ooij et al., 2017). Recently, Garcia, Barker and Mark (2019) described advanced flow quantification and visualization of aortic hemodynamic by 4D flow MRI data depicted by 3D streamlines in AS patients, which allows for assessment of flow patterns, wall shear stress, pressure gradients, and flow displacement. To summarize, the results suggest that AS alters hemodynamic and WSS in the ascending aorta, a stimulus for aortic wall remodeling. One limitation of these findings is that the impact of the wire on the integrity of the vessel should be considered.

Although the clinical translation of data obtained in mice is always challenging, the AS model based on wire-injury showed to be meaningful to mimic human disease considering the similarities regarding valvular, blood flow, and LV adaptions in our model.

5.3 Decreased NO bioavailability determines endothelial dysfunction in mice suffering from aortic valve stenosis

The association of decreased endothelial dysfunction and AVS was described for the first time by Poggianti et al. (2003). They identified a significant impairment of FMD in AVS patients compared to patients with a morphologically normal aortic valve (Poggianti et al., 2003). In 2006 Chenevard et al. extended the research in this field by investigating FMD in patients with relevant AS (Chenevard et al., 2006). They found impaired FMD in patients with AS. Interestingly, a further study showed that FMD was indeed significantly decreased in AS patients, but different from the previous findings of a persistent decrease in FMD, they found improvement of FMD in AS patients after TAVI (Horn et al., 2014). It is important to discuss the fact that impaired FMD in patients with AS might be an additional attempt to explain the high onset of cardiovascular events in these patients (Otto et al., 1999; Owens et al., 2012; Lee et al., 2021). In multiple studies, endothelial dysfunction measured by FMD was suggested as an independent predictor for future cardiovascular events (Brevetti et al., 2003; Gokce et al., 2003).

As mentioned previously, most animals studies of AS have focused on pathophysiological alterations of the valve. To the best of our knowledge, none of these models investigated vascular endothelial function in AS. For this reason one of the major aims of the present work was to evaluate the systemic effects of AS by a comprehensive analysis of vascular endothelial function with special regard to NO bioavailability, preceding with *in vivo* analysis by FMD in the left femoral artery. FMD is a reliable method to assess endothelial-dependent vasomotor function. The stimulus for *in-vivo* assessment of endothelium-dependent dilation was identified as flow associated shear stress, which induce signal transduction by mechanosensitive structures resulting in rapid synthesis of NO by eNOS (Celermajer et al., 1992; Rubanyi et al., 1986). Therefore, FMD is widely used as a read-out for NO bioavailability. Our data indicate that mice suffering from AS are characterized by a dysfunction of endothelium-mediated relaxation of VSMCs, identified by significantly impaired FMD. This deterioration was clearly attributable to the presence of AS, considering the impaired FMD before and after wire-injury, as well as the comparison to animals which underwent sham surgery. In addition, baseline femoral artery diameters, baseline blood flow and blood flow during hyperemia did not differ between sham and AS animals after four weeks. Consequently, it can be assumed that the stimulus to trigger the release of NO, the

increase in vascular wall shear stress, was not altered in peripheral arteries. Moreover, administration of eNOS inhibitor L-NAME prior to FMD abolished relaxation response within the first minutes after vessel reperfusion in sham and AS mice. These data implies that maximal relaxation response during FMD in the femoral artery is completely facilitated by NO triggered relaxation of VSMCs.

Next, mice identified with impaired FMD were also subjected to *ex-vivo* vascular reactivity studies of the femoral artery to elucidate whether receptor-induced endothelium-dependent relaxation was also affected in these animals. We observed unaltered endothelium-dependent relaxation, as well as endothelium-independent response to SNP compared to sham animals after four weeks. These findings provide evidence that receptor-mediated, intracellular NO release and sensitivity of VSMCs was fully preserved in AS animals. However, in line with previous findings from different investigators, we found acetylcholine-induced relaxation responses were only partly NO-dependent in these arteries. As reported in the previous section, with the decrease in vessel size, the contribution of the major vasodilators shifts from NO and PGI_2 towards EDHF-dependent vasodilation (Luksha et al., 2009).

5.3.1 Cell-free Hb mediated scavenging of NO is likely to determine impaired FMD in AS animals

At this stage of understanding, we were able to identify mice with AS with an impaired relaxation response during FMD studies. The key difference between sham and mice with AS was the presence of high turbulent flow in the ascending aorta due to valve orifice narrowing. High transvalvular velocity jet in stenotic aortic valves results in asymmetrical, disturbed flow patterns in the ascending aorta, with eccentrically elevated shear stress (Garcia et al., 2019; von Knobelsdorff-Brenkenhoff et al., 2016). Several lines of evidence suggest that alterations in blood flow velocities go along with high turbulent shear forces above the physiological level, which likely induce RBC damage. Depending on the magnitude of shear forces, this can induce immediate rupture of RBC or damage in the range of subhemolytic trauma (Baskurt, 2012). The compartmentalization of Hb within the RBCs is essential to limit the reaction with NO (Liu et al., 1998). Intravascular hemolysis-triggered release of cell-free Hb limits endothelium-mediated vasorelaxation by preventing NO diffusion to VSMCs resulting in altered vasomotor response (Rother et al., 2005). This reduction in NO bioavailability due to scavenging effects primarly takes place in the subendothelial space after dimerization and translocation of cell-free Hb (Kim-Shapiro et al.,2006).

The NO consumption by cell-free Hb in plasma was described as the deoxygenation reaction to form methemoglobin and NO_3^- via the iron-containing heme group. Moreover, NO reaction with deoxyhemoglobin induces nitrosylation.

Equation 3 NO consumption by oxyhemoglobin described as the deoxygenation reaction

$$Hb\text{-}Fe^{2+}(O_2) + NO \rightarrow Hb\text{-}Fe^{3+} + NO_3^-$$

$$Hb\text{-}Fe^{2+} + NO \rightarrow Hb(NO)$$

The scavenging of NO by cell-free Hb explains the multiple adverse effects, including acute hypertension, vasoconstriction, and vascular injury following the infusion of cell-free Hb in animal models (Boretti et al., 2009; Schaer et al., 2016; Hugelshofer et al., 2019). Moreover, infusion of stored RBCs increased cell-free Hb and vasoconstriction response (Baek et al., 2012).

Moreover, a broad range of studies reported the hematological consequences of prosthetic heart valves, but only a few studies investigated the consequences of native AS on RBC functional properties. Sugiura and colleagues demonstrated that AS is associated with intravascular hemolysis induced by high blood flow velocities in patients suffering from moderate to severe AS (Sugiura et al., 2016). They found that patients with AS showed higher values of erythrocyte creatine, which is a sensitive marker for erythrocyte survival. Additionally, they observed that erythrocyte creatine correlates positively with the peak flow velocity. Moreover, these patients were identified with increased levels of lactate dehydrogenase (LDH), decrease in RBC count, total Hb, and Hp compared to control patients. Despite several studies describing intravascular hemolysis in AS patients, the systemic effects of hemolytic conditions in AS are not very well understood.

We found that our experimental model of AS was associated with alterations in RBC integrity, indicated by an increased number of Annexin V positive RBCs and a significant increase in cell-free Hb. Vahidkhah et al. (2016) postulated by means of computational simulations that stenotic heart valves induce subhemolytic damage to RBCs (Vahidkhah et al. , 2016). In line with this idea, we assume that in our experimental model of AS, RBC damage is likely to occur in a subhemolytic manner as well. Hemolysis represents the final stage of RBC membrane damage and goes along with significant blood count changes, including the increase in reticulocytes, LDH, and a decrease in Hp (Bunn et al., 2010). We did not find any substantial changes in total Hb, RBC indices, reticulocyte levels, which in summary contradicts against severe RBC rupture and thus acute hemolysis. Moreover, the

analysis of RBC deformability did not show any significant changes in mice with AS. Several research groups have investigated the link between shear-induced RBC damage and RBC deformability. The specific RBC membrane properties rendered by a highly organized protein network allowing the RBC to elongate with an increase in shear stress and adapt its morphology during circulation, i.e. passes through the lumen of capillaries. However, shear stress beyond the physiological range can change the mechanical characteristics of RBC and consequently decline RBC's ability to deform (Lee et al., 2004). It has been shown that RBC deformability decrease with the magnitude of shear-induced membrane damage and with the exposure time to the applied shear stress.

As early as 1977, it was reported that subhemolytic trauma of RBC occurs even below the hemolytic threshold and can also go along with membrane alterations and release of cell-free Hb into the plasma (Sutera, 1977). Subhemotylic damage of RBCs was shown to decrease the life span of RBCs, increase trapping in the spleen, and might change their deformability (Sandza et al., 1974; Simmonds et al., 2014; Sutera, 1977). It was suggested that during subhemolytic damage of RBCs, Hb is released into the plasma via the temporary formation of pores on RBC membranes, which is favored during RBC membrane *tanktreading* under high shear flow (Sohrabi & Liu, 2017). Membrane *tanktreading* describes "*the movement of the membrane around the discoid shape without significant changes in the shape of the whole-cell"*(Kuhn et al., 2017 p.726).

We observed a significant 2-fold increase of cell-free Hb levels in AS animals. In disease states such as sickle-cell disease, chronic hemolysis occurs with the substantial release of Hb into the vasculature (Kato et al., 2006). Cell-free Hb levels showed a more than 10-fold increase compared to healthy controls in sickle-cell disease and are even reinforced during an acute pain crisis (Naumann et al., 1971). This acute disruption of RBCs results in substantial Hb release and thus rapid reduction in NO bioavailability. It was shown that plasma from sickle-cell patients consumes more NO than plasma from normal volunteers and that heme concentrations correlate with NO consumption (Reiter et al., 2002). The massive RBC damage further explains the serious systemic effects such as occlusion of small and large blood vessels, endothelial dysfunction, and tissue ischemia. It was shown that vasodilation response after forearm infusion of SNP was up to 80% decreased in sickle-cell disease patients (Reiter et al., 2002), explaining why the scavenger molecules Hp and hemopexin are depleted in such disease states (Santiago et al., 2016). Likewise, in severe hemolytic infections like malaria caused by plasmodium falciparum, cell-free Hb levels were

up to 5-fold increased and were associated with severe complications, such as renal failure, significant endothelial dysfunction and increased markers of EC activation (Yeo et al., 2009). Hence, cell-free Hb-driven physiological consequences, such as increased blood pressure, are expected at higher rates of cell-free Hb release than in our experiments. This might explain why we could not detect substantial changes in mean arterial pressure (MAP) and thus systemic vascular resistance (SVR). However, it was shown that NO is scavenged 600 times more rapidly by cell-free Hb than by RBC (Liu et al., 1998). In line with previous studies, our data indicate that even a mild increase in cell-free Hb can lead to relevant reduction in NO bioavailability and thus decrease VSMCs response to NO. This has been previously shown in computational and animal studies (Jeffers *et al*., 2006).

By contrast, we did not find any changes in NO_2^- or RXNO, but NO_3^- tend to be increased considering the well-known reaction of NO with oxyHb increasing the formation of NO_3^- and Hb(Fe^{3+}) (Olson et al., 2004). However, unaltered NO_2^- limiting precise interpretation of these results. Cell-free Hb limits slower reactions such as NO autoxidation to form *S*-nitrosothiols and NO_2^- (Reiter et al., 2002). In patients with sickle cell disease, *S*-nitrosothiols were found to be under the limit of detection (Reiter et al., 2002).

5.3.2 Haptoglobin administration restores FMD in aortic valve stenosis

To verify that cell-free Hb accounts for decreased FMD though scavenging of NO*,* Hp was administered during FMD studies. Hp is the major Hb binding protein in the plasma and prevents Hb-induced toxicity (D. J. Schaer et al., 2014). We found that administration of Hp induced a greater increase in diameter in AS animals within the first minute of reperfusion than vehicle-treated AS animals. From this data, it can be concluded that Hp is able to enhance NO mediated VSMCs relaxation by preventing NO scavenging by cell-free Hb. In recent years, the supplementation of purified Hp gained growing attention because it was found that Hp can effectively clear cell-free Hb from the vasculature, protect against Hb-induced vaso-occlusion and inflammation (Belcher et al., 2018), renal injury, and hypertension (Lipiski et al., 2013).

Furthermore, it was demonstrated that Hb, but not Hb-Hp, caused dose-dependent vasoconstriction of isolated porcine coronary arteries, and Hp maintains NO-dependent signaling in the vasculature (Schaer et al., 2016). However, the translocation of dimerized Hb across endothelial barriers is still a matter of debate. It was suggested to involve active transport mechanisms (Komarova & Malik, 2010).

Eventually, Hp facilitates the retention of Hb in the antioxidant-rich plasma environment (Butt et al., 2010). Consequently, the large Hp-Hb complex is unable to pass cell barriers, thus preventing cell-free Hb-driven tissue toxicity, including heme release (Buehler et al., 2020). Noteworthy, the secondary toxicity of cell-free Hb compromises the release of heme from accumulated Hb(Fe^{3+}) and its transfer to proteins or lipids (Schaer et al., 2013), promoting oxidative stress (G. Balla et al., 1991; J. Balla et al., 2005; Nagy et al., 2010).

To sum up, the mechanisms underlying the toxicity of cell-free Hb are complex and go beyond the scavenging of NO, even though this toxicity pathway is the most important one considering decreased VSMCs relaxation (Schaer et al., 2016). The presented data are in line with previous studies analyzing Hb-driven toxicity, particularly scavenging of NO and the ability of Hp to reverse Hb-induced decrease of NO effectively. To conclude, it can be assumed that the decrease in FMD is a consequence of limited NO bioavailability due to cell-free hemoglobin scavenging, causing endothelium-dependent decrease in vasomotor function.

Importantly, data collected from AS patients in our lab revealed increased cell-free Hb levels, which correlated with helical, turbulent flow peak velocities in the aorta (*unpublished data*). Notably, this increase in cell-free Hb reversed after aortic valve replacement after TAVI. Therefore, these findings support the notion that the improvement of FMD after aortic valve replacement, as reported previously (Horn, 2014; Takata et al., 2015), could be attributed to decrease in cell-free Hb levels. Regardless, future research is certainly required to disentangle these complexities in patients with AS.

5.3.3 Decreased FMD aggravated in AS animals after three months

Previous analysis revealed that AS associated decrease in FMD can be attributed to reduction in NO bioavailability. The analysis of FMD revealed an almost abolished relaxation response three months after wire-injury. Comparing the maximal increase in diameter of AS and sham animals at both time points, an again substantial deterioration becomes clear (four weeks: sham 18.93 ± 1.57 % vs. AS 14.00 ± 0.68 %, p=0.0085, three months: sham 17.25 ± 2.15 % vs. AS 6.18 ± 1.68 %, p=0.0007). However, baseline femoral artery diameters, baseline blood flow, nor blood flow during hyperemia was significantly altered in these animals. Importantly, there were no substantial differences in aortic peak velocities or pressure gradients in AS mice after four weeks or three months. Accordingly, the relative increase in cell-free Hb levels did not substantially differ between AS animals four weeks or three months after surgery. From the results, it becomes obvious, that not aging alone, but the

combination of aging and AS induce a strong aggravation of endothelial function. The analysis of PVW lead to similar conclusion, where PWV was significantly increased compared to age-matched sham animals and AS animals from the four weeks post-surgery time point. Aging is associated with increased arterial stiffening and is long known to be a critical determinants of cardiovascular risk (Blacher et al., 1999). In younger individuals, PWV is lower due to the more elastic properties of the vessel (McEniery et al., 2005). Therefore an increase in PWV in aging animals is not surprising. Previous research showed, a strong correlation between femoral arterial PWV and aortic valve severity and calcification was found in patients with AS (Liu et al., 2004). Nevertheless, our data suggest, that the presence of AS in aging animals determine significant increase in vessel stiffness, which in turn could affect the diameter change in FMD studies. Moreover, future research is needed to delimitate if compensatory increases of other vasoactive substances are co-responsible for these findings.

By contrast, *ex vivo* vascular reactivity studies of the femoral artery showed preserved endothelium-dependent relaxation in AS animals after three months. Correspondingly, VSMCs sensitivity to endothelium-independent response to SNP remained unaffected. Therefore, endothelium-dependent NO release was not affected and sensitivity of VSMCs was also fully preserved. Of note, vascular reactivity studies of the femoral artery showed that the endothelium-dependent dilation was more NO-dependent in older animals, irrespective of AS pathology. Experiments from organ bath facilitate the assessment of receptor-mediated vascular reactivity. Noteworthy, the vessel is removed from the organisms, thus important factors like the contact to the flowing blood, nervous system are missing. Future studies could investigate the mechanisms underlying the impaired FMD in aging AS animals by pharmacological intervention *in vivo*. Linking the observation that under certain disease states, eNOS-independent mechanisms, are predominant. To conclude, our data indicate that AS has an additive effect regarding the deterioration of NO bioavailability in aging animals *in vivo*.

5.4 Aortic endothelium-dependent relaxation was decreased in mice with aortic valve stenosis

In the present study, we show that impaired endothelium-mediated relaxation of VSMCs is a common feature in AS animals in the absence of any of the common comorbidities such as diabetes, hypertension, or CAD. However, endothelial function has been reported to vary between different vascular beds (Chiu & Chien, 2011). Consequently, endothelial dysfunction of one vascular tissue does not necessarily require endothelial dysfunction of other vascular beds.

Therefore, we conducted vascular endothelial function studies on isolated aortic rings in an organ bath setting from mice with AS. Our data suggest impaired aortic endothelium-dependent relaxation in mice suffering from AS. This was revealed by a significantly decreased endothelium-dependent relaxation response to acetylcholine in aortic ring assay. The endothelium-dependent response to acetylcholine tended to be decreased in the absence of COX inhibitor indomethacin, but only the presence of this inhibitor revealed the NO-dependent relaxation impairment in AS animals. As has been previously reported in the literature, decrease in synthesis and bioavailability of NO can lead to a shift in favor of the synthesis or effect of constrictive prostanoids (Laemmel et al., 2003) and contribute to endothelial dysfunction. These findings are in line with a considerable body of literature that has identified concomitant impairment of NO-dependent relaxation and increased synthesis of vasoconstrictors from the arachidonic acid pathway (Matz et al., 2000; Rodríguez-Mañas et al., 2009; Vanhoutte et al., 2005). Particularly the role of COX-derived vasoconstrictor products in the context of aging was pointed out previously (Kang et al., 2007). Considering the data from three months after wire-injury, we speculate that products of the arachidonic acid metabolism or their effect are increasing with age in mice with AS. Noteworthy, the relative decline in relaxation response to acetylcholine was comparably equal in the presence or absence of indomethacin in both groups after three months and four weeks.

In conclusion, the decreased efficacy of acetylcholine (maximal response) was almost similar in all mice with AS, even though reaching only significance in the animals four weeks after wire-injury. The observation of unaltered relaxation response to NO donor SNP demonstrates preserved sensitivity of VSMCs, and thus it can be assumed that NO-stimulated formation of cGMP was most likely not affected. Of note, the abolished vasodilator response to acetylcholine in the presence of L-NAME demonstrates that

endothelium-dependent relaxation was completely NO-dependent in aortic rings. Therefore, it can be concluded that impaired relaxation response to acetylcholine is attributable to a decrease of NO. This is either due to an altered eNOS-dependent formation of NO, eNOS uncoupling or scavenging of NO.

5.4.1 The decrease in aortic endothelium-dependent relaxation was associated with alterations in redox balance

We observed an increase in aortic eNOS expression levels of AS mice with impaired endothelium-dependent relaxation. Nevertheless, eNOS mRNA expression was similar in both experimental groups. Importantly, mRNA expression levels and protein expression levels might not necessarily correlate, considering factors such as posttranscriptional mechanisms and the variations in half-lives of mRNA and proteins (Greenbaum et al., 2003). Together with results from aortic rings, it becomes evident that even though aortic eNOS expression was increased, the enzyme's activity was not enhanced. Lacking information about eNOS phosphorylation state, which can alter the enzymes' activity towards increased activation by, e.g., phosphorylation at serine residue, or decreased activation by phosphorylation at threonine residue, limits the precise interpretation of the results. However, many physiological stimuli are known to regulate eNOS expression and thus influence NO generation. Several studies provide evidence of the role of enhanced vascular O_2^- in the pathology of endothelial function, associated with increased eNOS expression, e.g. in rats suffering from ischemic heart failure (Bauersachs et al., 1999). In line with these findings, it was demonstrated that oxidative stress contributes to endothelial dysfunction in spontaneously hypertensive rats with significantly enhanced eNOS expression (Ulker et al., 2003). Many other groups verified the association of oxidative stress and endothelial dysfunction in cardiovascular diseases (Brunner et al., 2005; Schulz et al., 2011; Silva et al., 2012; Tejero et al., 2019). All these studies suggested that the enhanced generation of O_2^-, results in the formation of $ONOO^-$, which is known to induce the phenomena of eNOS uncoupling by disruption of the eNOS dimer (Zou et al., 2002). Disease states, in which control of ROS by antioxidant enzymes are diminished, eNOS contributes to oxidative stress due to eNOS uncoupling (Förstermann & Münzel, 2006).

The tripeptide GSH is an abundant antioxidant (Meister, 1994), opposing harmful effects of ROS, thereby being crucial for redox homeostasis. Therefore, the ratio of reduced (GSH) and the oxidized forms (GSSG) are used as a marker for oxidative stress (Asensi et al., 1999; Xiong et al., 2011). The imbalance of GSH homeostasis was also reported in patients

diagnosed with arteriosclerosis and aortic valve sclerosis (Valerio et al., 2019) and in patients with AS (Cavalca et al., 2013).

We found that the GSH/GSSG ratio was significantly reduced in the aorta of animals with AS compared to sham mice, while plasma and heart ratios did not significantly differ. The aortic mRNA expression levels of glutathione reductase and glutathione peroxidase were not significantly different between sham and AS animals. Superoxide dismutase 1 tends to show an increased expression, whereas catalase expression was significantly enhanced in aortic tissue of AS animals. All of these enzymes together with SH-containing compounds and antioxidants such as tocopherol play an important role in the antioxidant buffering system (Sies et al., 2017). The imbalance between these antioxidant systems and excessive ROS reflects the condition of oxidative stress, in which the final stage causes damage to proteins, lipids and nucleic acids (Storz and Imlay, 1999). Interestingly, we observed an increase in the aortic mRNA expression of catalase. Catalase catalyzes the reaction of H_2O_2, formed by superoxide dismutase from O_2^- to oxygen and water. Previous studies showed that H_2O_2 is able to increase eNOS protein expression (Drummond et al., 2000, Thomas, Chen and Keaney, 2002). However, protein expression levels of nitrotyrosine, a posttranslational protein modification of tyrosine residues by oxidants originated from NO (Thomson, 2015), showed no alterations after four weeks in aortic tissue from AS mice. Thus, these results hint for an adaptive increase in antioxidative capacity, which was limited to the vessel at this stage. This increase in vascular ROS might be a secondary toxicity effect of cell-free Hb, as mentioned in the previous section. The effects of ROS in vascular tone regulation are complex and might affect both contraction and relaxation responses, but it was described to induce chronically increased expression of contractile proteins (Chettimada et al., 2014). However, further investigations are needed to clarify to what extent ROS contribute to impaired endothelium-dependent relaxation response in AS.

6 Summary and Outlook

Aortic valve stenosis is still the leading valvular heart disease in the western world, determining cardiovascular morbidity and mortality in AS patients. Although endothelial dysfunction in AS patients has been known for a long time, research progress was limited due to the lack of a suitable mouse model comprising the fundamental characteristics of AS. We hypothesized that turbulent blood flow alterations in AS trigger the release of cell-free Hb, which leads to a reduction in NO bioavailability. Therefore, the present work aimed to examine endothelial function in a murine model of AS induced by aortic valve injury without further metabolic intervention. Initially, the model was characterized by evaluating the consequences of valvular orifice narrowing on aortic blood flow, LV function and RBCs integrity. Based on our findings, the moderate wire-injury model can be considered mild in terms of myocardial afterload and RBCs membrane damage. However, the results of the present work hint that AS is sufficient to induce subhemolytic trauma to RBCs with release of cell-free Hb, consequently limits NO to activate soluble guanylyl cyclase and thus VSMCs relaxation. Furthermore, this was supported by improvement of FMD in the presence of the physiological scavenger of cell-free Hb, Hp. These experiments confirmed that Hp can improve NO relaxation response during FMD studies in the femoral artery in our AS model. In addition, we observed that older animals suffer from a substantially greater impaired NO-dependent dilation than younger animals with AS *in vivo*. Furthermore, *ex-vivo* vascular reactivity studies of isolated aortic segments, revealed the impairment of aortic endothelium-dependent relaxation in AS animals. Moreover, this research illustrates altered aortic antioxidant capacity, suggesting a potential increase in ROS in the aortic vessel, which might contribute to the observed decrease in aortic endothelium-dependent relaxation responses. Nevertheless, future research needs to identify the mechanisms underlying the imbalance of antioxidants. The excess of ROS might be an additional consequence of cell-free Hb-driven toxicity via heme release or eNOS uncoupling. For this purpose, further vascular reactivity studies could be implemented in the presence of different antioxidants. Further work is certainly required to disentangle the complexities in the involvement of eNOS phosphorylation by transcriptional modifications of different protein kinases, which are also of particular importance to understand mechanisms involved in AS-associated endothelial dysfunction. Notably, future research needs to reconsider the role of plasma derived Hp as a promising therapeutic tool in conditions associated with increased cell-free Hb. Although multiple animal studies disclosed the beneficial effects of Hp by

compartmentalization of cell-free Hb, future work needs to widen this data to clinical application. Globally spoken, the data of the present work provide a good initiation for future translational discussions on decreased NO bioavailability driven endothelial dysfunction in AS patients, especially considering the high onset of cardiovascular adverse events. To our knowledge, this is the first study that explored vascular endothelial function in an experimental model of AS.

7 References

Aikawa, E., Nahrendorf, M., Sosnovik, D., Lok, V. M., Jaffer, F. A., Aikawa, M., & Weissleder, R. (2007). Multimodality molecular imaging identifies proteolytic and osteogenic activities in early aortic valve disease. *Circulation*, *115*(3), 377–386. https://doi.org/10.1161/CIRCULATIONAHA.106.654913

Aird, W. C. (2007). Phenotypic Heterogeneity of the Endothelium. *Circulation Research*, *100*(2), 158–173. https://doi.org/10.1161/01.RES.0000255691.76142.4a

Aird, W. C. (2012). Endothelial cell heterogeneity. *Cold Spring Harbor Perspectives in Medicine*, *2*(1), 1–13. https://doi.org/10.1101/cshperspect.a006429

Amdahl, M. B., DeMartino, A. W., & Gladwin, M. T. (2019). Inorganic nitrite bioactivation and role in physiological signaling and therapeutics. *Biological Chemistry*, *401*(1), 201–211. https://doi.org/10.1515/hsz-2019-0349

Asakura, T., & Karino, T. (1990). Flow patterns and spatial distribution of atherosclerotic lesions in human coronary arteries. *Circulation Research*, *66*(4), 1045–1066. https://doi.org/10.1161/01.RES.66.4.1045

Asensi, M., Sastre, J., Pallardo, F. V., Lloret, A., Lehner, M., Garcia-de-la Asuncion, J., & Viña, J. (1999). [23] Ratio of reduced to oxidized glutathione as indicator of oxidative stress status and DNA damage. In *Methods in Enzymology* (Vol. 299, Issue 1978, pp. 267–276). https://doi.org/10.1016/S0076-6879(99)99026-2

Baek, J. H., D'Agnillo, F., Vallelian, F., Pereira, C. P., Williams, M. C., Jia, Y., Schaer, D. J., & Buehler, P. W. (2012). Hemoglobin-driven pathophysiology is an in vivo consequence of the red blood cell storage lesion that can be attenuated in guinea pigs by haptoglobin therapy. *Journal of Clinical Investigation*, *122*(4), 1444–1458. https://doi.org/10.1172/JCI59770

Balla, G., Jacob, H. S., Eaton, J. W., Belcher, J. D., & Vercellotti, G. M. (1991). Hemin: a possible physiological mediator of low density lipoprotein oxidation and endothelial injury. *Arteriosclerosis and Thrombosis: A Journal of Vascular Biology*, *11*(6), 1700–1711. https://doi.org/10.1161/01.ATV.11.6.1700

Balla, J., Vercellotti, G. M., Jeney, V., Yachie, A., Varga, Z., Eaton, J. W., & Balla, G. (2005). Heme, heme oxygenase and ferritin in vascular endothelial cell injury. *Molecular Nutrition & Food Research*, *49*(11), 1030–1043. https://doi.org/10.1002/mnfr.200500076

Balligand, J.-L., Feron, O., & Dessy, C. (2009). eNOS Activation by Physical Forces: From Short-Term Regulation of Contraction to Chronic Remodeling of Cardiovascular Tissues. *Physiological Reviews*, *89*(2), 481–534. https://doi.org/10.1152/physrev.00042.2007

Baron, S. J., Magnuson, E. A., Lu, M., Wang, K., Chinnakondepalli, K., Mack, M., Thourani, V. H., Kodali, S., Makkar, R., Herrmann, H. C., Kapadia, S., Babaliaros, V., Williams, M. R., Kereiakes, D., Zajarias, A., Alu, M. C., Webb, J. G., Smith, C. R., Leon, M. B., & Cohen, D. J. (2019). Health Status After Transcatheter Versus Surgical Aortic Valve Replacement in Low-Risk Patients With Aortic Stenosis. *Journal of the American College of Cardiology*, *74*(23), 2833–2842. https://doi.org/10.1016/j.jacc.2019.09.007

Baskurt, O. K. (2012). Red Blood Cell Mechanical Stability. *Engineering*, *04*(10), 8–10. https://doi.org/10.4236/eng.2012.410B003

Bauersachs, J., Bouloumie, A., Fraccarollo, D., Hu, K., Busse, R., & Ertl, G. (1999). Endothelial Dysfunction in Chronic Myocardial Infarction Despite Increased Vascular Endothelial Nitric Oxide Role of Enhanced Vascular Superoxide Production. *Circulation*, *100*(3), 292–298.

Baumgartner, H., Falk, V., Bax, J. J., De Bonis, M., Hamm, C., Holm, P. J., Iung, B., Lancellotti, P., Lansac, E., Rodriguez Muñoz, D., Rosenhek, R., Sjögren, J., Tornos Mas, P., Vahanian, A., Walther, T., Wendler, O., Windecker, S., Zamorano, J. L., Roffi, M., … Brecker, S. J. D. (2017). 2017 ESC/EACTS Guidelines for the management of valvular heart disease. *European Heart Journal*, *38*(36), 2739–2791. https://doi.org/10.1093/eurheartj/ehx391

Baumgartner, H., Hung, J., Bermejo, J., Chambers, J. B., Evangelista, A., Griffin, B. P., Iung, B., Otto, C. M., Pellikka, P. A., & Quiñones, M. (2009). Echocardiographic assessment of valve stenosis: EAE/ASE recommendations for clinical practice. *European Journal of Echocardiography*, *10*(1), 1–25. https://doi.org/10.1093/ejechocard/jen303

Belcher, J. D., Chen, C., Nguyen, J., Abdulla, F., Zhang, P., Nguyen, H., Nguyen, P., Killeen, T., Miescher, S. M., Brinkman, N., Nath, K. A., Steer, C. J., & Vercellotti, G. M. (2018). Haptoglobin and hemopexin inhibit vaso-occlusion and inflammation in murine sickle cell disease: Role of heme oxygenase-1 induction. *PLOS ONE*, *13*(4), e0196455. https://doi.org/10.1371/journal.pone.0196455

Blacher, J., Asmar, R., Djane, S., London, G. M., & Safar, M. E. (1999). Aortic Pulse Wave Velocity as a Marker of Cardiovascular Risk in Hypertensive Patients. *Hypertension*, *33*(5), 1111–1117. https://doi.org/10.1161/01.HYP.33.5.1111

Boas, F. E., Forman, L., & Beutler, E. (1998). Phosphatidylserine exposure and red cell viability in red cell aging and in hemolytic anemia. *Proceedings of the National Academy of Sciences*, *95*(6), 3077–3081. https://doi.org/10.1073/pnas.95.6.3077

Bohbot, Y., Renard, C., Manrique, A., Levy, F., Maréchaux, S., Gerber, B. L., & Tribouilloy, C. (2020). Usefulness of Cardiac Magnetic Resonance Imaging in Aortic Stenosis. *Circulation: Cardiovascular Imaging*, *13*(5), 1–16. https://doi.org/10.1161/CIRCIMAGING.119.010356

Bönner, F., Jacoby, C., Temme, S., Borg, N., Ding, Z., Schrader, J., & Flögel, U. (2014). Multifunctional MR monitoring of the healing process after myocardial infarction. *Basic Research in Cardiology*, *109*(5), 430. https://doi.org/10.1007/s00395-014-0430-0

Boretti, F. S., Buehler, P. W., D'Agnillo, F., Kluge, K., Glaus, T., Butt, O. I., Jia, Y., Goede, J., Pereira, C. P., Maggiorini, M., Schoedon, G., Alayash, A. I., & Schaer, D. J. (2009). Sequestration of extracellular hemoglobin within a haptoglobin complex decreases its hypertensive and oxidative effects in dogs and guinea pigs. *Journal of Clinical Investigation*, *119*(8), 2271–2280. https://doi.org/10.1172/JCI39115

Bredt, D. S., & Snyder, S. H. (1990). Isolation of nitric oxide synthetase, a calmodulin-requiring enzyme. *Proceedings of the National Academy of Sciences*, *87*(2), 682–685. https://doi.org/10.1073/pnas.87.2.682

Brevetti, G., Silvestro, A., Schiano, V., & Chiariello, M. (2003). Endothelial Dysfunction and Cardiovascular Risk Prediction in Peripheral Arterial Disease. *Circulation*, *108*(17), 2093–2098. https://doi.org/10.1161/01.CIR.0000095273.92468.D9

Brunner, H., Cockcroft, J. R., Deanfield, J., Donald, A., Ferrannini, E., Halcox, J., Kiowski, W., L??scher, T. F., Mancia, G., Natali, A., Oliver, J. J., Pessina, A. C., Rizzoni, D., Rossi, G. P., Salvetti, A., Spieker, L. E., Taddei, S., & Webb, D. J. (2005). Endothelial function and dysfunction. Part II: Association with cardiovascular risk factors and diseases. A statement by the Working Group on Endothelins and Endothelial Factors of the European Society of Hypertension*. *Journal of Hypertension*, *23*(2), 233–246. https://doi.org/10.1097/00004872-200502000-00001

Bryan, N. S., Fernandez, B. O., Bauer, S. M., Garcia-Saura, M. F., Milsom, A. B., Rassaf, T., Maloney, R. E., Bharti, A., Rodriguez, J., & Feelisch, M. (2005). Nitrite is a

signaling molecule and regulator of gene expression in mammalian tissues. *Nature Chemical Biology*, *1*(5), 290–297. https://doi.org/10.1038/nchembio734

Buehler, P. W., Humar, R., & Schaer, D. J. (2020). Haptoglobin Therapeutics and Compartmentalization of Cell-Free Hemoglobin Toxicity. *Trends in Molecular Medicine*, *26*(7), 683–697. https://doi.org/10.1016/j.molmed.2020.02.004

Buerck, J. P., Burke, D. K., Schmidtke, D. W., Snyder, T. A., Papavassiliou, D. V, & O'Rear, E. A. (2021). Production of erythrocyte microparticles in a sub-hemolytic environment. *Journal of Artificial Organs*, *24*(2), 135–145. https://doi.org/10.1007/s10047-020-01231-7

Bull, S., Loudon, M., Francis, J. M., Joseph, J., Gerry, S., Karamitsos, T. D., Prendergast, B. D., Banning, A. P., Neubauer, S., & Myerson, S. G. (2015). A prospective, double-blind, randomized controlled trial of the angiotensin-converting enzyme inhibitor Ramipril In Aortic Stenosis (RIAS trial). *European Heart Journal – Cardiovascular Imaging*, *16*(8), 834–841. https://doi.org/10.1093/ehjci/jev043

Bunn, H. F., Nathan, D. G., Dover, G. J., Hebbel, R. P., Platt, O. S., Rosse, W. F., & Ware, R. E. (2010). Pulmonary hypertension and nitric oxide depletion in sickle cell disease. *Blood*, *116*(5), 687–692. https://doi.org/10.1182/blood-2010-02-268193

Busse, R., Edwards, G., Félétou, M., Fleming, I., Vanhoutte, P. M., & Weston, A. H. (2002). EDHF: bringing the concepts together. *Trends in Pharmacological Sciences*, *23*(8), 374–380. https://doi.org/10.1016/S0165-6147(02)02050-3

Butcher, J. T., Penrod, A. M., García, A. J., & Nerem, R. M. (2004). Unique Morphology and Focal Adhesion Development of Valvular Endothelial Cells in Static and Fluid Flow Environments. *Arteriosclerosis, Thrombosis, and Vascular Biology*, *24*(8), 1429–1434. https://doi.org/10.1161/01.ATV.0000130462.50769.5a

Butcher, J. T., Tressel, S., Johnson, T., Turner, D., Sorescu, G., Jo, H., & Nerem, R. M. (2006). Transcriptional Profiles of Valvular and Vascular Endothelial Cells Reveal Phenotypic Differences. *Arteriosclerosis, Thrombosis, and Vascular Biology*, *26*(1), 69–77. https://doi.org/10.1161/01.ATV.0000196624.70507.0d

Butt, O. I., Buehler, P. W., & D'Agnillo, F. (2010). Differential Induction of Renal Heme Oxygenase and Ferritin in Ascorbate and Nonascorbate Producing Species Transfused with Modified Cell-Free Hemoglobin. *Antioxidants & Redox Signaling*, *12*(2), 199–208. https://doi.org/10.1089/ars.2009.2798

Cavalca, V., Tremoli, E., Porro, B., Veglia, F., Myasoedova, V., Squellerio, I., Manzone, D., Zanobini, M., Trezzi, M., Di Minno, M. N. D., Werba, J. P., Tedesco, C., Alamanni, F., & Parolari, A. (2013). Oxidative stress and nitric oxide pathway in adult patients who are candidates for cardiac surgery: Patterns and differences. *Interactive Cardiovascular and Thoracic Surgery*, *17*(6), 923–930. https://doi.org/10.1093/icvts/ivt386

Celermajer, D. S., Sorensen, K. E., Gooch, V. M., Spiegelhalter, D. J., Miller, O. I., Sullivan, I. D., Lloyd, J. K., & Deanfield, J. E. (1992). Non-invasive detection of endothelial dysfunction in children and adults at risk of atherosclerosis. *The Lancet*, *340*(8828), 1111–1115. https://doi.org/10.1016/0140-6736(92)93147-F

Chan, K. L., Teo, K., Dumesnil, J. G., Ni, A., & Tam, J. (2010). Effect of lipid lowering with rosuvastatin on progression of aortic stenosis: Results of the aortic stenosis progression observation: Measuring effects of rosuvastatin (Astronomer) trial. *Circulation*, *121*(2), 306–314. https://doi.org/10.1161/CIRCULATIONAHA.109.900027

Chenevard, R., Bechir, M., Hurlimann, D., Ruschitzka, F., Turina, J., Luscher, T. F., & Noll, G. (2006). Persistent endothelial dysfunction in calcified aortic stenosis beyond valve replacement surgery. *Heart*, *92*(12), 1862–1863. https://doi.org/10.1136/hrt.2006.087437

Chettimada, S., Ata, H., Rawat, D. K., Gulati, S., Kahn, A. G., Edwards, J. G., & Gupte, S.

A. (2014). Contractile protein expression is upregulated by reactive oxygen species in aorta of Goto-Kakizaki rat. *American Journal of Physiology-Heart and Circulatory Physiology*, *306*(2), H214–H224. https://doi.org/10.1152/ajpheart.00310.2013

Chi, J.-T., Chang, H. Y., Haraldsen, G., Jahnsen, F. L., Troyanskaya, O. G., Chang, D. S., Wang, Z., Rockson, S. G., van de Rijn, M., Botstein, D., & Brown, P. O. (2003). Endothelial cell diversity revealed by global expression profiling. *Proceedings of the National Academy of Sciences*, *100*(19), 10623–10628. https://doi.org/10.1073/pnas.1434429100

Chiu, J. J., & Chien, S. (2011). Effects of disturbed flow on vascular endothelium: Pathophysiological basis and clinical perspectives. *Physiological Reviews*, *91*(1), 327–387. https://doi.org/10.1152/physrev.00047.2009

Coffey, S., Cairns, B. J., & Iung, B. (2016). The modern epidemiology of heart valve disease. *Heart*, *102*(1), 75–85. https://doi.org/10.1136/heartjnl-2014-307020

Coffey, S., Cox, B., & Williams, M. J. A. (2014). The Prevalence, Incidence, Progression, and Risks of Aortic Valve Sclerosis. *Journal of the American College of Cardiology*, *63*(25), 2852–2861. https://doi.org/10.1016/j.jacc.2014.04.018

Cook, S., Hugli, O., Egli, M., Menard, B., Thalmann, S., Sartori, C., Perrin, C., Nicod, P., Thorens, B., Vollenweider, P., Scherrer, U., & Burcelin, R. (2004). Partial Gene Deletion of Endothelial Nitric Oxide Synthase Predisposes to Exaggerated High-Fat Diet--Induced Insulin Resistance and Arterial Hypertension. *Diabetes*, *53*(8), 2067–2072. https://doi.org/10.2337/diabetes.53.8.2067

Corretti, M. C., Anderson, T. J., Benjamin, E. J., Celermajer, D., Charbonneau, F., Creager, M. A., Deanfield, J., Drexler, H., Gerhard-Herman, M., Herrington, D., Vallance, P., Vita, J., & Vogel, R. (2002). Guidelines for the ultrasound assessment of endothelial-dependent flow-mediated vasodilation of the brachial artery. *Journal of the American College of Cardiology*, *39*(2), 257–265. https://doi.org/10.1016/S0735-1097(01)01746-6

Cortese-Krott, M. M., & Kelm, M. (2014). Endothelial nitric oxide synthase in red blood cells: Key to a new erythrocrine function? *Redox Biology*, *2*(1), 251–258. https://doi.org/10.1016/j.redox.2013.12.027

Cortese-Krott, M. M., Rodriguez-Mateos, A., Sansone, R., Kuhnle, G. G. C., Thasian-Sivarajah, S., Krenz, T., Horn, P., Krisp, C., Wolters, D., Heiß, C., Kröncke, K.-D., Hogg, N., Feelisch, M., & Kelm, M. (2012). Human red blood cells at work: identification and visualization of erythrocytic eNOS activity in health and disease. *Blood*, *120*(20), 4229–4237. https://doi.org/10.1182/blood-2012-07-442277

Cosby, K., Partovi, K. S., Crawford, J. H., Patel, R. P., Reiter, C. D., Martyr, S., Yang, B. K., Waclawiw, M. A., Zalos, G., Xu, X., Huang, K. T., Shields, H., Kim-Shapiro, D. B., Schechter, A. N., Cannon, R. O., & Gladwin, M. T. (2003). Nitrite reduction to nitric oxide by deoxyhemoglobin vasodilates the human circulation. *Nature Medicine*, *9*(12), 1498–1505. https://doi.org/10.1038/nm954

Côté, N., Couture, C., Pibarot, P., Després, J.-P., & Mathieu, P. (2011). Angiotensin receptor blockers are associated with a lower remodelling score of stenotic aortic valves. *European Journal of Clinical Investigation*, *41*(11), 1172–1179. https://doi.org/10.1111/j.1365-2362.2011.02522.x

Cowell, S. J., Newby, D. E., Prescott, R. J., Bloomfield, P., Reid, J., Northridge, D. B., & Boon, N. A. (2005). A Randomized Trial of Intensive Lipid-Lowering Therapy in Calcific Aortic Stenosis. *New England Journal of Medicine*, *352*(23), 2389–2397. https://doi.org/10.1056/NEJMoa043876

Dasi, L. P., Simon, H. A., Sucosky, P., & Yoganathan, A. P. (2009). FLUID MECHANICS OF ARTIFICIAL HEART VALVES. *Clinical and Experimental Pharmacology and*

Physiology, *36*(2), 225–237. https://doi.org/10.1111/j.1440-1681.2008.05099.x

Davies, P. F. (1995). Flow-mediated endothelial mechanotransduction. *Physiological Reviews*, *75*(3), 519–560. https://doi.org/10.1152/physrev.1995.75.3.519

Deonikar, P., & Kavdia, M. (2013). Contribution of membrane permeability and unstirred layer diffusion to nitric oxide–red blood cell interaction. *Journal of Theoretical Biology*, *317*, 321–330. https://doi.org/10.1016/j.jtbi.2012.10.025

Dichtl, W., Alber, H. F., Feuchtner, G. M., Hintringer, F., Reinthaler, M., Bartel, T., Süssenbacher, A., Grander, W., Ulmer, H., Pachinger, O., & Müller, S. (2008). Prognosis and Risk Factors in Patients With Asymptomatic Aortic Stenosis and Their Modulation by Atorvastatin (20 mg). *The American Journal of Cardiology*, *102*(6), 743–748. https://doi.org/10.1016/j.amjcard.2008.04.060

Doherty, D. H., Doyle, M. P., Curry, S. R., Vali, R. J., Fattor, T. J., Olson, J. S., & Lemon, D. D. (1998). Rate of reaction with nitric oxide determines the hypertensive effect of cell-free hemoglobin. *Nature Biotechnology*, *16*(7), 672–676. https://doi.org/10.1038/nbt0798-672

Dweck, M. R., Boon, N. A., & Newby, D. E. (2012). Calcific aortic stenosis: A disease of the valve and the myocardium. *Journal of the American College of Cardiology*, *60*(19), 1854–1863. https://doi.org/10.1016/j.jacc.2012.02.093

Dweck, M. R., Joshi, S., Murigu, T., Alpendurada, F., Jabbour, A., Melina, G., Banya, W., Gulati, A., Roussin, I., Raza, S., Prasad, N. A., Wage, R., Quarto, C., Angeloni, E., Refice, S., Sheppard, M., Cook, S. A., Kilner, P. J., Pennell, D. J., … Prasad, S. K. (2011). Midwall Fibrosis Is an Independent Predictor of Mortality in Patients With Aortic Stenosis. *Journal of the American College of Cardiology*, *58*(12), 1271–1279. https://doi.org/10.1016/j.jacc.2011.03.064

El Accaoui, Ramzi N., Gould, S. T., Hajj, G. P., Chu, Y., Davis, M. K., Kraft, D. C., Lund, D. D., Brooks, R. M., Doshi, H., Zimmerman, K. A., Kutschke, W., Anseth, K. S., Heistad, D. D., & Weiss, R. M. (2014). Aortic valve sclerosis in mice deficient in endothelial nitric oxide synthase. *American Journal of Physiology-Heart and Circulatory Physiology*, *306*(9), H1302–H1313. https://doi.org/10.1152/ajpheart.00392.2013

Elmariah, S., Cimmino, G., Fuster, V., & Badimon, J. J. (2010). BISPHOSPHONATES PREVENT OXIDIZED LOW-DENSITY LIPOPROTEIN-INDUCED EXPRESSION OF OSTEOGENIC MARKERS IN AORTIC VALVE MYOFIBROBLASTS. *Journal of the American College of Cardiology*, *55*(10), A149.E1398. https://doi.org/10.1016/S0735-1097(10)61399-X

Erkens, R., Kramer, C. M., Lückstädt, W., Panknin, C., Krause, L., Weidenbach, M., Dirzka, J., Krenz, T., Mergia, E., Suvorava, T., Kelm, M., & Cortese-Krott, M. M. (2015). Left ventricular diastolic dysfunction in Nrf2 knock out mice is associated with cardiac hypertrophy, decreased expression of SERCA2a, and preserved endothelial function. *Free Radical Biology and Medicine*, *89*, 906–917. https://doi.org/10.1016/j.freeradbiomed.2015.10.409

Erkens, R., Suvorava, T., Kramer, C. M., Diederich, L. D., Kelm, M., & Cortese-Krott, M. M. (2017). Modulation of Local and Systemic Heterocellular Communication by Mechanical Forces: A Role of Endothelial Nitric Oxide Synthase. *Antioxidants & Redox Signaling*, *26*(16), 917–935. https://doi.org/10.1089/ars.2016.6904

Everett, R. J., Tastet, L., Clavel, M.-A., Chin, C. W. L., Capoulade, R., Vassiliou, V. S., Kwiecinski, J., Gomez, M., van Beek, E. J. R., White, A. C., Prasad, S. K., Larose, E., Tuck, C., Semple, S., Newby, D. E., Pibarot, P., & Dweck, M. R. (2018). Progression of Hypertrophy and Myocardial Fibrosis in Aortic Stenosis. *Circulation: Cardiovascular Imaging*, *11*(6), 1–11.

https://doi.org/10.1161/CIRCIMAGING.117.007451

Feletou, M., & Vanhoutte, P. M. (1988). Endothelium-dependent hyperpolarization of canine coronary smooth muscle. *British Journal of Pharmacology*, *93*(3), 515–524. https://doi.org/10.1111/j.1476-5381.1988.tb10306.x

Fleming, I. (2010). Molecular mechanisms underlying the activation of eNOS. *Pflügers Archiv - European Journal of Physiology*, *459*(6), 793–806. https://doi.org/10.1007/s00424-009-0767-7

Fleming, I., Bauersachs, J., Fisslthaler, B., & Busse, R. (1998). Ca 2+ -Independent Activation of the Endothelial Nitric Oxide Synthase in Response to Tyrosine Phosphatase Inhibitors and Fluid Shear Stress. *Circulation Research*, *82*(6), 686–695. https://doi.org/10.1161/01.RES.82.6.686

Förstermann, U., Closs, E. I., Pollock, J. S., Nakane, M., Schwarz, P., Gath, I., & Kleinert, H. (1994). Nitric oxide synthase isozymes antibodies. *The Histochemical Journal*, *23*(6), 738–744. https://doi.org/10.1007/BF02388299

Förstermann, U., & Münzel, T. (2006a). Endothelial Nitric Oxide Synthase in Vascular Disease. *Circulation*, *113*(13), 1708–1714. https://doi.org/10.1161/CIRCULATIONAHA.105.602532

Furchgott, R. F., & Zawadzki, J. V. (1980). The obligatory role of endothelial cells in the relaxation of arterial smooth muscle by acetylcholine. *Nature*, *288*(5789), 373–376. https://doi.org/10.1038/288373a0

Garcia, J., Barker, A. J., & Markl, M. (2019). The Role of Imaging of Flow Patterns by 4D Flow MRI in Aortic Stenosis. *JACC: Cardiovascular Imaging*, *12*(2), 252–266. https://doi.org/10.1016/j.jcmg.2018.10.034

Gardiner, S. M., Compton, A. M., Bennett, T., Palmer, R. M. J., & Moncada, S. (1990). Control of regional blood flow by endothelium-derived nitric oxide. *Hypertension*, *15*(5), 486–492. https://doi.org/10.1161/01.HYP.15.5.486

Garg, V., Muth, A. N., Ransom, J. F., Schluterman, M. K., Barnes, R., King, I. N., Grossfeld, P. D., & Srivastava, D. (2005). Mutations in NOTCH1 cause aortic valve disease. *Nature*, *437*(7056), 270–274. https://doi.org/10.1038/nature03940

Garland, C. J., & McPherson, G. A. (1992). Evidence that nitric oxide does not mediate the hyperpolarization and relaxation to acetylcholine in the rat small mesenteric artery. *British Journal of Pharmacology*, *105*(2), 429–435. https://doi.org/10.1111/j.1476-5381.1992.tb14270.x

Ghaisas, N. K., Foley, J. B., O'Briain, D. S., Crean, P., Kelleher, D., & Walsh, M. (2000). Adhesion molecules in nonrheumatic aortic valve disease: endothelial expression, serum levels and effects of valve replacement. *Journal of the American College of Cardiology*, *36*(7), 2257–2262. https://doi.org/10.1016/S0735-1097(00)00998-0

Gladwin, M. T., Crawford, J. H., & Patel, R. P. (2004). The biochemistry of nitric oxide, nitrite, and hemoglobin: role in blood flow regulation. *Free Radical Biology and Medicine*, *36*(6), 707–717. https://doi.org/10.1016/j.freeradbiomed.2003.11.032

Gladwin, M. T., Raat, N. J. H., Shiva, S., Dezfulian, C., Hogg, N., Kim-Shapiro, D. B., & Patel, R. P. (2006). Nitrite as a vascular endocrine nitric oxide reservoir that contributes to hypoxic signaling, cytoprotection, and vasodilation. *American Journal of Physiology-Heart and Circulatory Physiology*, *291*(5), H2026–H2035. https://doi.org/10.1152/ajpheart.00407.2006

Gödecke, A., Decking, U. K. M., Ding, Z., Hirchenhain, J., Bidmon, H.-J., Gödecke, S., & Schrader, J. (1998). Coronary Hemodynamics in Endothelial NO Synthase Knockout Mice. *Circulation Research*, *82*(2), 186–194. https://doi.org/10.1161/01.RES.82.2.186

Gokce, N., Keaney, J. F., Hunter, L. M., Watkins, M. T., Nedeljkovic, Z. S., Menzoian, J. O., & Vita, J. A. (2003). Predictive value of noninvasivelydetermined endothelial

dysfunction for long-term cardiovascular events inpatients with peripheral vascular disease. *Journal of the American College of Cardiology*, *41*(10), 1769–1775. https://doi.org/10.1016/S0735-1097(03)00333-4

Goody, P. R., Hosen, M. R., Christmann, D., Niepmann, S. T., Zietzer, A., Adam, M., Bönner, F., Zimmer, S., Nickenig, G., & Jansen, F. (2020). Aortic Valve Stenosis. *Arteriosclerosis, Thrombosis, and Vascular Biology*, *40*(4), 885–900. https://doi.org/10.1161/ATVBAHA.119.313067

Gould, S. T., Srigunapalan, S., Simmons, C. A., & Anseth, K. S. (2013). Hemodynamic and Cellular Response Feedback in Calcific Aortic Valve Disease. *Circulation Research*, *113*(2), 186–197. https://doi.org/10.1161/CIRCRESAHA.112.300154

Green, D. J., Jones, H., Thijssen, D., Cable, N. T., & Atkinson, G. (2011). Flow-Mediated Dilation and Cardiovascular Event Prediction. *Hypertension*, *57*(3), 363–369. https://doi.org/10.1161/HYPERTENSIONAHA.110.167015

Greenbaum, D., Colangelo, C., Williams, K., & Gerstein, M. (2003). Comparing protein abundance and mRNA expression levels on a genomic scale. *Genome Biology*, *4*(117). https://doi.org/10.1186/gb-2003-4-9-117

Haberkorn, S. M., Jacoby, C., Ding, Z., Keul, P., Bönner, F., Polzin, A., Levkau, B., Schrader, J., Kelm, M., & Flögel, U. (2017). Cardiovascular Magnetic Resonance Relaxometry Predicts Regional Functional Outcome After Experimental Myocardial Infarction. *Circulation: Cardiovascular Imaging*, *10*(8), 1–12. https://doi.org/10.1161/CIRCIMAGING.116.006025

Hanley, D. A., Adachi, J. D., Bell, A., & Brown, V. (2012). Denosumab: mechanism of action and clinical outcomes. *International Journal of Clinical Practice*, *66*(12), 1139–1146. https://doi.org/10.1111/ijcp.12022

Hardeman, M. R., Goedhart, P. T., Dobbe, J. G. G., & Lettinga, K. P. (1994). Laser-assisted optical rotational cell analyser (L.O.R.C.A.); I. A new instrument for measurement of various structural hemorheological parameters. *Clinical Hemorheology and Microcirculation*, *14*(4), 605–618. https://doi.org/10.3233/CH-1994-14416

Harris, R. A., Nishiyama, S. K., Wray, W. D., & Richardson Russel S.S. (2010). Ultrasound assessment pf flow-mediated dilation: a tutorial. *Hypertension*, *55*(5), 1075–1085. https://doi.org/10.1161/HYPERTENSIONAHA.110.150821.ULTRASOUND

Hein, T. W., Zhang, C., Wang, W., Chang, C., Thengchaisri, N., & Kuo, L. (2003). Ischemia-reperfusion selectively impairs nitric oxide- mediated dilation in coronary arterioles: counteracting role of arginase. *The FASEB Journal*, *17*(15), 2328–2330. https://doi.org/10.1096/fj.03-0115fje

Heiss, C., Lauer, T., Dejam, A., Kleinbongard, P., Hamada, S., Rassaf, T., Matern, S., Feelisch, M., & Kelm, M. (2006). Plasma Nitroso Compounds Are Decreased in Patients With Endothelial Dysfunction. *Journal of the American College of Cardiology*, *47*(3), 573–579. https://doi.org/10.1016/j.jacc.2005.06.089

Heiss, C., Sievers, R. E., Amabile, N., Momma, T. Y., Chen, Q., Natarajan, S., Yeghiazarians, Y., & Springer, M. L. (2008). In vivo measurement of flow-mediated vasodilation in living rats using high-resolution ultrasound. *American Journal of Physiology-Heart and Circulatory Physiology*, *294*(2), H1086–H1093. https://doi.org/10.1152/ajpheart.00811.2007

Honda, S., Miyamoto, T., Watanabe, T., Narumi, T., Kadowaki, S., Honda, Y., Otaki, Y., Hasegawa, H., Netsu, S., Funayama, A., Ishino, M., Nishiyama, S., Takahashi, H., Arimoto, T., Shishido, T., Miyashita, T., & Kubota, I. (2014b). A Novel Mouse Model of Aortic Valve Stenosis Induced by Direct Wire Injury. *Arteriosclerosis, Thrombosis, and Vascular Biology*, *34*(2), 270–278. https://doi.org/10.1161/ATVBAHA.113.302610

Horn, P., Stern, D., Veulemans, V., Heiss, C., Zeus, T., Merx, M. W., Kelm, M., & Westenfeld, R. (2015). Improved endothelial function and decreased levels of endothelium-derived microparticles after transcatheter aortic valve implantation. *EuroIntervention*, *10*(12), 1456–1463. https://doi.org/10.4244/EIJY14M10_02

Huang, P. L., Huang, Z., Mashimo, H., Bloch, K. D., Moskowitz, M. A., Bevan, J. A., & Fishman, M. C. (1995). Hypertension in mice lacking the gene for endothelial nitric oxide synthase. *Nature*, *377*(6546), 239–242. https://doi.org/10.1038/377239a0

Hugelshofer, M., Buzzi, R. M., Schaer, C. A., Richter, H., Akeret, K., Anagnostakou, V., Mahmoudi, L., Vaccani, R., Vallelian, F., Deuel, J. W., Kronen, P. W., Kulcsar, Z., Regli, L., Baek, J. H., Pires, I. S., Palmer, A. F., Dennler, M., Humar, R., Buehler, P. W., … Schaer, D. J. (2019). Haptoglobin administration into the subarachnoid space prevents hemoglobin-induced cerebral vasospasm. *Journal of Clinical Investigation*, *129*(12), 5219–5235. https://doi.org/10.1172/JCI130630

Ignarro, L. J., Buga, G. M., Wood, K. S., Byrns, R. E., & Chaudhuri, G. (1987). Endothelium-derived relaxing factor produced and released from artery and vein is nitric oxide. *Proceedings of the National Academy of Sciences of the United States of America*, *84*(24), 9265–9269. https://doi.org/10.1073/pnas.84.24.9265

Intengan, H. D., & Schiffrin, E. L. (2000). Structure and Mechanical Properties of Resistance Arteries in Hypertension. *Hypertension*, *36*(3), 312–318. https://doi.org/10.1161/01.HYP.36.3.312

JA Frangos, Eskin, S., McIntire, L., & Ives, C. (1983). *Flow Effects on Prostacyclin Production by Cultured I __ Overflow Lowt9a*. *227*(4693), 1477–1480.

Jacobson, R. J., Rath, C. E., & Perloff, J. K. (1973). Intravascular haemolysis and thrombocytopenia in left ventricular outflow obstruction. *Heart*, *35*(8), 849–854. https://doi.org/10.1136/hrt.35.8.849

Jeffers, G. and K.-S. (2006). NIH Public Access. *Bone*, *23*(1), 1–7. https://www.ncbi.nlm.nih.gov/pmc/articles/PMC3624763/pdf/nihms412728.pdf

Ju, H., Zou, R., Venema, V. J., & Venema, R. C. (1997). Direct Interaction of Endothelial Nitric-oxide Synthase and Caveolin-1 Inhibits Synthase Activity. *Journal of Biological Chemistry*, *272*(30), 18522–18525. https://doi.org/10.1074/jbc.272.30.18522

Kang, K. B., Rajanayagam, M. A. S., van der Zypp, A., & Majewski, H. (2007). A role for cyclooxygenase in aging-related changes of β-adrenoceptor-mediated relaxation in rat aortas. *Naunyn-Schmiedeberg's Archives of Pharmacology*, *375*(4), 273–281. https://doi.org/10.1007/s00210-007-0153-y

Kato, G. J., McGowan, V., Machado, R. F., Little, J. A., Taylor, J., Morris, C. R., Nichols, J. S., Wang, X., Poljakovic, M., Morris, S. M., & Gladwin, M. T. (2006). Lactate dehydrogenase as a biomarker of hemolysis-associated nitric oxide resistance, priapism, leg ulceration, pulmonary hypertension, and death in patients with sickle cell disease. *Blood*, *107*(6), 2279–2285. https://doi.org/10.1182/blood-2005-06-2373

Kawakami, R., Nakagami, H., Noma, T., Ohmori, K., Kohno, M., & Morishita, R. (2016). RANKL system in vascular and valve calcification with aging. *Inflammation and Regeneration*, *36*(1), 10. https://doi.org/10.1186/s41232-016-0016-3

Kelm, M. (1999). Nitric oxide metabolism and breakdown. *Biochimica et Biophysica Acta - Bioenergetics*, *1411*(2–3), 273–289. https://doi.org/10.1016/S0005-2728(99)00020-1

Kim-Shapiro, D. B., Schechter, A. N., & Gladwin, M. T. (2006). Unraveling the Reactions of Nitric Oxide, Nitrite, and Hemoglobin in Physiology and Therapeutics. *Arteriosclerosis, Thrombosis, and Vascular Biology*, *26*(4), 697–705. https://doi.org/10.1161/01.ATV.0000204350.44226.9a

Kleinbongard, P., Dejam, A., Lauer, T., Jax, T., Kerber, S., Gharini, P., Balzer, J., Zotz, R. B., Scharf, R. E., Willers, R., Schechter, A. N., Feelisch, M., & Kelm, M. (2006).

Plasma nitrite concentrations reflect the degree of endothelial dysfunction in humans. *Free Radical Biology and Medicine*, *40*(2), 295–302. https://doi.org/10.1016/j.freeradbiomed.2005.08.025

Kleinbongard, P., Dejam, A., Lauer, T., Rassaf, T., Schindler, A., Picker, O., Scheeren, T., Gödecke, A., Schrader, J., Schulz, R., Heusch, G., Schaub, G. A., Bryan, N. S., Feelisch, M., & Kelm, M. (2003). Plasma nitrite reflects constitutive nitric oxide synthase activity in mammals. *Free Radical Biology and Medicine*, *35*(7), 790–796. https://doi.org/10.1016/S0891-5849(03)00406-4

Knowles, R. G., & Moncada, S. (1994). Nitric oxide synthases in mammals. *Biochemical Journal*, *298*(2), 249–258. https://doi.org/10.1042/bj2980249

Kolluru, G. K., Siamwala, J. H., & Chatterjee, S. (2010). ENOS phosphorylation in health and disease. *Biochimie*, *92*(9), 1186–1198. https://doi.org/10.1016/j.biochi.2010.03.020

Komarova, Y., & Malik, A. B. (2010). Regulation of Endothelial Permeability via Paracellular and Transcellular Transport Pathways. *Annual Review of Physiology*, *72*(1), 463–493. https://doi.org/10.1146/annurev-physiol-021909-135833

Kostyunin, A. E., Yuzhalin, A. E., Ovcharenko, E. A., & Kutikhin, A. G. (2019). Development of calcific aortic valve disease: Do we know enough for new clinical trials? *Journal of Molecular and Cellular Cardiology*, *132*(May), 189–209. https://doi.org/10.1016/j.yjmcc.2019.05.016

Kristiansen, M., Graversen, J. H., Jacobsen, C., Sonne, O., Hoffman, H.-J., Law, S. K. A., & Moestrup, S. K. (2001). Identification of the haemoglobin scavenger receptor. *Nature*, *409*(6817), 198–201. https://doi.org/10.1038/35051594

Kubes, P., Suzuki, M., & Granger, D. N. (1991). Nitric oxide: an endogenous modulator of leukocyte adhesion. *Proceedings of the National Academy of Sciences*, *88*(11), 4651–4655. https://doi.org/10.1073/pnas.88.11.4651

Kuhlencordt, P. J., Gyurko, R., Han, F., Scherrer-Crosbie, M., Aretz, T. H., Hajjar, R., Picard, M. H., & Huang, P. L. (2001). Accelerated Atherosclerosis, Aortic Aneurysm Formation, and Ischemic Heart Disease in Apolipoprotein E/Endothelial Nitric Oxide Synthase Double-Knockout Mice. *Circulation*, *104*(4), 448–454. https://doi.org/10.1161/hc2901.091399

Kuhn, V., Diederich, L., Keller, T. C. S., Kramer, C. M., Lückstädt, W., Panknin, C., Suvorava, T., Isakson, B. E., Kelm, M., & Cortese-Krott, M. M. (2017). Red Blood Cell Function and Dysfunction: Redox Regulation, Nitric Oxide Metabolism, Anemia. *Antioxidants & Redox Signaling*, *26*(13), 718–742. https://doi.org/10.1089/ars.2016.6954

Kupari, M., Turto, H., & Lommi, J. (2005). Left ventricular hypertrophy in aortic valve stenosis: preventive or promotive of systolic dysfunction and heart failure? *European Heart Journal*, *26*(17), 1790–1796. https://doi.org/10.1093/eurheartj/ehi290

Laemmel, E., Bonnardel-Phu, E., Hou, X., Seror, J., & Vicaut, E. (2003). Interaction between nitric oxide and prostanoids in arterioles of rat cremaster muscle in vivo. *American Journal of Physiology-Heart and Circulatory Physiology*, *285*(3), H1254–H1260. https://doi.org/10.1152/ajpheart.00839.2002

Lancellotti, P., Magne, J., Dulgheru, R., Clavel, M.-A., Donal, E., Vannan, M. A., Chambers, J., Rosenhek, R., Habib, G., Lloyd, G., Nistri, S., Garbi, M., Marchetta, S., Fattouch, K., Coisne, A., Montaigne, D., Modine, T., Davin, L., Gach, O., … Oury, C. (2018). Outcomes of Patients With Asymptomatic Aortic Stenosis Followed Up in Heart Valve Clinics. *JAMA Cardiology*, *3*(11), 1060. https://doi.org/10.1001/jamacardio.2018.3152

Langlois, M. R., & Delanghe, J. R. (1996). Biological and clinical significance of haptoglobin polymorphism in humans. *Clinical Chemistry*, *42*(10), 1589–1600.

https://doi.org/10.1093/clinchem/42.10.1589

Laurent, S., & Boutouyrie, P. (2015). The Structural Factor of Hypertension. *Circulation Research*, *116*(6), 1007–1021. https://doi.org/10.1161/CIRCRESAHA.116.303596

Lee, S. S., Ahn, K. H., Lee, S. J., Sun, K., Goedhart, P. T., & Hardeman, M. R. (2004). Shear induced damage of red blood cells monitored by the decrease of their deformability. In *Korea Australia Rheology Journal* (Vol. 16, Issue 3, pp. 141–146).

Lee, T. C., Zhao, Y. D., Courtman, D. W., & Stewart, D. J. (2000). Abnormal Aortic Valve Development in Mice Lacking Endothelial Nitric Oxide Synthase. *Circulation*, *101*(20), 2345–2348. https://doi.org/10.1161/01.CIR.101.20.2345

Lee, W., Choi, W., Kang, S.-H., Hwang, I.-C., Choi, H.-M., Yoon, Y. E., & Cho, G.-Y. (2021). Long-term Prognosis of Mild to Moderate Aortic Stenosis and Coronary Artery Disease. *Journal of Korean Medical Science*, *36*(6), 1–9. https://doi.org/10.3346/jkms.2021.36.e47

Lerman, D. A., Prasad, S., & Alotti, N. (2015). Calcific Aortic Valve Disease: Molecular Mechanisms And Therapeutic Approaches. *European Cardiology Review*, *10*(2), 108. https://doi.org/10.15420/ecr.2015.10.2.108

Liakos, C. I., Grassos, C. A., Papadopoulos, D. P., Dimitriadis, K. S., Tsioufis, C. P., & Tousoulis, D. (2017). Arterial hypertension and aortic valve stenosis: Shedding light on a common "liaison." *Hellenic Journal of Cardiology*, *58*(4), 261–266. https://doi.org/10.1016/j.hjc.2017.03.005

Liao, J. K. (2013). Linking endothelial dysfunction with endothelial cell activation. *Journal of Clinical Investigation*, *123*(2), 540–541. https://doi.org/10.1172/JCI66843

Lim, S.-K., Ferraro, B., Moore, K., & Halliwell, B. (2001). Role of haptoglobin in free hemoglobin metabolism. *Redox Report*, *6*(4), 219–227. https://doi.org/10.1179/135100001101536364

Lipiski, M., Deuel, J. W., Baek, J. H., Engelsberger, W. R., Buehler, P. W., & Schaer, D. J. (2013). Human Hp1-1 and Hp2-2 Phenotype-Specific Haptoglobin Therapeutics Are Both Effective In Vitro and in Guinea Pigs to Attenuate Hemoglobin Toxicity. *Antioxidants & Redox Signaling*, *19*(14), 1619–1633. https://doi.org/10.1089/ars.2012.5089

LIU, P.-Y., TSAI, W.-C., LIN, C.-C., HSU, C.-H., HAUNG, Y.-Y., & CHEN, J.-H. (2004). Invasive measurements of pulse wave velocity correlate with the degree of aortic valve calcification and severity associated with matrix metalloproteinases in elderly patients with aortic valve stenosis. *Clinical Science*, *107*(4), 415–422. https://doi.org/10.1042/CS20040098

Liu, X., Miller, M. J. S., Joshi, M. S., Sadowska-krowicka, H., Clark, D. A., & Lancaster, J. R. (1998). Diffusion-limited Reaction of Free Nitric Oxide with Erythrocytes *. *Journal of Biological Chemistry*, *273*(30), 18709–18713. https://doi.org/10.1074/jbc.273.30.18709

Livak, K. J., & Schmittgen, T. D. (2001). Analysis of Relative Gene Expression Data Using Real-Time Quantitative PCR and the 2−ΔΔCT Method. *Methods*, *25*(4), 402–408. https://doi.org/10.1006/meth.2001.1262

Loot, A. E., Schreiber, J. G., Fisslthaler, B., & Fleming, I. (2009). Angiotensin II impairs endothelial function via tyrosine phosphorylation of the endothelial nitric oxide synthase. *Journal of Experimental Medicine*, *206*(13), 2889–2896. https://doi.org/10.1084/jem.20090449

Luksha, L., Agewall, S., & Kublickiene, K. (2009). Endothelium-derived hyperpolarizing factor in vascular physiology and cardiovascular disease. *Atherosclerosis*, *202*(2), 330–344. https://doi.org/10.1016/j.atherosclerosis.2008.06.008

Lundberg, J. O., Weitzberg, E., & Gladwin, M. T. (2008). The nitrate-nitrite-nitric oxide

pathway in physiology and therapeutics. *Nature Reviews Drug Discovery*, *7*(2), 156–167. https://doi.org/10.1038/nrd2466

Marquis-Gravel, G., Redfors, B., Leon, M. B., & Généreux, P. (2016). Medical Treatment of Aortic Stenosis. *Circulation*, *134*(22), 1766–1784. https://doi.org/10.1161/CIRCULATIONAHA.116.023997

Maruhashi, T., Soga, J., Fujimura, N., Idei, N., Mikami, S., Iwamoto, Y., Iwamoto, A., Kajikawa, M., Matsumoto, T., Oda, N., Kishimoto, S., Matsui, S., Hashimoto, H., Aibara, Y., Mohamad Yusoff, F., Hidaka, T., Kihara, Y., Chayama, K., Noma, K., … Higashi, Y. (2018). Endothelial Dysfunction, Increased Arterial Stiffness, and Cardiovascular Risk Prediction in Patients With Coronary Artery Disease: FMD-J (Flow-Mediated Dilation Japan) Study A. *Journal of the American Heart Association*, *7*(14). https://doi.org/10.1161/JAHA.118.008588

Matz, R. L., De Sotomayor, M. A., Schott, C., Stoclet, J., & Andriantsitohaina, R. (2000). Vascular bed heterogeneity in age-related endothelial dysfunction with respect to NO and eicosanoids. *British Journal of Pharmacology*, *131*(2), 303–311. https://doi.org/10.1038/sj.bjp.0703568

McEniery, C. M., Yasmin, Hall, I. R., Qasem, A., Wilkinson, I. B., & Cockcroft, J. R. (2005). Normal Vascular Aging: Differential Effects on Wave Reflection and Aortic Pulse Wave Velocity. *Journal of the American College of Cardiology*, *46*(9), 1753–1760. https://doi.org/10.1016/j.jacc.2005.07.037

Mecozzi, G., Milano, A. D., De Carlo, M., Sorrentino, F., Pratali, S., Nardi, C., & Bortolotti, U. (2002). Intravascular hemolysis in patients with new-generation prosthetic heart valves: A prospective study. *The Journal of Thoracic and Cardiovascular Surgery*, *123*(3), 550–556. https://doi.org/10.1067/mtc.2002.120337

Meister, A. (1994). Glutathione-ascorbic acid antioxidant system in animals. *Journal of Biological Chemistry*, *269*(13), 9397–9400. https://doi.org/10.1016/S0021-9258(17)36891-6

Miller, J. D., Weiss, R. M., Serrano, K. M., Castaneda, L. E., Brooks, R. M., Zimmerman, K., & Heistad, D. D. (2010). Evidence for Active Regulation of Pro-Osteogenic Signaling in Advanced Aortic Valve Disease. *Arteriosclerosis, Thrombosis, and Vascular Biology*, *30*(12), 2482–2486. https://doi.org/10.1161/ATVBAHA.110.211029

Misfeld, M., & Sievers, H.-H. (2007). Heart valve macro- and microstructure. *Philosophical Transactions of the Royal Society B: Biological Sciences*, *362*(1484), 1421–1436. https://doi.org/10.1098/rstb.2007.2125

Mohler, E. R., Gannon, F., Reynolds, C., Zimmerman, R., Keane, M. G., & Kaplan, F. S. (2001). Bone Formation and Inflammation in Cardiac Valves. *Circulation*, *103*(11), 1522–1528. https://doi.org/10.1161/01.CIR.103.11.1522

Moncada, S, Gryglewski, R., Bunting, S., & Vane, J. R. (1976). An enzyme isolated from arteries transforms prostaglandin endoperoxides to an unstable substance that inhibits platelet aggregation. *Nature*, *263*(5579), 663–665. https://doi.org/10.1038/263663a0

Moncada, Salvador, Higgs, E. A., & Vane, J. R. (1977). HUMAN ARTERIAL AND VENOUS TISSUES GENERATE PROSTACYCLIN (PROSTAGLANDIN X), A POTENT INHIBITOR OF PLATELET AGGREGATION. *The Lancet*, *309*(8001), 18–21. https://doi.org/10.1016/S0140-6736(77)91655-5

Monod, J., Wyman, J., & Changeux, J.-P. (1965). On the nature of allosteric transitions: A plausible model. *Journal of Molecular Biology*, *12*(1), 88–118. https://doi.org/10.1016/S0022-2836(65)80285-6

Moscarelli, M., Devito, F., Fattouch, K., Lancellotti, P., Ciccone, M. M., Rizzo, P., Gaudino, M., Marchese, A., Angelini, G., & Speziale, G. (2019). The effect of surgical versus

transcatheter aortic valve replacement on endothelial function. An observational study. *International Journal of Surgery*, *63*(January), 1–7. https://doi.org/10.1016/j.ijsu.2019.01.014

Mulvany, M. J., & Halpern, W. (1977). Contractile properties of small arterial resistance vessels in spontaneously hypertensive and normotensive rats. *Circulation Research*, *41*(1), 19–26. https://doi.org/10.1161/01.RES.41.1.19

Murohara, T., Asahara, T., Silver, M., Bauters, C., Masuda, H., Kalka, C., Kearney, M., Chen, D., Symes, J. F., Fishman, M. C., Huang, P. L., & Isner, J. M. (1998). Nitric oxide synthase modulates angiogenesis in response to tissue ischemia. *Journal of Clinical Investigation*, *101*(11), 2567–2578. https://doi.org/10.1172/JCI1560

Nagao, T., & Vanhoutte, P. M. (1992). Hyperpolarization as a mechanism for endothelium-dependent relaxations in the porcine coronary artery. *The Journal of Physiology*, *445*(1), 355–367. https://doi.org/10.1113/jphysiol.1992.sp018928

Nagy, E., Eaton, J. W., Jeney, V., Soares, M. P., Varga, Z., Galajda, Z., & Szentmiklósi, J. (2010). Red Cells, Hemoglobin, Heme, Iron and Atherogenesis. *Arteriosclerosis, Thrombosis, and Vascular Biology*, *30*(7), 1347–1353. https://doi.org/10.1161/ATVBAHA.110.206433.Red

Naumann, H. N., Diggs, L. W., Barreras, L., & Williams, B. J. (1971). Plasma Hemoglobin and Hemoglobin Fractions in Sickle Cell Crisis. *American Journal of Clinical Pathology*, *56*(2), 137–145. https://doi.org/10.1093/ajcp/56.2.137

Niepmann, S. T., Steffen, E., Zietzer, A., Adam, M., Nordsiek, J., Gyamfi-Poku, I., Piayda, K., Sinning, J.-M., Baldus, S., Kelm, M., Nickenig, G., Zimmer, S., & Quast, C. (2019). Graded murine wire-induced aortic valve stenosis model mimics human functional and morphological disease phenotype. *Clinical Research in Cardiology*, *108*(8), 847–856. https://doi.org/10.1007/s00392-019-01413-1

Nkomo, V. T., Gardin, J. M., Skelton, T. N., Gottdiener, J. S., Scott, C. G., & Enriquez-Sarano, M. (2006). Burden of valvular heart diseases: a population-based study. *The Lancet*, *368*(9540), 1005–1011. https://doi.org/10.1016/S0140-6736(06)69208-8

Novaro, G. M., Tiong, I. Y., Pearce, G. L., Lauer, M. S., Sprecher, D. L., & Griffin, B. P. (2001). Effect of Hydroxymethylglutaryl Coenzyme A Reductase Inhibitors on the Progression of Calcific Aortic Stenosis. *Circulation*, *104*(18), 2205–2209. https://doi.org/10.1161/hc4301.098249

O'Brien, K. D., Probstfield, J. L., Caulfield, M. T., Nasir, K., Takasu, J., Shavelle, D. M., Wu, A. H., Zhao, X.-Q., & Budoff, M. J. (2005). Angiotensin-Converting Enzyme Inhibitors and Change in Aortic Valve Calcium. *Archives of Internal Medicine*, *165*(8), 858. https://doi.org/10.1001/archinte.165.8.858

Olson, J. S., Foley, E. W., Rogge, C., Tsai, A.-L., Doyle, M. P., & Lemon, D. D. (2004). No scavenging and the hypertensive effect of hemoglobin-based blood substitutes. *Free Radical Biology and Medicine*, *36*(6), 685–697. https://doi.org/10.1016/j.freeradbiomed.2003.11.030

Olsson, M., Thyberg, J., & Nilsson, J. (1999). Presence of Oxidized Low Density Lipoprotein in Nonrheumatic Stenotic Aortic Valves. *Arteriosclerosis, Thrombosis, and Vascular Biology*, *19*(5), 1218–1222. https://doi.org/10.1161/01.ATV.19.5.1218

Osnabrugge, R. L. J., Mylotte, D., Head, S. J., Van Mieghem, N. M., Nkomo, V. T., LeReun, C. M., Bogers, A. J. J. C., Piazza, N., & Kappetein, A. P. (2013). Aortic Stenosis in the Elderly. *Journal of the American College of Cardiology*, *62*(11), 1002–1012. https://doi.org/10.1016/j.jacc.2013.05.015

Otto, C. M., Lind, B. K., Kitzman, D. W., Gersh, B. J., & Siscovick, D. S. (1999). Association of Aortic-Valve Sclerosis with Cardiovascular Mortality and Morbidity in the Elderly. *New England Journal of Medicine*, *341*(3), 142–147.

https://doi.org/10.1056/NEJM199907153410302

Owens, D. S., Budoff, M. J., Katz, R., Takasu, J., Shavelle, D. M., Carr, J. J., Heckbert, S. R., Otto, C. M., Probstfield, J. L., Kronmal, R. A., & O'Brien, K. D. (2012). Aortic Valve Calcium Independently Predicts Coronary and Cardiovascular Events in a Primary Prevention Population. *JACC: Cardiovascular Imaging*, *5*(6), 619–625. https://doi.org/10.1016/j.jcmg.2011.12.023

Ozkor, M. A., & Quyyumi, A. A. (2011). Endothelium-Derived Hyperpolarizing Factor and Vascular Function. *Cardiology Research and Practice*, *2011*(1), 1–12. https://doi.org/10.4061/2011/156146

Palacios, M., Knowles, R. G., Palmer, R. M. J., & Moncada, S. (1989). Nitric oxide from L-arginine stimulates the soluble guanylate cyclase in adrenal glands. *Biochemical and Biophysical Research Communications*, *165*(2), 802–809. https://doi.org/10.1016/S0006-291X(89)80037-3

Palmer, R. M. J., Ashton, D. S., & Moncada, S. (1988). Vascular endothelial cells synthesize nitric oxide from L-arginine. *Nature*, *333*(6174), 664–666. https://doi.org/10.1038/333664a0

Palmer, Richard M.J., & Moncada, S. (1989). A novel citrulline-forming enzyme implicated in the formation of nitric oxide by vascular endothelial cells. *Biochemical and Biophysical Research Communications*, *158*(1), 348–352. https://doi.org/10.1016/S0006-291X(89)80219-0

Papapetropoulos, A., García-Cardeña, G., Madri, J. A., & Sessa, W. C. (1997). Nitric oxide production contributes to the angiogenic properties of vascular endothelial growth factor in human endothelial cells. *Journal of Clinical Investigation*, *100*(12), 3131–3139. https://doi.org/10.1172/JCI119868

Park, K., Park, T.-H., Jo, Y.-S., Cho, Y.-R., Park, J.-S., Kim, M.-H., & Kim, Y.-D. (2021). Prognostic effect of increased left ventricular wall thickness in severe aortic stenosis. *Cardiovascular Ultrasound*, *19*(1), 5. https://doi.org/10.1186/s12947-020-00234-x

Pawade, T. A., Doris, M. K., Bing, R., White, A. C., Forsyth, L., Evans, E., Graham, C., Williams, M. C., van Beek, E. J. R., Fletcher, A., Adamson, P. D., Andrews, J. P. M., Cartlidge, T. R. G., Jenkins, W. S. A., Syed, M., Fujisawa, T., Lucatelli, C., Fraser, W., Ralston, S. H., … Dweck, M. R. (2021). Effect of Denosumab or Alendronic Acid on the Progression of Aortic Stenosis: A Double-Blind Randomized Controlled Trial. *Circulation*, *143*(25), 2418–2427. https://doi.org/10.1161/CIRCULATIONAHA.121.053708

Pawade, T. A., Newby, D. E., & Dweck, M. R. (2015). Calcification in Aortic Stenosis. *Journal of the American College of Cardiology*, *66*(5), 561–577. https://doi.org/10.1016/j.jacc.2015.05.066

Perutz, M. F. (1978). Hemoglobin Structure and Respiratory Transport. *Scientific American*, *239*(6), 92–125. https://doi.org/10.1038/scientificamerican1278-92

Perutz, M. F., Wilkinson, A. J., Paoli, M., & Dodson, G. G. (1998). THE STEREOCHEMICAL MECHANISM OF THE COOPERATIVE EFFECTS IN HEMOGLOBIN REVISITED. *Annual Review of Biophysics and Biomolecular Structure*, *27*(1), 1–34. https://doi.org/10.1146/annurev.biophys.27.1.1

Poggianti, E., Venneri, L., Chubuchny, V., Jambrik, Z., Baroncini, L. A., & Picano, E. (2003). Aortic valve sclerosis is associatedwith systemic endothelial dysfunction. *Journal of the American College of Cardiology*, *41*(1), 136–141. https://doi.org/10.1016/S0735-1097(02)02622-0

Pyke, K. E., & Tschakovsky, M. E. (2005). The relationship between shear stress and flow-mediated dilatation: implications for the assessment of endothelial function. *The Journal of Physiology*, *568*(2), 357–369. https://doi.org/10.1113/jphysiol.2005.089755

Quast, C, Erkens, R., Piayda, K., Wolff, G., Kelm, M., & Cortese-Krott, M. M. (2018). P5125 Lack of endothelial nitric oxide synthase leads to aortic valve stenosis in aging mice. *European Heart Journal*, *39*(suppl_1), 126. https://doi.org/10.1093/eurheartj/ehy566.P5125

Quast, Christine, Kober, F., Becker, K., Zweck, E., Hoffe, J., Jacoby, C., Flocke, V., Gyamfi-Poku, I., Keyser, F., Piayda, K., Erkens, R., Niepmann, S., Adam, M., Baldus, S., Zimmer, S., Nickenig, G., Grandoch, M., Bönner, F., Kelm, M., & Flögel, U. (2022). Multiparametric MRI identifies subtle adaptations for demarcation of disease transition in murine aortic valve stenosis. *Basic Research in Cardiology*, *117*(1), 29. https://doi.org/10.1007/s00395-022-00936-5

Radomski, M. W., Palmer, R. M. J., & Moncada, S. (1987). The role of nitric oxide and cGMP in platelet adhesion to vascular endothelium. *Biochemical and Biophysical Research Communications*, *148*(3), 1482–1489. https://doi.org/10.1016/S0006-291X(87)80299-1

Rajamannan, N. M., Evans, F. J., Aikawa, E., Grande-Allen, K. J., Demer, L. L., Heistad, D. D., Simmons, C. A., Masters, K. S., Mathieu, P., O'Brien, K. D., Schoen, F. J., Towler, D. A., Yoganathan, A. P., & Otto, C. M. (2011). Calcific Aortic Valve Disease: Not Simply a Degenerative Process. *Circulation*, *124*(16), 1783–1791. https://doi.org/10.1161/CIRCULATIONAHA.110.006767

Raman, C. ., Li, H., Martásek, P., Král, V., Masters, B. S. S., & Poulos, T. L. (1998). Crystal Structure of Constitutive Endothelial Nitric Oxide Synthase. *Cell*, *95*(7), 939–950. https://doi.org/10.1016/S0092-8674(00)81718-3

Rassaf, T., Bryan, N. S., Kelm, M., & Feelisch, M. (2002). Concomitant presence of N-nitroso and S-nitroso proteins in human plasma. *Free Radical Biology and Medicine*, *33*(11), 1590–1596. https://doi.org/10.1016/S0891-5849(02)01183-8

Rassaf, T., Flögel, U., Drexhage, C., Hendgen-Cotta, U., Kelm, M., & Schrader, J. (2007). Nitrite Reductase Function of Deoxymyoglobin. *Circulation Research*, *100*(12), 1749–1754. https://doi.org/10.1161/CIRCRESAHA.107.152488

Rassaf, T., Heiss, C., Hendgen-Cotta, U., Balzer, J., Matern, S., Kleinbongard, P., Lee, A., Lauer, T., & Kelm, M. (2006). Plasma nitrite reserve and endothelial function in the human forearm circulation. *Free Radical Biology and Medicine*, *41*(2), 295–301. https://doi.org/10.1016/j.freeradbiomed.2006.04.006

Reiter, C. D., Wang, X., Tanus-Santos, J. E., Hogg, N., Cannon, R. O., Schechter, A. N., & Gladwin, M. T. (2002). Cell-free hemoglobin limits nitric oxide bioavailability in sickle-cell disease. *Nature Medicine*, *8*(12), 1383–1389. https://doi.org/10.1038/nm799

Rezzoug, N., Vaes, B., Pasquet, A., Gerber, B., de Meester, C., Van Pottelbergh, G., Adriaensen, W., Matheï, C., DeGryse, J., & Vanoverschelde, J.-L. (2015). Prevalence and Prognostic Impact of Valve Area—Gradient Patterns in Patients ≥80 Years With Moderate-to-Severe Aortic Stenosis (from the Prospective BELFRAIL Study). *The American Journal of Cardiology*, *116*(6), 925–932. https://doi.org/10.1016/j.amjcard.2015.05.062

Richards, J., El-Hamamsy, I., Chen, S., Sarang, Z., Sarathchandra, P., Yacoub, M. H., Chester, A. H., & Butcher, J. T. (2013a). Side-Specific Endothelial-Dependent Regulation of Aortic Valve Calcification. *The American Journal of Pathology*, *182*(5), 1922–1931. https://doi.org/10.1016/j.ajpath.2013.01.037

Richards, J., El-Hamamsy, I., Chen, S., Sarang, Z., Sarathchandra, P., Yacoub, M. H., Chester, A. H., & Butcher, J. T. (2013b). Side-Specific Endothelial-Dependent Regulation of Aortic Valve Calcification. *The American Journal of Pathology*, *182*(5), 1922–1931. https://doi.org/10.1016/j.ajpath.2013.01.037

Rieck, Å. E., Cramariuc, D., Boman, K., Gohlke-Bärwolf, C., Staal, E. M., Lønnebakken,

M. T., Rossebø, A. B., & Gerdts, E. (2012). Hypertension in Aortic Stenosis. *Hypertension*, *60*(1), 90–97. https://doi.org/10.1161/HYPERTENSIONAHA.112.194878

Rodríguez-Mañas, L., El-Assar, M., Vallejo, S., López-Dóriga, P., Solís, J., Petidier, R., Montes, M., Nevado, J., Castro, M., Gómez-Guerrero, C., Peiró, C., & Sánchez-Ferrer, C. F. (2009). Endothelial dysfunction in aged humans is related with oxidative stress and vascular inflammation. *Aging Cell*, *8*(3), 226–238. https://doi.org/10.1111/j.1474-9726.2009.00466.x

Rosca, M., Magne, J., Calin, A., Popescu, B. A., Pierard, L. A., & Lancellotti, P. (2011). Impact of aortic stiffness on left ventricular function and B-type natriuretic peptide release in severe aortic stenosis. *European Journal of Echocardiography*, *12*(11), 850–856. https://doi.org/10.1093/ejechocard/jer120

Rosenhek, R., Rader, F., Loho, N., Gabriel, H., Heger, M., Klaar, U., Schemper, M., Binder, T., Maurer, G., & Baumgartner, H. (2004). Statins but Not Angiotensin-Converting Enzyme Inhibitors Delay Progression of Aortic Stenosis. *Circulation*, *110*(10), 1291–1295. https://doi.org/10.1161/01.CIR.0000140723.15274.53

Rossebø, A. B., Pedersen, T. R., Boman, K., Brudi, P., Chambers, J. B., Egstrup, K., Gerdts, E., Gohlke-Bärwolf, C., Holme, I., Kesäniemi, Y. A., Malbecq, W., Nienaber, C. A., Ray, S., Skjærpe, T., Wachtell, K., & Willenheimer, R. (2008). Intensive Lipid Lowering with Simvastatin and Ezetimibe in Aortic Stenosis. *New England Journal of Medicine*, *359*(13), 1343–1356. https://doi.org/10.1056/NEJMoa0804602

Rother, R. P., Bell, L., Hillmen, P., & Gladwin, M. T. (2005). The Clinical Sequelae of Intravascular Hemolysis and Extracellular Plasma Hemoglobin. *JAMA*, *293*(13), 1653. https://doi.org/10.1001/jama.293.13.1653

Rubanyi, G. M., Romero, J. C., & Vanhoutte, P. M. (1986). Flow-induced release of endothelium-derived relaxing factor. *American Journal of Physiology-Heart and Circulatory Physiology*, *250*(6), H1145–H1149. https://doi.org/10.1152/ajpheart.1986.250.6.H1145

Rubanyi, G. M., & Vanhoutte, P. M. (1986). Superoxide anions and hyperoxia inactivate endothelium-derived relaxing factor. *American Journal of Physiology-Heart and Circulatory Physiology*, *250*(5), H822–H827. https://doi.org/10.1152/ajpheart.1986.250.5.H822

Rudolph, T. K., Messika-Zeitoun, D., Frey, N., Thambyrajah, J., Serra, A., Schulz, E., Maly, J., Aiello, M., Lloyd, G., Bortone, A. S., Clerici, A., Delle-Karth, G., Rieber, J., Indolfi, C., Mancone, M., Belle, L., Lauten, A., Arnold, M., Bouma, B. J., … Steeds, R. P. (2020). Impact of selected comorbidities on the presentation and management of aortic stenosis. *Open Heart*, *7*(2), e001271. https://doi.org/10.1136/openhrt-2020-001271

Salinger, T., Hu, K., Liu, D., Taleh, S., Herrmann, S., Oder, D., Gensler, D., Müntze, J., Ertl, G., Lorenz, K., Frantz, S., Weidemann, F., & Nordbeck, P. (2018). Association between Comorbidities and Progression of Transvalvular Pressure Gradients in Patients with Moderate and Severe Aortic Valve Stenosis. *Cardiology Research and Practice*, *2018*, 1–7. https://doi.org/10.1155/2018/3713897

Sandza, J., Clark, E. E., Weldon, C. S., & Sutera, S. P. (1974). *Subhemolytic trauma of erythrocytes: recognition and sequestration by the spleen as a function of shear* (pp. 457–462).

Santiago, R. P., Guarda, C. C., Figueiredo, C. V. B., Fiuza, L. M., Adanho, C. S. A., Aleluia, M. M., Zanette, D. L., Carvalho, M. O. S., Lyra, I. M., Lopes, V. M., Nguyen, J., Killeen, T., Nguyen, H., Vercellotti, G. M., Belcher, J. D., & Goncalves, M. S. (2016). Serum Haptoglobin and Hemopexin Levels in Pediatric SS and SC Disease Patients: Biomarker of Hemolysis and Inflammation. *Blood*, *128*(22), 3649–3649.

https://doi.org/10.1182/blood.V128.22.3649.3649

Schaer, C. A., Deuel, J. W., Schildknecht, D., Mahmoudi, L., Garcia-Rubio, I., Owczarek, C., Schauer, S., Kissner, R., Banerjee, U., Palmer, A. F., Spahn, D. R., Irwin, D. C., Vallelian, F., Buehler, P. W., & Schaer, D. J. (2016). Haptoglobin Preserves Vascular Nitric Oxide Signaling during Hemolysis. *American Journal of Respiratory and Critical Care Medicine*, *193*(10), 1111–1122. https://doi.org/10.1164/rccm.201510-2058OC

Schaer, D. J., Buehler, P. W., Alayash, A. I., Belcher, J. D., & Vercellotti, G. M. (2013). Hemolysis and free hemoglobin revisited: exploring hemoglobin and hemin scavengers as a novel class of therapeutic proteins. *Blood*, *121*(8), 1276–1284. https://doi.org/10.1182/blood-2012-11-451229

Schaer, D. J., Vinchi, F., Ingoglia, G., Tolosano, E., & Buehler, P. W. (2014). Haptoglobin, hemopexin, and related defense pathwaysâ€"basic science, clinical perspectives, and drug development. *Frontiers in Physiology*, *5*(OCT), 1–13. https://doi.org/10.3389/fphys.2014.00415

Schoen, F. J. (2008). Evolving Concepts of Cardiac Valve Dynamics. *Circulation*, *118*(18), 1864–1880. https://doi.org/10.1161/CIRCULATIONAHA.108.805911

Schuler, D., Sansone, R., Freudenberger, T., Rodriguez-Mateos, A., Weber, G., Momma, T. Y., Goy, C., Altschmied, J., Haendeler, J., Fischer, J. W., Kelm, M., & Heiss, C. (2014). Measurement of Endothelium-Dependent Vasodilation in Mice—Brief Report. *Arteriosclerosis, Thrombosis, and Vascular Biology*, *34*(12), 2651–2657. https://doi.org/10.1161/ATVBAHA.114.304699

Schulz, E., Gori, T., & Münzel, T. (2011). Oxidative stress and endothelial dysfunction in hypertension. *Hypertension Research*, *34*(6), 665–673. https://doi.org/10.1038/hr.2011.39

Searles, C. D. (2006). Transcriptional and posttranscriptional regulation of endothelial nitric oxide synthase expression. *American Journal of Physiology-Cell Physiology*, *291*(5), C803–C816. https://doi.org/10.1152/ajpcell.00457.2005

Shavelle, D. M., Takasu, J., Budoff, M. J., Mao, S., Zhao, X.-Q., & O'Brien, K. D. (2002). HMG CoA reductase inhibitor (statin) and aortic valve calcium. *The Lancet*, *359*(9312), 1125–1126. https://doi.org/10.1016/S0140-6736(02)08161-8

Shesely, E. G., Maeda, N., Kim, H. S., Desai, K. M., Krege, J. H., Laubach, V. E., Sherman, P. A., Sessa, W. C., & Smithies, O. (1996). Elevated blood pressures in mice lacking endothelial nitric oxide synthase. *Proceedings of the National Academy of Sciences*, *93*(23), 13176–13181. https://doi.org/10.1073/pnas.93.23.13176

Shin, W., Berkowitz, D. E., & Ryoo, S. (2012). Increased arginase II activity contributes to endothelial dysfunction through endothelial nitric oxide synthase uncoupling in aged mice. *Experimental & Molecular Medicine*, *44*(10), 594. https://doi.org/10.3858/emm.2012.44.10.068

Sider, K. L., Blaser, M. C., & Simmons, C. A. (2011). Animal Models of Calcific Aortic Valve Disease. *International Journal of Inflammation*, *2011*(Ldl), 1–18. https://doi.org/10.4061/2011/364310

Sies, H., Berndt, C., & Jones, D. P. (2017). Oxidative Stress. *Annual Review of Biochemistry*, *86*(1), 715–748. https://doi.org/10.1146/annurev-biochem-061516-045037

Silva, B. R., Pernomian, L., & Bendhack, L. M. (2012). Contribution of oxidative stress to endothelial dysfunction in hypertension. *Frontiers in Physiology*, *3*(December), 1–5. https://doi.org/10.3389/fphys.2012.00441

Simmonds, M. J., Atac, N., Baskurt, O. K., Meiselman, H. J., & Yalcin, O. (2014). Erythrocyte deformability responses to intermittent and continuous subhemolytic shear stress. *Biorheology*, *51*(2–3), 171–185. https://doi.org/10.3233/BIR-140665

Simmons, C. A., Grant, G. R., Manduchi, E., & Davies, P. F. (2005). Spatial Heterogeneity of Endothelial Phenotypes Correlates With Side-Specific Vulnerability to Calcification in Normal Porcine Aortic Valves. *Circulation Research*, *96*(7), 792–799. https://doi.org/10.1161/01.RES.0000161998.92009.64

Siragusa, M., & Fleming, I. (2016). The eNOS signalosome and its link to endothelial dysfunction. *Pflugers Archiv European Journal of Physiology*, *468*(7), 1125–1137. https://doi.org/10.1007/s00424-016-1839-0

Smith, J. G., Luk, K., Schulz, C., Engert, J. C., Do, R., Hindy, G., Rukh, G., Dufresne, L., Almgren, P., Owens, D. S., Harris, T. B., Peloso, G. M., Kerr, K. F., Wong, Q., Smith, A. V, Budoff, M. J., Rotter, J. I., Cupples, L. A., Rich, S., … Thanassoulis, G. (2014). Association of Low-Density Lipoprotein Cholesterol–Related Genetic Variants With Aortic Valve Calcium and Incident Aortic Stenosis. *JAMA*, *312*(17), 1764. https://doi.org/10.1001/jama.2014.13959

Sohrabi, S., & Liu, Y. (2017). A Cellular Model of Shear-Induced Hemolysis. *Artificial Organs*, *41*(9), E80–E91. https://doi.org/10.1111/aor.12832

Srivatsa, S. S., Harrity, P. J., Maercklein, P. B., Kleppe, L., Veinot, J., Edwards, W. D., Johnson, C. M., & Fitzpatrick, L. A. (1997). Increased cellular expression of matrix proteins that regulate mineralization is associated with calcification of native human and porcine xenograft bioprosthetic heart valves. *Journal of Clinical Investigation*, *99*(5), 996–1009. https://doi.org/10.1172/JCI119265

Storz, G., & Imlayt, J. A. (1999). Oxidative stress. *Current Opinion in Microbiology*, *2*(2), 188–194. https://doi.org/10.1016/S1369-5274(99)80033-2

Stuehr, D. J., Kwon, N. S., Nathan, C. F., Griffith, O. W., Feldman, P. L., & Wiseman, J. (1991). N omega-hydroxy-L-arginine is an intermediate in the biosynthesis of nitric oxide from L-arginine. *Journal of Biological Chemistry*, *266*(10), 6259–6263. https://doi.org/10.1016/S0021-9258(18)38112-2

Sucosky, P., Balachandran, K., Elhammali, A., Jo, H., & Yoganathan, A. P. (2009). Altered Shear Stress Stimulates Upregulation of Endothelial VCAM-1 and ICAM-1 in a BMP-4– and TGF-β1–Dependent Pathway. *Arteriosclerosis, Thrombosis, and Vascular Biology*, *29*(2), 254–260. https://doi.org/10.1161/ATVBAHA.108.176347

Sugiura, T., Okumiya, T., Kubo, T., Takeuchi, H., & Matsumura, Y. (2016). Evaluation of Intravascular Hemolysis With Erythrocyte Creatine in Patients With Aortic Stenosis. *International Heart Journal*, *57*(4), 430–433. https://doi.org/10.1536/ihj.15-433

Sutera, S. P. (1977). Flow-induced trauma to blood cells. *Circulation Research*, *41*(1), 2–8. https://doi.org/10.1161/01.RES.41.1.2

Suwa, K., Rahman, O. A., Bollache, E., Rose, M. J., Rahsepar, A. A., Carr, J. C., Collins, J. D., Barker, A. J., & Markl, M. (2020). Effect of Aortic Valve Disease on 3D Hemodynamics in Patients With Aortic Dilation and Trileaflet Aortic Valve Morphology. *Journal of Magnetic Resonance Imaging*, *51*(2), 481–491. https://doi.org/10.1002/jmri.26804

Suwaidi, J. Al, Hamasaki, S., Higano, S. T., Nishimura, R. A., Holmes, D. R., & Lerman, A. (2000). Long-Term Follow-Up of Patients With Mild Coronary Artery Disease and Endothelial Dysfunction. *Circulation*, *101*(9), 948–954. https://doi.org/10.1161/01.CIR.101.9.948

Synetos, A., Toutouzas, K., Drakopoulou, M., Koutagiar, I., Benetos, G., Kotronias, R., Anousakis-Vlachochristou, N., Latsios, G., Karanasos, A., Agrogiannis, G., Metaxas, M., Stathogiannis, K., Papanikolaou, A., Georgakopoulos, A., Pianou, N., Tsiamis, E., Patsouris, E., Papalois, A., Cokkinos, D., … Tousoulis, D. (2018). Inhibition of Aortic Valve Calcification by Local Delivery of Zoledronic Acid—an Experimental Study. *Journal of Cardiovascular Translational Research*, *11*(3), 192–200.

https://doi.org/10.1007/s12265-018-9802-4

Takata, M., Amiya, E., Watanabe, M., Ozeki, A., Watanabe, A., Kawarasaki, S., Nakao, T., Hosoya, Y., Uno, K., Saito, A., Murasawa, T., Ono, M., Nagai, R., & Komuro, I. (2015). Brachial artery diameter has a predictive value in the improvement of flow-mediated dilation after aortic valve replacement for aortic stenosis. *Heart and Vessels*, *30*(2), 218–226. https://doi.org/10.1007/s00380-014-0475-x

Tanaka, K., Sata, M., Fukuda, D., Suematsu, Y., Motomura, N., Takamoto, S., Hirata, Y., & Nagai, R. (2005). Age-Associated Aortic Stenosis in Apolipoprotein E-Deficient Mice. *Journal of the American College of Cardiology*, *46*(1), 134–141. https://doi.org/10.1016/j.jacc.2005.03.058

Tejero, J., Shiva, S., & Gladwin, M. T. (2019). Sources of Vascular Nitric Oxide and Reactive Oxygen Species and Their Regulation. *Physiological Reviews*, *99*(1), 311–379. https://doi.org/10.1152/physrev.00036.2017

Thomas, S. R., Witting, P. K., & Drummond, G. R. (2008). Redox Control of Endothelial Function and Dysfunction: Molecular Mechanisms and Therapeutic Opportunities. *Antioxidants & Redox Signaling*, *10*(10), 1713–1766. https://doi.org/10.1089/ars.2008.2027

Thomson, L. (2015). 3-Nitrotyrosine Modified Proteins in Atherosclerosis. *Disease Markers*, *2015*(2), 1–8. https://doi.org/10.1155/2015/708282

Thubrikar, M. J., Aouad, J., & Nolan, S. P. (1986). Patterns of calcific deposits in operatively excised stenotic or purely regurgitant aortic valves and their relation to mechanical stress. *The American Journal of Cardiology*, *58*(3), 304–308. https://doi.org/10.1016/0002-9149(86)90067-6

TSUJI, A., TANABE, M., ONISHI, K., KITAMURA, T., OKINAKA, T., ITO, M., ISAKA, N., & NAKANO, T. (2004). Intravascular Hemolysis in Aortic Stenosis. *Internal Medicine*, *43*(10), 935–938. https://doi.org/10.2169/internalmedicine.43.935

ULKER, S., MCMASTER, D., MCKEOWN, P., & BAYRAKTUTAN, U. (2003). Impaired activities of antioxidant enzymes elicit endothelial dysfunction in spontaneous hypertensive rats despite enhanced vascular nitric oxide generation. *Cardiovascular Research*, *59*(2), 488–500. https://doi.org/10.1016/S0008-6363(03)00424-3

Vahanian, A., Beyersdorf, F., Praz, F., Milojevic, M., Baldus, S., Bauersachs, J., Capodanno, D., Conradi, L., De Bonis, M., De Paulis, R., Delgado, V., Freemantle, N., Gilard, M., Haugaa, K. H., Jeppsson, A., Jüni, P., Pierard, L., Prendergast, B. D., Sádaba, J. R., … Wojakowski, W. (2021). 2021 ESC/EACTS Guidelines for the management of valvular heart disease. *European Heart Journal*, 1–72. https://doi.org/10.1093/eurheartj/ehab395

Vahidkhah K., Cordasco D., Abbasi M., Ge L., Tseng E., Bagchi P., A. A. (2016). *Flow-Induced Damage to Blood Cells in Aortic Valve Stenosis*. *44*(9), 2724–2736. https://doi.org/10.1007/s10439-016-1577-7

Valerio, V., Myasoedova, V. A., Moschetta, D., Porro, B., Perrucci, G. L., Cavalca, V., Cavallotti, L., Songia, P., & Poggio, P. (2019). Impact of Oxidative Stress and Protein S-Glutathionylation in Aortic Valve Sclerosis Patients with Overt Atherosclerosis. *Journal of Clinical Medicine*, *8*(4), 552. https://doi.org/10.3390/jcm8040552

van Ooij, P., Markl, M., Collins, J. D., Carr, J. C., Rigsby, C., Bonow, R. O., Malaisrie, S. C., McCarthy, P. M., Fedak, P. W. M., & Barker, A. J. (2017). Aortic Valve Stenosis Alters Expression of Regional Aortic Wall Shear Stress: New Insights From a 4-Dimensional Flow Magnetic Resonance Imaging Study of 571 Subjects. *Journal of the American Heart Association*, *6*(9), 1–13. https://doi.org/10.1161/JAHA.117.005959

Vanhoutte, P. M., Feletou, M., & Taddei, S. (2005). Endothelium-dependent contractions in hypertension. *British Journal of Pharmacology*, *144*(4), 449–458.

https://doi.org/10.1038/sj.bjp.0706042

Vaughn, M. W., Huang, K., Kuo, L., & Liao, J. C. (2000). Erythrocytes Possess an Intrinsic Barrier to Nitric Oxide Consumption. *Journal of Biological Chemistry*, *275*(4), 2342–2348. https://doi.org/10.1074/jbc.275.4.2342

Vaughn, M. W., Kuo, L., & Liao, J. C. (1998). Effective diffusion distance of nitric oxide in the microcirculation. *American Journal of Physiology-Heart and Circulatory Physiology*, *274*(5), H1705–H1714. https://doi.org/10.1152/ajpheart.1998.274.5.H1705

von Knobelsdorff-Brenkenhoff, F., Karunaharamoorthy, A., Trauzeddel, R. F., Barker, A. J., Blaszczyk, E., Markl, M., & Schulz-Menger, J. (2016). Evaluation of Aortic Blood Flow and Wall Shear Stress in Aortic Stenosis and Its Association With Left Ventricular Remodeling. *Circulation: Cardiovascular Imaging*, *9*(3), 1–11. https://doi.org/10.1161/CIRCIMAGING.115.004038

Weisell, J., Ruotsalainen, A., Laakso, H., Ylä-Herttuala, E., Näpänkangas, J., Levonen, A., Liimatainen, T., & Rysä, J. (2019). Characterizing valve dynamics in mice by high-resolution cine-MRI. *NMR in Biomedicine*, *32*(8), e4108. https://doi.org/10.1002/nbm.4108

Weiss, R. M., Ohashi, M., Miller, J. D., Young, S. G., & Heistad, D. D. (2006). Calcific Aortic Valve Stenosis in Old Hypercholesterolemic Mice. *Circulation*, *114*(19), 2065–2069. https://doi.org/10.1161/CIRCULATIONAHA.106.634139

Wood, K. C., Cortese-Krott, M. M., Kovacic, J. C., Noguchi, A., Liu, V. B., Wang, X., Raghavachari, N., Boehm, M., Kato, G. J., Kelm, M., & Gladwin, M. T. (2013). Circulating Blood Endothelial Nitric Oxide Synthase Contributes to the Regulation of Systemic Blood Pressure and Nitrite Homeostasis. *Arteriosclerosis, Thrombosis, and Vascular Biology*, *33*(8), 1861–1871. https://doi.org/10.1161/ATVBAHA.112.301068

Xiong, Y., Uys, J. D., Tew, K. D., & Townsend, D. M. (2011). S-Glutathionylation: From Molecular Mechanisms to Health Outcomes. *Antioxidants & Redox Signaling*, *15*(1), 233–270. https://doi.org/10.1089/ars.2010.3540

Yadgir, S., Johnson, C. O., Aboyans, V., Adebayo, O. M., Adedoyin, R. A., Afarideh, M., Alahdab, F., Alashi, A., Alipour, V., Arabloo, J., Azari, S., Barthelemy, C. M., Benziger, C. P., Berman, A. E., Bijani, A., Carrero, J. J., Carvalho, F., Daryani, A., Durães, A. R., … Roth, G. A. (2020). Global, Regional, and National Burden of Calcific Aortic Valve and Degenerative Mitral Valve Diseases, 1990–2017. *Circulation*, *141*(21), 1670–1680. https://doi.org/10.1161/CIRCULATIONAHA.119.043391

Yang, X., Fullerton, D. A., Su, X., Ao, L., Cleveland, J. C., & Meng, X. (2009). Pro-Osteogenic Phenotype of Human Aortic Valve Interstitial Cells Is Associated With Higher Levels of Toll-Like Receptors 2 and 4 and Enhanced Expression of Bone Morphogenetic Protein 2. *Journal of the American College of Cardiology*, *53*(6), 491–500. https://doi.org/10.1016/j.jacc.2008.09.052

Yeboah, J., Folsom, A. R., Burke, G. L., Johnson, C., Polak, J. F., Post, W., Lima, J. A., Crouse, J. R., & Herrington, D. M. (2009). Predictive Value of Brachial Flow-Mediated Dilation for Incident Cardiovascular Events in a Population-Based Study. *Circulation*, *120*(6), 502–509. https://doi.org/10.1161/CIRCULATIONAHA.109.864801

Yeo, T. W., Lampah, D. A., Tjitra, E., Gitawati, R., Kenangalem, E., Piera, K., Granger, D. L., Lopansri, B. K., Weinberg, J. B., Price, R. N., Duffull, S. B., Celermajer, D. S., & Anstey, N. M. (2009). Relationship of Cell-Free Hemoglobin to Impaired Endothelial Nitric Oxide Bioavailability and Perfusion in Severe Falciparum Malaria. *The Journal of Infectious Diseases*, *200*(10), 1522–1529. https://doi.org/10.1086/644641

Zarins, C. K., Giddens, D. P., Bharadvaj, B. K., Sottiurai, V. S., Mabon, R. F., & Glagov, S. (1983). Carotid bifurcation atherosclerosis. Quantitative correlation of plaque

localization with flow velocity profiles and wall shear stress. *Circulation Research*, *53*(4), 502–514. https://doi.org/10.1161/01.RES.53.4.502

Zhang, C. (2008). The role of inflammatory cytokines in endothelial dysfunction. *Basic Research in Cardiology*, *103*(5), 398–406. https://doi.org/10.1007/s00395-008-0733-0

Zhang, M., & Vogel, H. J. (1994). Characterization of the calmodulin-binding domain of rat cerebellar nitric oxide synthase. *Journal of Biological Chemistry*, *269*(2), 981–985. https://doi.org/10.1016/S0021-9258(17)42208-3

Zou, M., Shi, C., & Cohen, R. A. (2002). Oxidation of the zinc-thiolate complex and uncoupling of endothelial nitric oxide synthase by peroxynitrite. *Journal of Clinical Investigation*, *109*(6), 817–826. https://doi.org/10.1172/JCI200214442

Zweier, J. L., Wang, P., Samouilov, A., & Kuppusamy, P. (1995). Enzyme-independent formation of nitric oxide in biological tissues. *Nature Medicine*, *1*(8), 804–809. https://doi.org/10.1038/nm0895-804